Energy Management System Design for Fuel Cell Vehicles

by

Di Shen

Thesis submitted for the degree of

Doctor of Philosophy

in

School of Electrical & Electronic Engineering
Faculty of Engineering, Computer & Mathematical Sciences
The University of Adelaide, Australia

October 2020

© 2020
Di Shen
All Rights Reserved

THE UNIVERSITY of ADELAIDE

Contents

Abstract

Fuel cell vehicles combine the benefits of fuel cell stacks and energy storage systems to achieve fuel economy and zero emission. Energy management systems are vital to fuel cell vehicles in fuel economy and system durability since it determines the distribution of power from the fuel cell stack and energy storage system.

In this thesis, we propose three novel energy management system designs for fuel cell vehicles to improve the vehicle energy system stability, optimality and durability.

We first present a non-myopic energy management system for controlling multiple energy flows in fuel cell hybrid vehicles. The control problem is solved by convex programming under a partially observable Markov decision process based framework. We propose an average-reward approximator to estimate a long-term average cost instead of using a model to predict future power demand. Thus, the dependency between the system closed-loop performance and the model accuracy for predicting the future power demand is decoupled in the energy management design for fuel cell vehicles. The energy management scheme consists of a real-time self-learning system, an average-reward filter based on the Markov chain Monte Carlo sampling, and an action selector system through the rollout algorithm with convex programming based policy. The performance evaluation of the energy management strategy is conducted via simulation studies using data obtained from real-world driving experiments and its performance is compared with three benchmark schemes.

To increase the applicability of the energy management system to various driving scenarios and multiple drivers, we propose an energy management scheme in fuel cell vehicle systems. The energy management problem is cast in the form of a nonlinear infinite-time optimisation problem. A model-based fuzzy control method is employed to design the control law. By linear matrix inequality approach, sufficient conditions are proposed to design the control strategy such that the energy system is robustly stable with a desired mixed H_2/H_∞ performance. The effectiveness and potential of the new design technique developed are demonstrated by different real-world driving scenarios.

By using optimal control principle, we further improve the energy management system performance in terms of reducing hydrogen consumption while maintaining the battery state of charge under practical operating constraints and uncertain future power demand. The fuzzy modelling approach is employed to describe the nonlinear power plant and a robust model predictive based control is designed to achieve the desired system performance. Moreover, traffic condition is incorporated into the energy management controller design to further improve the system performance. The effectiveness and advantages of the proposed control scheme are illustrated by a simulator developed based on real-world experimental data.

Finally, we investigate the problem of controlling energy flow in fuel cell vehicles by considering system stability, optimality, and durability. The energy management problem is transformed into a nonlinear optimisation problem with multi-objectives to improve fuel economy, maintain battery state of charge, and reduce the incidence of factors affecting the fuel cell performance degradation. A robust model-predictive-based fuzzy control method is employed to design the nonlinear control law. The energy management system is capable of coordinating with a fuel cell stack state of health estimator and an energy storage system scheduler to achieve the optimisation objectives in the presence of uncertainty of the driver's power demand. The effectiveness of the new design technique developed is demonstrated by conducting studies on control performance over typical urban/highway driving scenarios.

Statement of Originality

I certify that this work contains no material which has been accepted for the award of any other degree or diploma in my name, in any university or other tertiary institution and, to the best of my knowledge and belief, contains no material previously published or written by another person, except where due reference has been made in the text. In addition, I certify that no part of this work will, in the future, be used in a submission in my name, for any other degree or diploma in any university or other tertiary institution without the prior approval of the University of Adelaide and where applicable, any partner institution responsible for the joint-award of this degree.

I acknowledge that copyright of published works contained within this thesis resides with the copyright holder(s) of those works.

I also give permission for the digital version of my thesis to be made available on the web, via the University's digital research repository, the Library Search and also through web search engines, unless permission has been granted by the University to restrict access for a period of time.

Signed: .... Date: 10/22/2020 .....

Acknowledgements

I wish to express my sincere appreciation to my PhD supervisors, Professors Cheng-Chew Lim and Peng Shi, for their support, guidance and encouragement during the past four years of my study. Professor Lim shares insightful suggestions about the research. I am also very grateful to his scientific advice and knowledge and many valuable comments. He always provides insightful discussions for getting my science questions answered and helping me polishing my research writing skills. I would also like to extend my deepest gratitude to Professor Shi for his care, guidance, and constant support to my study. He always provides valuable suggestions when I met difficulties in my work, and encourages me to apply theoretic results to practical applications. Without their persistent support and advice, this project would not have achieved its goals.

I greatly appreciate the support received from the School of Electrical and Electronic Engineering at The University of Adelaide. The world-class research facilities and laboratory in the school have helped me a lot during my study. I also would like to acknowledge Mr Danny Di Giacomo who provides helpful support on the laboratory facilities and Mr Muhammad Saeed Aslam who gives constructive criticism of the thesis.

I am also deeply indebted to my former colleague Dr Piotr Bujlo. He provided the experimental data used in my first work and gave useful comments on the experiments design and results discussion. My thanks also go out to the support I received from our System & Control research group. The helpful research discussion and suggestions extended a great amount of assistance on the project.

Last but not least, my heartfelt thanks to my family, friends and partner for their continued love, support and encouragement.

Di Shen
Aug 2020
Adelaide, SA, Australia

Publications

Journal publications

DI SHEN, CHENG-CHEW LIM, PENG SHI, PIOTR BUJLO (2018). Energy management of fuel cell hybrid vehicle based on partially observable Markov decision process, *IEEE Transactions on Control Systems Technology*, **28**(2), pp. 318–330.

DI SHEN, CHENG-CHEW LIM, PENG SHI (2020). Robust fuzzy model predictive control for energy management systems in fuel cell vehicles, *Control Engineering Practice*, **98**, pp. 104364.

DI SHEN, CHENG-CHEW LIM, PENG SHI (2020). Fuzzy model based energy management system design for fuel cell vehicles, *IEEE Transactions on Vehicular Technology*, minor revision.

Conference publication

DI SHEN, CHENG-CHEW LIM, PENG SHI (2019). Predictive modeling for energy control in hybrid electric vehicle systems, *International Conference on Machine Learning and Cybernetics (ICMLC)*, **2019-July**, pp. 18–20 (Lotfi Zadeh Best Paper Awards).

List of Figures

List of Tables

Chapter 1

Introduction

ENERGY management system is a core technology for the electrification of traditional internal combustion engine vehicles. Fuel cells receive growing attention from the industrial and academic community as promising alternative energy systems for environment-friendly transportation applications. This introductory chapter offers a brief background of fuel cell vehicles, research problems of the energy management system design, motivations and contributions of the thesis, and the thesis outline.

1.1 Fuel cell vehicle introduction

In recent years, the energy efficiency of traditional vehicles has been markedly improved. Dependence on fossil fuels and pollution is significant shortcomings of traditional vehicles. One solution is the electrification of internal combustion engine vehicles.

In the automotive market, there is considerable interest in developing advanced electrified vehicles, including battery electric vehicles (BEVs), hybrid electric vehicles (HEVs) and fuel cell vehicles (FCVs) (Kasimalla and Velisala 2018, Axsen and Kurani 2013). They share similar vehicle control technologies but differ in the energy sources used to propel the vehicle.

Battery electric vehicles use an electric motor for traction, and batteries as the sole energy source to power the vehicle. battery electric vehicles offer many advantages over traditional internal combustion engines vehicles (ICEVs), such as zero emissions, high efficiency, independence on fossil fuels (Yan *et al.* 2006). However, they suffer from limited driving mileage and require long battery charging time.

Hybrid electric vehicles propulsion systems are equipped with two energy sources, the engine with a chemical fuel in liquid or gaseous form, and a rechargeable energy storage system (typically batteries or supercapacitors) that can serve as an energy storage buffer and recover vehicle kinetic energy during vehicle braking (Onori *et al.* 2016, Krithika and Subramani 2018). Hybrid electric vehicles offer longer driving mileage and greatly lower emissions compared to internal combustion engines vehicles but fossil fuel dependence and pollution from the engine are critical concerns.

Enhancing fuel economy with alternate fuel has led to usage of fuel cells as advanced power sources for transportation (Daud *et al.* 2017, Ehsani *et al.* 2018, Burke 2007). Fuel cells are efficient and cleanly convert the chemical energy to electric energy with high efficiency and much significantly lower greenhouse-gas emission as compared to traditional internal combustion engines (Wang and Jiang 2017). To improve the dynamics response and durability of fuel cell systems, hybridization of fuel cells with energy storage systems such as lithium-ion batteries or supercapacitors is necessary (Motapon *et al.* 2013).

Fig. 1.1 shows the basic layout of a typical a fuel cell drive train. Its propulsion system comprises a fuel cell stack and an energy storage system to drive the vehicle. Thus,

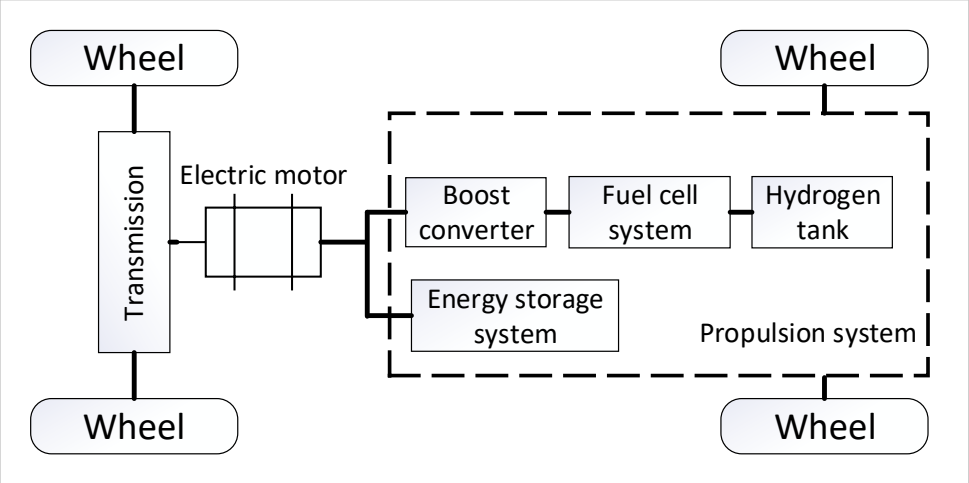

Figure 1.1. Basic configuration of a typical a fuel cell drive train

this kind of propulsion system combines the advantages of BEVs and HEVs and offers efficient, pollution-free and long range driving experience.

1.2 Research problems

In an FCV, an effective energy management system is vital to the system since it determines the distribution of power from the fuel cell system and energy storage system at each instant in the vehicle while meeting several constraints (Sulaiman *et al.* 2018, Hrovat *et al.* 2012).

Fuel cell systems use hydrogen and oxygen to generate electricity and emit only water. Consequently, they receive growing attention from the industrial and academic community as a promising alternative energy system for environment-friendly applications. Those promising converters, however, suffer from a limited lifespan due to performance degradation that impedes their widespread deployment.

The first research problem is how to reduce the negative factors caused fuel cell performance degradation during driving. The power demand during driving is determined by the driver's driving behaviour. In practice, predicting a human's behaviours is always a challenge.

Second, as a transportation application, how to minimise the fuel (hydrogen) consumption and maintain the battery SoC within the admissible range under practical operating constraints and uncertain future power demand?

Third, how to design a real-time energy management system to respond instantaneously to the power demand ?

Designing an effective energy management system to address the three energy management problems in the primary objective in this research work.

1.3 Motivation

The main practical challenge of the prediction-based energy management system design in FCVs is that the control system may perform poorly when the future power demand is not well described by the predictive model. From an energy point of view, the power demand is determined by the driver's driving behavior. In real-world driving scenarios, drivers have quite different driving behaviors. It is challenging to predict human's behavior even if the driving conditions are given.. Finding an efficient and effective way to design a universal energy management system for all driving conditions without explicit prediction of future power demand has been the first motivation of this research.

The energy management system design for traditional hybrid vehicles is well-developed. Nevertheless, the new requirements render the approaches not easy to be implemented in fuel cell vehicles since we should consider the dynamic performance of the fuel cell systems, and the efficiency of auxiliary devices, such as the boost converter, in fuel cell vehicles. Overcoming the shortcoming of the method compatibility and the model accuracy in traditional hybrid vehicle based energy management system has been the second motivation of this research.

Developing an effective real-time energy management controller to reduce the incidence of factors affecting the fuel cell performance degradation while improving system optimality has been the third task in the energy management system design for fuel cell vehicles.

1.4 Summary of contributions

This thesis offers the following contributions:

- A novel technique to solve the energy management problem for fuel cell vehicles under a partially observable Markov decision process framework is proposed, which decouples the dependency between the system closed-loop performance and the model accuracy for predicting the future power demand in the energy management design.

- A novel control law is developed by considering system stability, system optimality for charge-sustaining fuel cell vehicles and a fuzzy-model based energy management controller capable of providing H_∞ control performance for the charge sustenance of the battery pack and H_2 control performance for reducing the total fuel consumption over various driving scenarios.

- A robust fuzzy model predictive based control scheme with the T-S fuzzy modelling framework that optimises the power distribution in fuel cell vehicles while maintaining battery charge-sustaining in the presence of disturbance, a theoretical analysis for stability, robustness and performance that is applicable to the energy management system design in fuel cell vehicles, and an improved robust fuzzy model predictive control by incorporating traffic condition for further improving the system performance in terms of fuel consumption.

- Finally, a reformulated T-S fuzzy modelling framework is proposed to transform the energy management system for fuel cell vehicles into a nonlinear control law, which allows to concurrently take battery state of charge sustenance, fuel cell stack durability and vehicle fuel economy into account in the energy management system design and a novel fuzzy robust-model-predictive based energy management controller is developed, which ensures Lyapunov stability of the vehicle power system for all driving conditions and offers the compatibility with the state estimation and dynamic optimization.

1.5 Thesis outline

The thesis is organised as follows.

Chapter 2 gives a literature review of the energy management system design for fuel cell vehicles. Firstly, the historical background of the development of the fuel

cell vehicles is presented. Then, the chapter overviews the energy management system design for fuel cell vehicles in the literature.

Chapter 3 presents an energy management system for fuel cell vehicles under partially observable Markov decision process where a Markov chain Monte Carlo sampling-based approximator is developed to predict long term average power demand and the energy management problem is then solved by convex programming. Since the predictive model of the future power demand is not required in the energy management strategy, the dependency between the system closed-loop performance and the model accuracy for predicting the future power demand is decoupled in the energy management design.

Chapter 4 provides a mixed H_2/H_∞ control based energy management system for fuel cell vehicles to increase the system's applicability over various driving scenarios. The energy management problem is cast in a mixed H_2/H_∞ framework in which H_2 control improves the fuel economy to achieve optimal performance and H_∞ control maintains battery charge sustainability in the presence of system uncertainty and disturbance to achieve robustness specifications.

Chapter 5 proposes a robust model predictive based control scheme under a fuzzy modelling framework to design the energy management system for fuel cell vehicles. The fuzzy modelling approach is employed to describe the nonlinear energy system and a robust model predictive based control is designed to achieve the desired system performance. By using receding horizon control principle, the available driving information is leveraged in the energy management system design to reduce fuel consumption.

Chapter 6 incorporates the fuel cell system optimisation into the energy management system design. The energy management system consists of a fuel cell stack state of health estimator, an energy management system scheduler, and an energy management controller. The energy management problem is transformed to a nonlinear optimization problem with multi-objectives to improve fuel economy, maintain battery state of charge, reduce deterioration in fuel cell performance and the fuzzy robust model predictive control is employed to design the energy management controller.

Chapter 7 concludes this study and discusses some directions for future research to achieve optimal system performance in terms of fuel economy and energy system durability.

Chapter 2

Literature Review

THIS chapter provides a brief review of the historical background of the fuel cell vehicle development and literature review of the energy management system design for fuel-cell electric vehicles.

2.1 Introduction

Owing to increased public awareness of environmental and energy crisis concerns, vehicle manufacturers are turning to the electrification of traditional internal combustion engine vehicles in an effort to reduce greenhouse gas emissions, embrace alternative energy and increase energy system efficiency. Fuel cells have been attracting significant attention as a potential alternative to the combustion engine for the absence of CO_2 emissions during vehicle operation.

Besides this, compared with battery-powered electric vehicles, fuel cell vehicles promise benefits for drivers/owners among multiple dimensions (Rücker 2020):

- Quick charging time. Less than five minutes (like for internal combustion engine engines) will be needed to refill the tank compared to the longer duration expected to recharge battery-powered electric vehicles.
- Longer driving range. With more than 450km of driving allowance, fuel cell vehicles are already commercially attractive and, on average, they support larger ranges than battery-powered electric vehicles.
- Applicability of various driving condition. The range of fuel cell vehicles does not deteriorate in cold weather.

This chapter presents a short review of the historical background of the fuel cell vehicle development in Section 2.2 and the literature review of the energy management system design for fuel cell vehicles in Section 2.3.

2.2 Fuel cell vehicle development

The concept of using fuel cells to generate electricity was first invented in 1839 by Sir William Grove, a Welsh physicist (Andújar and Segura 2009). The first notable commercial fuel cell application was developed a century later in the early 1960s. NASA's Gemini spacecraft uses fuel cells to provide electrical power during manned space missions (Cook 2002, Burke 2003). In 1966, General Motors tested the Electrovan, the world's first hydrogen-powered fuel cell vehicle (Rodrigues *et al.* 2010). The vehicle provides a range of 120 miles and 70 mph maximum speed.

Table 2.1. List of the latest fuel cell vehicles commercially produced

FCV model	Vehicle Power (ps)	FCS power (kW)	Range (km)	Battery capacity (kWh)
Toyota Mirai 2019	151	114	502	1.6
Hyundi NEXO 2019	163	95	611	1.56
Honda Clarity 2020	174	103	580	-
Mercedes-Benz GLC F-CELL 2019	217	-	478	13.5
Audi A7 Quattro	220	-	500	8.8

Although fuel cell applications were still limited to the aerospace industry in the 1970s-1980s, the 1970s oil crisis brought significant research into hydrogen fuel cells. By 1990s, many car manufacturers, such as Daimler Chrysler, General Motors, Hyundai, and Toyota, had demonstrated their fuel cell vehicle prototypes. In the 2000s, commercial fuel cell vehicles began to appear in the automotive leasing market. Some examples are: Honda(FCX-V4,2002-2007), Ford (Focus FCV, 2003-2006), Chevrolet (Equinox FC, 2007-2009), Mercedes-Benz (F-Cell 2007-2009).

With the rapid iteration of the fuel cell system, energy storage system and other improvements, substantial progress has been made in fuel cell vehicle development in the last decade. Table 2.1 summarises the latest fuel cell vehicle models in the market (Yoshida and Kojima 2015, Nassif and de Almeida 2020, Tanaka *et al.* 2020, Kurtz *et al.* 2019).

Although fuel cell vehicles reach the first stage of commercialisation with more than 6500 on the road in the US for a wide array of transportation purposes in 2019 (Thompson and Papageorgopoulos 2019), research and development in the area of energy system performance and durability in fuel cell vehicles remain a top priority (Borup *et al.* 2020).

2.3 Energy management system design

Energy management systems are the brain of the fuel cell vehicles since it regulates the power flow between the fuel cell stack and energy storage system. Developing a new generation of fuel cell vehicle energy management system to reduce the fuel consumption, optimise the durability of the fuel cell stack, and improve vehicle performance remains the primary task of scientific research (Teng *et al.* 2020).

In the energy management system design for FCVs, there are two main categories proposed to address the energy management problem, that is, heuristic-based and optimisation-based control techniques.

Heuristic-based control techniques, such as equivalent consumption minimisation strategy (ECMS) (Paganelli *et al.* 2002, Yu *et al.* 2011) and fuzzy logic (Tekin *et al.* 2007, Zandi *et al.* 2010, Martinez *et al.* 2011), decompose the task of control design into a group of local tasks and solve optimization the problem in real-time. As model-free based control techniques, the control schemes are simple and straightforward and easy for implementation. These techniques are suitable in a real application, but one major shortcoming is that the optimality can only be guaranteed in few driving cycles since the fuzzy rules or factors must be chosen in advance.

The optimisation-based control techniques are based on minimising/maximising a cost function over a finite predictive horizon (Lewis *et al.* 2012, Sethi and Thompson 2000). Commonly used optimization methods, such as convex programming and dynamic programming, have been implemented to achieve optimality. For example, in (Ansarey *et al.* 2014), multi-dimensional dynamic programming is adopted to address the energy management problem in fuel cell vehicles. In (Chen *et al.* 2013), dynamic programming with two neural network modules is proposed to design the energy management system for hybrid vehicles. In (Hu *et al.* 2013, Elbert *et al.* 2014, Nüesch *et al.* 2014), the energy management problem is cast into a convex form and solved by convex programming. Those primary shortcomings of the EMSs based on those methods required prior information of the future power demand and heavy computational burden, thus they are challenging to apply in a real vehicle.

Finding an energy management controller to overcome the limitations of the above techniques has been one major motivation in the EMS design for FCVs.

To tackle the problem, adaptive and stochastic features are incorporated into the energy management system design for FCVs, with an aim to improve fuel economy by leveraging available driving information while maintaining battery charge in an admissible range.

A widely used strategy is the adaptive optimal supervisory control technique. It is based on heuristic-based control techniques, such as fuzzy logic, Pontryagin's Minimum Principle(PMP) and ECMS. The main improvement of the control technique is that the co-state/fuzzy-rules is estimated online as driving scenarios vary, which is

called co-state adaptation (Nguyen *et al.* 2018, Li *et al.* 2019). For example, in (Musardo *et al.* 2005, Sun *et al.* 2017), adaptive ECMS based EMSs are proposed in which the equivalence factor is updated online based on the driving condition. In (Ou *et al.* 2018, Onori and Tribioli 2015), the adaptive-PMP based energy manage management strategy is developed to minimise the fuel consumption and maintain the battery charge level in hybrid vehicles. In (Chen *et al.* 2016, Yin *et al.* 2016), the adaptive fuzzy logic control strategy is proposed to adjust the fuzzy system membership function online for improving the system applicability.

Future information of the driving power demand is not readily exploited by traditional optimal control strategies, but model predictive control (MPC) appears to be one suitable control technique for this purpose. The idea behind MPC is to formulate the optimal control problem over a finite time-interval and repeatedly optimise a control sequence over a receding horizon by predicting future system behaviour (Shen *et al.* 2020b, Zhang *et al.* 2017, Golchoubian and Azad 2017, Huang *et al.* 2017). For instance, in (Cairano *et al.* 2014), a stochastic model predictive control is adopted to design an EMS for FCVs. The power demand is represented by a Markov-chain based predictive model; then the optimisation problem is solved online in a stochastic finite horizon with stability constraints. In (Wang *et al.* 2016), a model predictive based control is proposed to solve the energy management problem in a hybrid electric tracked bulldozer. In (Zeng and Wang 2015), the authors proposed a stochastic MPC based EMS using the prediction of the vehicle location, travelling direction, and terrain information.

Another recent approach is to use control Lyapunov functions to design energy management control laws. Unlike the prediction-based approach, control-Lyapunov based approach focuses on system stability and treats the vehicle power request as a disturbance to the power system (Shen *et al.* 2020a). In (Mura *et al.* 2015, Sampathnarayanan *et al.* 2014), the energy management problem is cast in the form of a nonlinear optimal regulation (with disturbance rejection) problem (Haddad and Chellaboina 2011), and a control Lyapunov function is used to design the control law. In (Song *et al.* 2017), a Lyapunov function based sliding-mode controller is proposed to regulate the power flow in electric vehicles. In (Zhang *et al.* 2019), a control-Lyapunov based nonlinear control is proposed for regulating the power flow between the fuel cell stack and the Li-ion battery in fuel cell vehicles.

Owing to increased public awareness of environmental and energy crisis concerns, fuel-cell based electrochemical converters receive growing attention from the industrial and scientific community as a promising internal combustion engine substitute for environment-friendly transportation applications. Unlike conventional internal combustion engine, fuel cell system dynamics brings model uncertainty to the system and impacts on the control performance of the EMS. The dynamic behavior of the fuel cell is affected by the operating condition of the stack, such as inlet pressure, humidity, temperature, fuel stoichiometry and load variation (Mueller *et al.* 2007, Yan *et al.* 2006). The results shown in (Wu *et al.* 2017) shows that up to 5% fuel economy improvement on New York city cycle by incorporating fuel cell dynamics in the EMS design. This is an indication of the effects of fuel cell dynamics on energy management design in FCVs. Moreover, those promising converters suffer from a limited lifespan due to performance degradation that impede their widespread deployment (Mueller *et al.* 2007, Yan *et al.* 2006, Bressel *et al.* 2016). Prolonging fuel cell life is another important consideration when designing the EMS (Wang *et al.* 2019, Liu *et al.* 2019).

Developing an EMS considering fuel cell system optimisation is generally formulated as a multi-objective problem. The objectives of the EMS consist of is not only improving fuel economy and maintaining battery charge level but also prolonging the system lifespan (Yue *et al.* 2019). Because these objectives are often conflicting, a compromise needs to be taken with trade-offs among the multiple objectives.

The fuel cell system optimisation has been considered in both heuristic-based and optimisation-based EMSs for FCVs in recent years.

Heuristic-based EMSs aim to find efficient operation points that reduce the energy system degradation in their local tasks/rules. For instance, in (Marx *et al.* 2017), a fuzzy logic based energy management strategy is proposed to reduce energy system degradation by using multi-stack fuel cell architecture where the fuzzy rules decide how many fuel cell stacks should be turned on and the corresponding output power level. However, the optimality of the system has not been discussed in the paper. In (Marx *et al.* 2017), a frequency split EMS has been proposed by using wavelet transforms. Since the frequencies of the attributed signals are in the range of admissible frequencies, the fuel cell system and battery pack can operate in their health modes. However, the autoregressive integrated moving average model used in the method requires expert knowledge and cannot be generalised.

Optimisation-based EMSs usually take the energy system degradation factor into account in their cost functions or set several constraints into the control actions to reduce the energy system degradation. In (García-Triviño *et al.* 2016), a multi-objective optimisation problem is formulated by combining energy system operational cost, efficiency and lifetime. The optimisation problem is then solved by particle swarm optimisation method where three objectives were integrated into a single cost function through weight aggregation approach. In (Arce *et al.* 2009), model predictive control is proposed for the energy management system design where fuel cell system degradation is limited by setting the threshold of fuel cell output power and reduce its start-ups and shut-downs frequency. However, the various operation conditions and heavy computational burden impede their widespread deployment in real-time implementation.

2.4 Chapter summary

This chapter introduces the historical background of fuel cell vehicle development and energy management system design for fuel cell vehicles in the literature. Two main categories, heuristic-based control techniques and optimisation-based control techniques, that proposed to address the energy management problem are given, as well as the fuel cell system optimisation in the energy management system development.

The next chapter will present our first energy management system design under a partially observable Markov decision process framework for fuel cell vehicles. Based on this control scheme, the dependency between the system closed-loop performance and the predictive model accuracy can be decoupled.

Chapter 3

Energy Management System Design under POMDP Framework

THE main problem of previous predictive based energy management systems is that the closed-loop performance of the control system is highly dependent on the predictive model. In this chapter, we propose a novel energy management system for fuel cell vehicles, an average-reward approximator under a partially observable Markov decision process framework to improve system optimality in terms of fuel consumption and battery charge-sustaining. A vector of random variables describing the long-term average power demand to be the unobservable state. A Markov chain Monte Carlo sampling method based average-reward filter is developed, along with observations, to determine the posterior distribution of the unobservable state. Then an optimal action is selected by convex programming based on a long-term average cost. The simulation result shows that the proposed energy management system provides 8% - 12% improvement compared with a standard charge-depleting charge-sustaining energy management system in terms of fuel consumption over five real-world driving experiments.

3.1 Introduction

The power demand in fuel cell vehicles is determined by a driver's driving behavior. In real-world driving conditions, it is a challenge to predict specific future human's behavior in a receding horizon even if the driving route is known in advance. To better understand this issue, we conducted a real-world driving experiment and collected the raw data of the power demand from a golf cart prototype in a four-lap (fixed route) driving experiment on a campus with the same driver at a weekend (few students on the campus). Fig. 3.1 shows the power demand in the four-lap driving experiment. In the experiment environment, we assume that the driving conditions in the four laps are almost the same. As observed from the plots, the driver performed different driving behavior in four laps. It is clear that even when the environment of driving is almost the same, the power demand is difficult to predict.

In order to deal with the problem of the coupling between the closed-loop performance and the model predictive accuracy, we propose a novel technique to solve the energy management problem for fuel cell vehicles. The action selector is based not on a predictive model forecasting the future power demand, but on an average-reward distribution representing the long-term average power demand. Given the measurements of the driver's performance in a driving route, we determine the average-reward distribution using an average-filtering method under a partially observable Markov decision process (POMDP) framework.

This chapter is organised as follows. Section 3.2 describes the energy management problem of a fuel cell hybrid vehicle. Section 3.3 explains the design of the new EMS for HEVs, where the control problem is solved under a POMDP based framework, and an average-reward filter is designed. In Section 3.4, the proposed energy management system is implemented in a vehicle simulator based on real-world driving experiments, and the results are evaluated against three benchmark solutions.

3.2 Problem formulation

This work relates to controlling the energy flow from a fuel cell based hybrid vehicle in response to the real-time power demand during driving. For simplicity, the DC-DC converter efficiency η_{dc} and the auxiliaries power requirement P_a taken as constant average values.

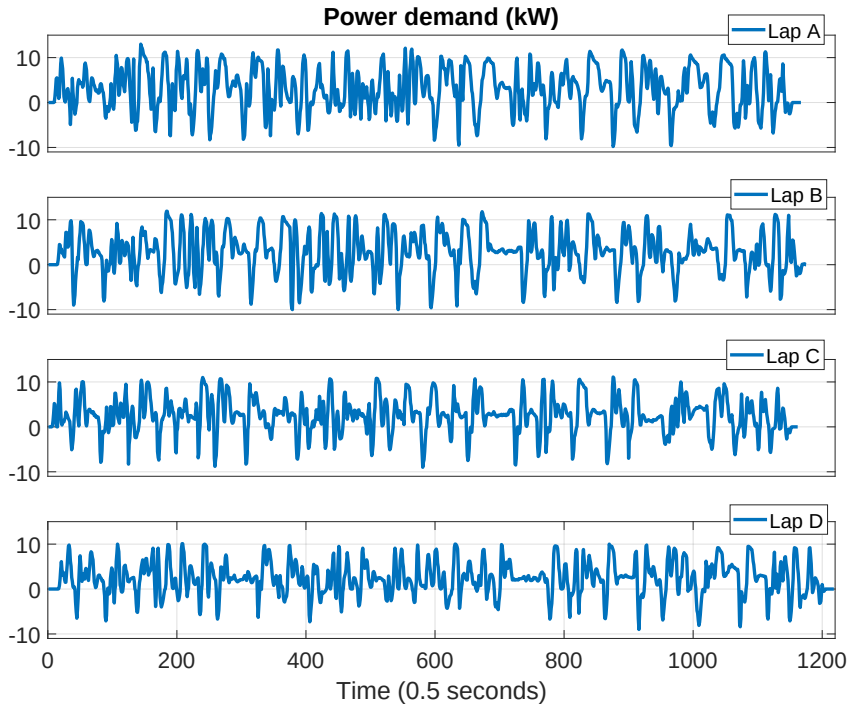

Figure 3.1. Power demand by the golf cart in a four-lap driving experiment on a campus

To formulate the EMS design problem, we first present the system dynamic model.

3.2.1 System energy flow

The vehicle model used in this chapter is a fuel cell hybrid golf cart prototype (Tolj *et al.* 2013). The electric motor is used as the propulsion system of the vehicle which is powered by hybrid power sources including a proton-exchange-membrane fuel cell system (PEMFCS) and a lithium-ion battery pack system. The DC-DC converter, which links the PEMFCS and the DC-BUS, plays the role of an actuator between the PEMFCS and the lithium-ion battery pack system to regulate the energy flow.

The total energy balancing equation in the system is

$$P_{fcs} + P_{bo} \geq P_{require} + P_a \tag{3.1}$$

$$P_{require} = P_v + P_{eloss} \tag{3.2}$$

where P_{fcs} is the output power (kW) from the PEMFCS, P_{bo} is the output power (kW) from the battery pack, $P_{require}$ is the power demand (kW) by the electric motor, P_a is the

power consumption of the auxiliary systems, P_v is the power demand (kW) from the vehicle, and P_{eloss} is the electric motor internal power loss (kW).

Combining (3.1) and (3.2) yields the system energy flow

$$P_{fcs} - P_{dcdc} + P_{bo} - P_a - P_{eloss} \geq P_v \tag{3.3}$$

where P_{dcdc} denotes the output power (kW) from the DC-DC converter. The left hand side of (3.3) represents the power provided by the power sources, and the right hand side of (3.3) represents the power demand from the vehicle.

The function of an EMS is to regulate the energy flow from P_{fcs} and P_{bo} via the DC-DC converter such that the energy flow meets the power demand $P_{require}$ and minimises certain cost function J, such as the fuel consumption. Fig. 3.2 shows the schematic diagram of the fuel cell hybrid vehicle.

3.2.2 System modelling and convexification

This section describes the system model corresponding to the energy flow in (3.3) and formulates the multiple energy flow control problem under a convex optimisation framework.

The convexification of power sources found in (Hu *et al.* 2015, Egardt *et al.* 2014, Murgovski *et al.* 2012) is adopted in our EMS design. The system model is as follows.

Power-demand P_v

We define the vehicle power-demand P_v as the output power from the electric motor to the drive wheel or the generated power from the drive wheel to the electric motor. P_v is obtained by

$$P_v = \frac{\tau \cdot \omega}{9.5488} \tag{3.4}$$

where τ is the motor output torque in N.m, and ω is the motor rotational speed in rpm. The calculation of τ and ω is based on the dynamic of the vehicle system. Fig. 3.3 shows a vehicle system. The forces experienced by the vehicle are modeled as,

$$F_t = F_w + F_f + F_i + F_a \tag{3.5}$$

where F_t denotes the driving force, F_w denotes the air resistance, F_f denotes the rolling resistance, F_i denotes the ramp resistance, and F_a denotes the acceleration resistance. These forces are obtained from

$$\begin{cases} F_t = \tau \cdot i_0 \cdot i_k \cdot \eta_r / R_{wheel} \\ F_w = \frac{1}{2} \cdot \rho \cdot C_{drag} \cdot A \cdot v(t)^2 \\ F_f = m \cdot g \cdot C_{rollR} \cdot \cos\alpha \\ F_i = m \cdot g \cdot \sin\alpha \\ F_a = \epsilon \cdot m \cdot \frac{dv(t)}{dt} \end{cases} \tag{3.6}$$

where i_0 and i_k are the transmission ratio, R_{wheel} is the vehicle wheel radius, m is the vehicle total mass, η_r denotes the transmission efficiency, ρ denotes the air density (kg/m^3), C_{drag} denotes the air resistance coefficient, $v(t)$ denotes the vehicle speed (m/s), g denotes the acceleration of gravity (m/s^2), α denotes the road slope angle (rad), C_{rollR} denotes the rolling resistance coefficient, A denotes the car frontal area (m^2), and ϵ denotes the rotating mass conversion factor.

Substituting (3.6) into (3.5) yields the expression for the motor output torque τ

$$\tau = \frac{R_{wheel} \cdot (F_w + F_f + F_i + F_a)}{i_0 \cdot i_k \cdot \eta_r} \tag{3.7}$$

The motor rotational speed ω is calculated from

$$\omega = 2.653 \cdot \frac{v(t) \cdot i_0 \cdot i_k}{R_{wheel}} \tag{3.8}$$

Substituting (3.7) and (3.8) into (3.4) gives the vehicle power-demand P_v. Accordingly, the following remark is obtained.

If all the model parameters of a specific vehicle are known in advance, the vehicle power-demand P_v is determined by the vehicle's velocity and the road information.

Power-supply P_s

The vehicle power-supply P_s is defined as the power provided by the power system to drive the vehicle and to overcome the power loss through the DC-DC converter and the electric motor. That is,

$$P_s = P_{fcs} + P_{bo} - P_a - P_{eloss} - P_{dcdc} \tag{3.9}$$

The convexification of the PEMFCS, the battery pack, and the electric motor in FCVs is presented as follows.

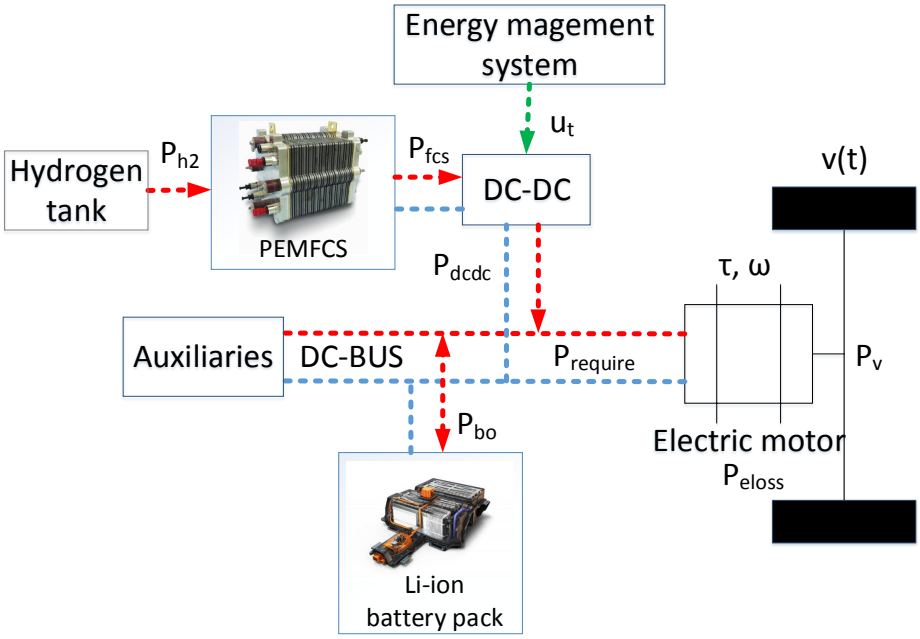

Figure 3.2. Schematic diagram of a fuel cell hybrid vehicle

Fuel cell system Fuel cell stack modeling is an indispensable tool for designing fuel-cell-powered systems. Numerous modeling techniques, from electrochemical-based to electrical-based, are used to develop fuel cell stack models (Springer *et al.* 1991, Corrêa *et al.* 2004). In this study, our focus is on the energy management design, and the fuel cell stack is assumed to operate at optimal conditions. Thus, using the relationship between input power P_{h_2} and output power P_{fcs} of a PEMFCS under optimal conditions is sufficient for our EMS design.

To analyse the convexification of a fuel cell system model, a 15kW PEMFCS from Ballard Power Systems FCvelocity ®-9SSL is used as the test model, and the experiment is performed on the Greenlight Innovation FCATS™-G500 stack testing station. When the fuel cell stack operates at optimum conditions and all recommendations and requirements specified in the product manual and integration guide from Ballard Power Systems (Inc. 2011) are met, the relationship between hydrogen input power P_{h_2} and output power of the PEMFCS P_{fcs} is described in Fig. 3.4. We observe that a quadratic function can be used to describe the relationship

$$P_{h_2}(t) \geq b_0 \cdot P_{fcs}^2(t) + b_1 \cdot P_{fcs}(t) + b_2 \tag{3.10}$$

where b_0, b_1 and b_2 are the constant fitting parameters in the model.

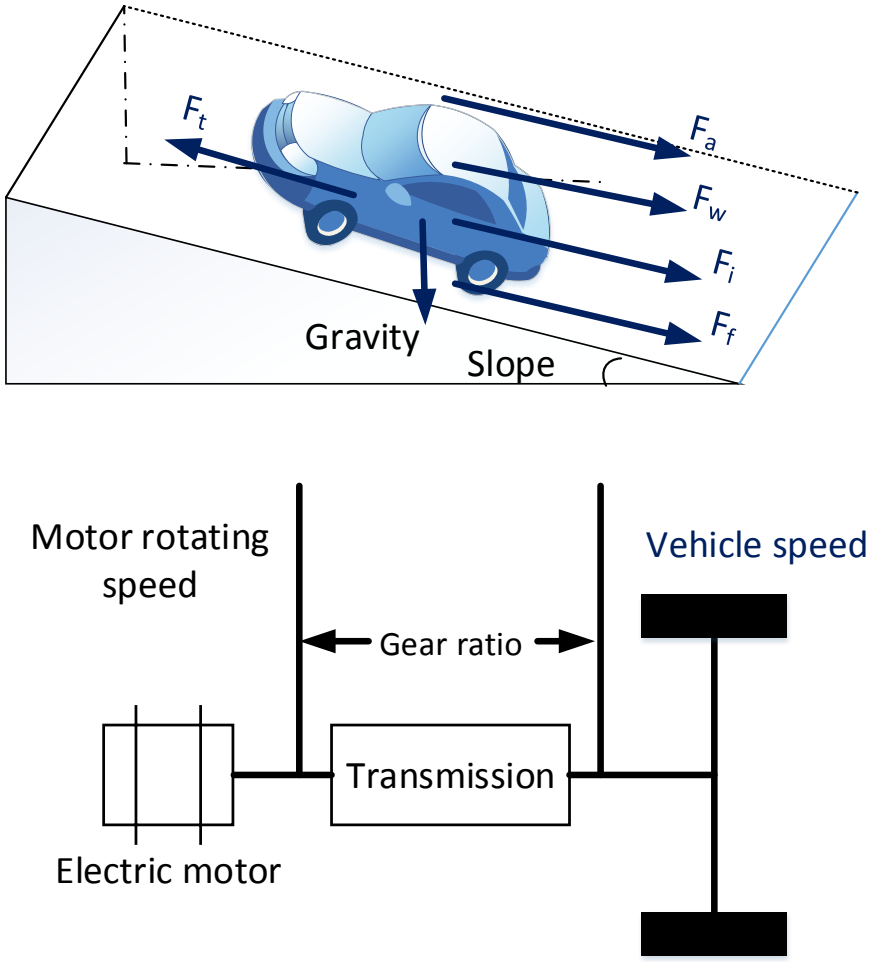

Figure 3.3. Schematic diagram of a vehicle system: a two-axle longitudinal vehicle model (top) and a transmission system (bottom)

Battery pack A battery cell can be modeled by an open-circuit voltage (OCV) u_{soc} in series with an internal resistance R.

$$P_{bin}(t) = u_{soc}(t) \cdot i(t) \tag{3.11}$$

$$P_{bloss}(t) = R \cdot i^2(t) \tag{3.12}$$

$$P_{bo}(t) = P_{bin}(t) - P_{bloss}(t) \tag{3.13}$$

where $i(t)$ is the instantaneous cell current (positive for discharge, negative for charge), P_{bin} denotes the cell internal power, and P_{bloss} denotes the cell internal power loss.

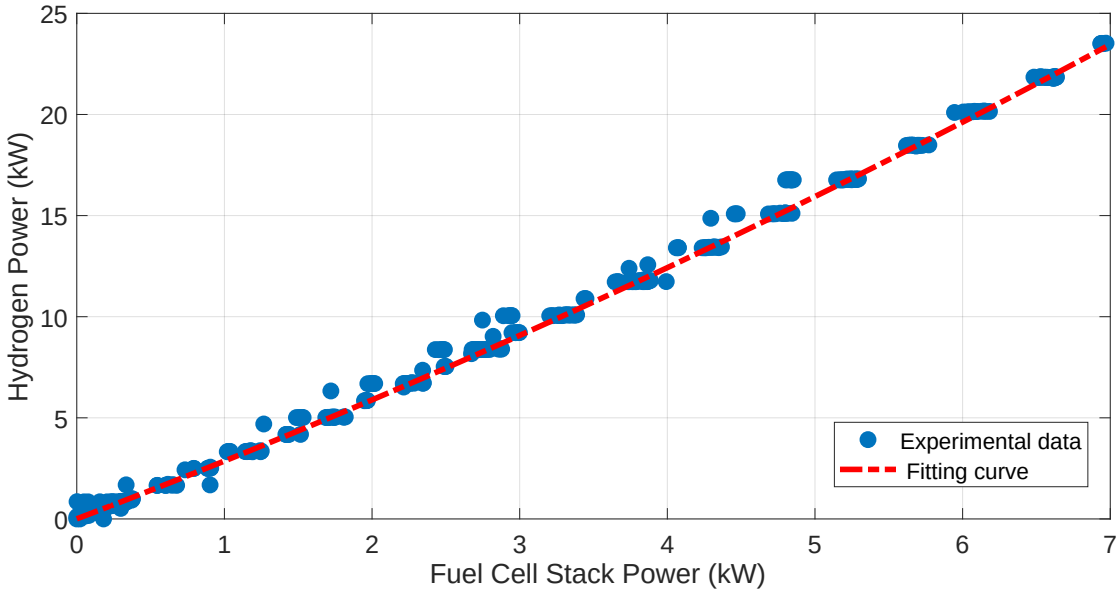

Figure 3.4. Relationship between fuel cell system output power and hydrogen power consumption

Substituting (3.11) and (3.12) into (3.13) yields

$$i(t) = \frac{1}{2R}\left(u_{soc}(t) - \sqrt{u_{soc}^2(t) - 4RP_{bo}(t)} \right) \tag{3.14}$$

$$i(t) \in [i_{min}, i_{max}] \tag{3.15}$$

$$P_{bo} \leq \frac{u_{soc}^2(t)}{4R} \tag{3.16}$$

where $[i_{min}, i_{max}]$ is the permissible range of current. The residual energy in a cell is defined by the state of charge (SoC), which is the ratio of the residual capacity to the nominal capacity of the cell, where the residual capacity is the number of ampere-hours that can be drawn from the battery at room temperature at the C/30 rate before it is fully discharged (Plett 2004).

A standard calculation of a cell's SoC is coulomb counting, that is, by measuring the battery current and integrating it in time. The model of the SoC is described and constrained by

$$SoC(t) = SoC(0) - \int_0^t \frac{\eta_b i(\zeta)}{C_n} d\zeta \tag{3.17}$$

$$SoC(t) \in [SoC_{min}, SoC_{max}] \tag{3.18}$$

where $SoC(0)$ is the cell's SoC at the initial time, $SoC(t)$ is the cell's SoC at time t, C_n is the cell's nominal capacitor, η_b is the cell's Faraday efficiency, and $[SoC_{min}, SoC_{max}]$ is the permissible range of the cell's SoC.

To analyse the convexification of a battery cell model, we use a 20Ah lithium-ion polymer battery for charge and discharge experiments on the Arbin Instruments BT2000 battery test station. The experimental results of the relationship between SoC and u_{soc} are shown in Fig. 3.5. The curve illustrates the non-linear characteristics of u_{soc} related to the cell SoC. It is clear that a typical battery cell model is non-convex.

To make the battery model convex, an energy concept ε_{soc} is introduced to replace SoC. With the total number of cells assumed to be γ,

$$\varepsilon_{soc} = \gamma \cdot \int_{0}^{SoC} u(\zeta) d(\zeta) \tag{3.19}$$

Furthermore, the range of the SoC is set to between 20% and 80%. Thus the relationship between OCV and SoC in a single battery cell is approximated (as shown in Fig. 3.5) by

$$u_{soc} = c_0 \cdot SoC + c_1 \tag{3.20}$$

where c_0 and c_1 are the fitting parameters of the model. Substituting (3.20) into (3.19) gives

$$\varepsilon_{soc} = \gamma \cdot (\frac{c_0}{2} \cdot SoC^2 + c_1 \cdot SoC) \tag{3.21}$$

Combining (3.11), (3.17), (3.19), (3.20) and (3.21), we have

$$\varepsilon_{soc} = \frac{\gamma}{2c_0} \cdot (u(soc)^2 - c_1^2) \tag{3.22}$$

$$\frac{d\varepsilon_{soc}}{dt} = \frac{d\varepsilon_{soc}}{dSoC} \cdot \frac{dSoC}{dt} = -\frac{P_{bin}(t)}{C_n} \tag{3.23}$$

Substituting (3.11) and (3.22) into (3.12), we have

$$P_{bloss}(t) = \frac{R \cdot P_{bin}(t)^2}{2c_0 \cdot \varepsilon_{soc} + \gamma \cdot c_1^2} \tag{3.24}$$

$$P_{bo}(t) = P_{bin}(t) - P_{bloss}(t) \tag{3.25}$$

As (3.24) is in quadratic-over-linear form, P_{bloss} has the required convexity property.

The constraints on P_{bloss} and ε_{soc} are

$$P_{bloss} \leq \gamma \cdot R \cdot i_{max}^2 \tag{3.26}$$

$$\varepsilon_{min} \leq \varepsilon_{soc} \leq \varepsilon_{max} \tag{3.27}$$

where $[\varepsilon_{min}, \varepsilon_{max}]$ is the available range of the battery pack.

Substituting (3.24) into (3.26) gives

$$P_{bin} \geq i_{min} \cdot \gamma \cdot \sqrt{\frac{2 \cdot c_0 \cdot \varepsilon_{soc}}{n} + c_1^2} \tag{3.28}$$

$$P_{bin} \leq i_{max} \cdot \gamma \cdot \sqrt{\frac{2 \cdot c_0 \cdot \varepsilon_{soc}}{n} + c_1^2} \tag{3.29}$$

Since the geometric mean is a concave function and $i_{min} \leq 0$, the inequalities provide the convexity property.

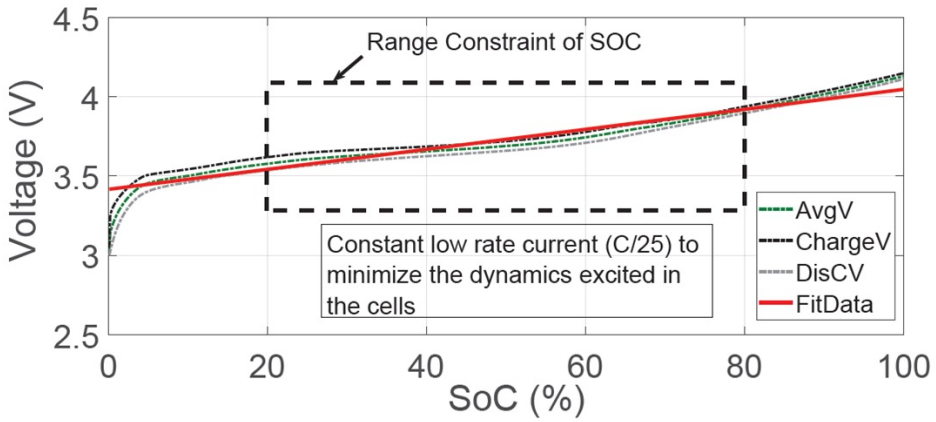

Figure 3.5. Relationship between OCV and SoC of the Lithium-ion polymer battery pack

3.2.3 Objective function for energy management system

The objective of an EMS in FCVs is to control the energy flow between multiple power sources that minimises a cost function while satisfying constraints from each component, such as maintaining battery charge, providing acceptable driving performance, and ensuring the durability of power sources.

To decouple the dependence on the accuracy of the predictive model, we adopt the following average-reward cost function

$$J = \lim_{t_h \to \infty} [\frac{1}{t_h} \int_{t_0}^{t_h} \dot{m}_f(u_t) dt] \tag{3.30}$$

where $\dot{m}_f$ is the instantaneous fuel flow rate, $[t_0, t_h]$ is the time horizon, and u_t is the control action which is selected by the EMS.

We are ready to state the problem addressed in this chapter. The energy management problem in a fuel cell hybrid vehicle is to design an EMS that regulates the energy flow between the fuel cell stack and the battery pack to minimise the long-term average cost (3.30), subject to meeting system dynamics (3.3) and (3.10), and constraints (3.25)-(3.29).

3.3 Energy management design for fuel cell vehicles

This section presents a novel EMS design method for an FCV based on an average-reward approximator to optimise the long-term average cost (3.30) under a POMDP framework by convex programming without forecasting future power demand.

First, we describe the following tuples in the POMDP used in this study.

- **Unobservable state** is the long-term average power demand described by a vector of random variables.
- **Action** is the output power from the fuel cell stack for regulating the energy flow via the DC-DC converter.
- **Measurements** (observations) are obtained from current velocity V_c, driver's driving behavior ρ_{avg} and road information α_{avg}.
- **Transition function** is approximated by an average-reward filter that updates the belief state. The filter includes a self-learning system which provides a recursive update mechanism on measurements, and an approximator, which is based on the MCMC sampling method to estimate the posterior distribution of the belief state.
- **Reward function** is represented by the long-term average cost function (3.30).

The POMDP-based EMS design framework is shown in Fig. 3.6.

We describe the belief state by a posterior average-reward distribution instead of a posterior probability distribution since we do not seek to forecast the future power demand. That is, the belief state in this study does not play the role of the predictive function of the future power demand but represents the power demand on average described by a vector of random variables. Given the measurements (V_c, ρ_{avg}, α_{avg}),

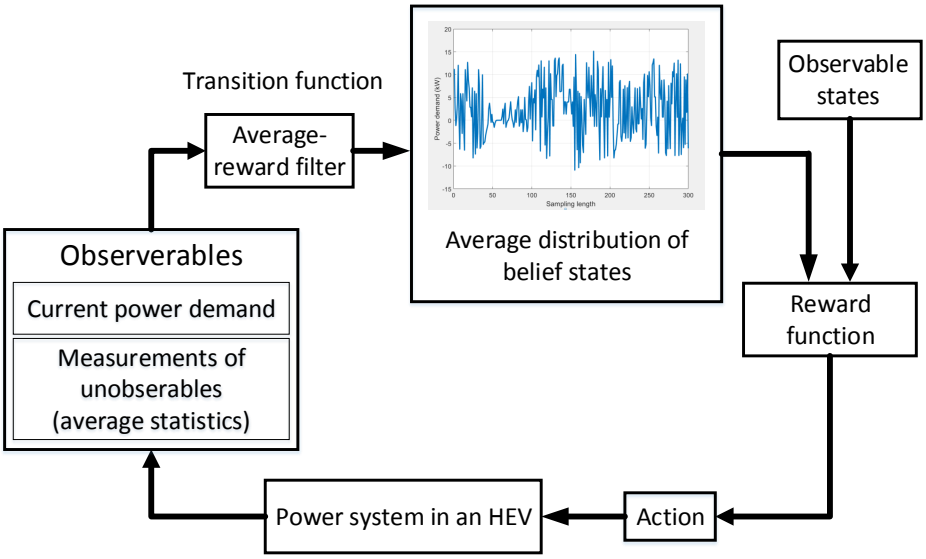

Figure 3.6. Block diagram of the POMDP for energy management strategy design

we determine the belief state using an average-filtering method. More specifically, we use the MCMC sampling method to calculate the posterior distribution.

The block diagram of the EMS is shown in Fig. 3.7. Presented below are the details of the EMS design.

3.3.1 Average-reward filter design

Cost function (3.30) is to minimise the long-term average cost. How to design an average-reward filter for optimisation is addressed here.

The average-reward filter comprises two subsystems: a self-learning system and an approximator.

Self-learning system

The self-learning system provides a recursive update mechanism on the observations. According to the law of large numbers, the average of the results obtained from a large number of trials should be close to the expected value when more tests are performed (Hsu and Robbins 1947). Thus, if the measurements (V_c, ρ_{avg}, α_{avg}) is updated recursively, the value finally converges to the real average driving performance.

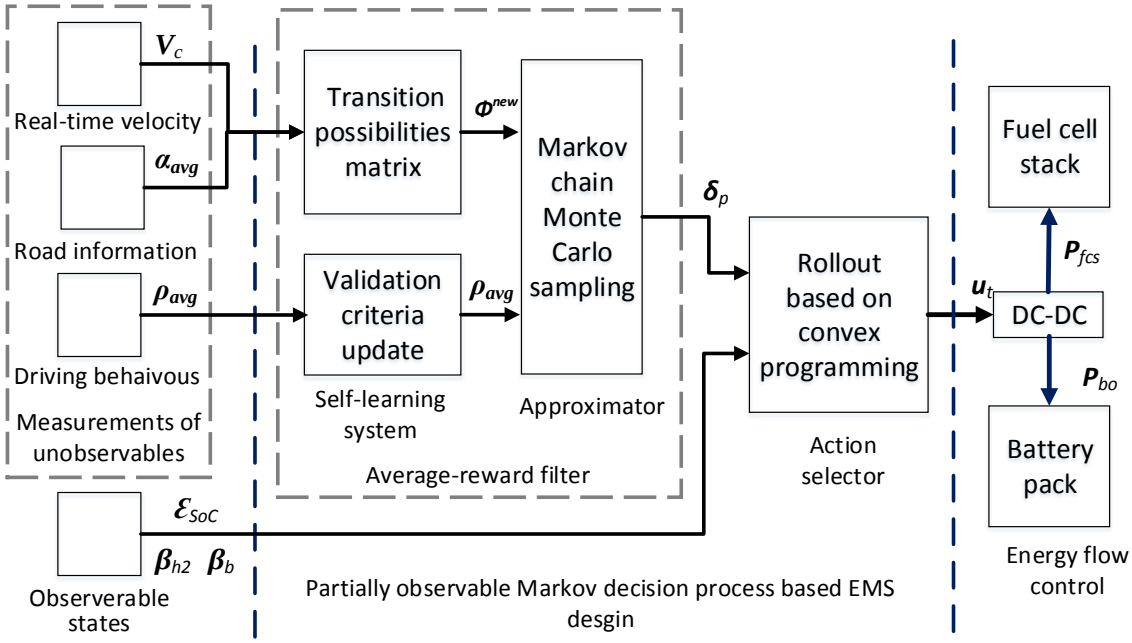

Figure 3.7. Block diagram of the POMDP based power control unit

We present the recursive update mechanism of each measurement as follows.

Real-time velocity V_c All the vehicle velocity values are segmented into discrete velocity classes of a 1 km/h bin width

$$\boldsymbol{V} = \left[\underbrace{[0 \leq V_c \leq 1]}_{\boldsymbol{V}_1}, \underbrace{[1 \leq V_c \leq 2]}_{\boldsymbol{V}_2}, ..., \underbrace{[(v_{max} - 1) \leq V_c \leq v_{max}]}_{\boldsymbol{V}_n} \right] \tag{3.31}$$

where v_{max} is the maximum value of the vehicle velocity.

Then, we define the transition probability matrix (TPM) based on the kth-order Markov chain $\boldsymbol{\Phi}$,

$$\boldsymbol{\Phi} = \begin{matrix} \boldsymbol{V}_1, \boldsymbol{V}_2, ..., \boldsymbol{V}_n \\ \left[\begin{array}{c} \text{Update} \\ \text{from real-time} \\ \text{vehicle velocity} \end{array} \right] \end{matrix} \begin{matrix} \\ \kappa_1 \\ \kappa_2 \\ \vdots \\ \kappa_i \end{matrix}$$

where $\boldsymbol{\kappa}_i$ is defined as the velocities in previous k time steps and arranged in lexicographic order.

When a new V_c is observed, its location in $\boldsymbol{\Phi}$ is identified, and the probability distribution in that row is updated.

Road information α_{avg} From Section 3.2.2, we know that the vehicle velocity and the road information are the two main factors that affect the vehicle power-demand P_v. Although we do not need to predict the specific future power demand in our EMS design, a more accurate average-reward approximator could be achieved by using the road information. One way to represent both the vehicle velocity and the road information is to build a 2-D Markov transition probability matrix. In the 2-D case, $\boldsymbol{\Phi}$ is defined by two states: $v(t)$ and $\alpha(t)$, where $\alpha(t)$ belongs to the discrete observation space for the road information Ω. Therefore, $\boldsymbol{\Phi}$ is the transition probability from the velocity and the road information in previous k time steps to velocity class V_j and road information class Ω_j in the next time step. Note that this 2-D matrix was introduced and analysed in (Lee *et al.* 2011) and (Silvas *et al.* 2016).

In practice, as the dimensionality of the matrix increases, the amount of data grows exponentially with the dimensionality. To contain the dimensionality problem, we use the average value of the road information in our EMS design. The use of average values is compatibly with the use of the long-term average cost function in the reward function.

Driving behavior Let ρ_{avg} denote the driving behaviors. We define ρ_{avg} based on the following eight validation criteria

$$\rho_{avg} = [v_{mean}, v_{std}, ac_{mean}, de_{mean}, ac_{std}, de_{std}, ac_{perc}, de_{perc}]$$

where v_{mean} is the average velocity, v_{std} is the average standard deviation velocity, ac_{mean} is the average acceleration, de_{mean} is the average deceleration, ac_{std} is the average standard deviation acceleration, de_{std} is the average standard deviation deceleration, ac_{perc} is the average driving time under acceleration, and de_{perc} is the average driving time under deceleration.

Furthermore, if the road information is available, we include additional four validation criteria: average slope α_{mean}, average standard deviation slope α_{std}, maximal slope α_{max} and minimal slope α_{min}.

To trade off between the computational burden and the timeliness of updating information, we only update ρ_{avg} after each driving cycle.

Approximator

The function of the approximation is to estimate belief state δ_p.

We adopt the MCMC sampling method (Gilks 2005) for the approximation. This MCMC technique has been successfully applied in the driving cycle generation (Lee *et al.* 2011, Silvas *et al.* 2016) and the power system (Hansen *et al.* 2018).

First, we denote the vehicle velocity and the road slope as

$$v(t) \in V = \{V_1, V_2, \cdots, V_n\}$$
$$\alpha(t) \in \Omega = \{\Omega_1, \Omega_2, \cdots, \Omega_m\}$$

where V is defined in (3.31) and Ω is defined in the same way of V by segmenting all the road information values into m classes.

Therefore, the new 2-D TPM $\mathbf{\Phi}^{new} \in \mathbb{R}^{N\times M}$ has N rows for the vehicle velocity classes and M columns for the road information classes. Each entry of the $\mathbf{\Phi}^{new}$ consists of a $(N \times M)$ matrix and is denoted by $\boldsymbol{\phi} \in \mathbb{R}^{N\times M}$. It represents the transition probability from current step s_k to the next step s_{k+1}.

Based on the sampling mechanism of the MCMC method, v_{k+1} and α_{k+1} are selected by a randomly generated number $\mu \in [0,1]$ to be in the interval of the cumulative vector $\Psi_{v_k,\alpha_k}(z)$ of $\mathbf{\Phi}^{new}$, that is

$$v_{k+1} = V(\lceil \frac{z}{M} \rceil) \tag{3.32}$$
$$\alpha_{k+1} = \Omega(z - \lfloor \frac{z-1}{M} \rfloor \cdot M) \tag{3.33}$$

where z is the index selected by the MCMC sampling, $\lfloor\ \rfloor$ denotes the floor function and $\lceil\ \rceil$ stands for the ceil function.

After selecting $v_{k+1} \in V_i$ and $\alpha_{k+1} \in \Omega_j$, the new velocity sample $\hat{v}_{k+1}$ and the new road slope $\hat{\alpha}_{k+1}$ are obtained by

$$\hat{v}_{k+1} = v_{avg}(\sigma) \quad \text{for all } \sigma \in V_i \tag{3.34}$$

Table 3.1. Parameters used in approximator generated cycle

Parameter	Tolerance
Initial velocity $(\mathrm{km/h})$ set to V_c	
Standard deviation velocity $(\mathrm{km/h})$	$\pm 10\%$
Average velocity $(\mathrm{km/h})$	
Average acceleration $(\mathrm{m/s^2})$	
Average deceleration $(\mathrm{m/s^2})$	
Standard deviation acceleration $(\mathrm{m/s^2})$	
Standard deviation deceleration $(\mathrm{m/s^2})$	
Percentage of driving time under acceleration $(\%)$	
Percentage of driving time under deceleration $(\%)$	
Additional parameter (if road information is included)	**Tolerance**
Standard deviation slope (degree)	$\pm 10\%$
Average slope (degree)	
Maximal slope (degree)	
Minimal slope (degree)	

$$\hat{\alpha}_{k+1} = \alpha_{avg}(\sigma) \quad \text{for all } \sigma \in \Omega_j \tag{3.35}$$

where v_{avg} and α_{avg} are the average values the permissible range of class σ by assuming a normal distribution within each class. The flow chart of the cycle generation is presented in Fig. 3.8. A random sampling $\mu \in [0, 1]$ is selected to generate new samples until the desired sampling length and criteria in ρ_{avg} are reached. In Table 3.1, we define the criteria of ρ_{avg} for the generated cycle. Since the first point of the generated synthetic cycle is the current power demand of the driver, the generated synthetic cycle is able to satisfy the dynamic demand of the driver.

Note that the sampling length in the average-reward filter can be set arbitrarily. Thus, we could solve the optimisation problem in a short receding horizon. We use the 1-D Markov transition probability matrix with the average value of the road information instead of a 2-D model for reducing the computational complexity.

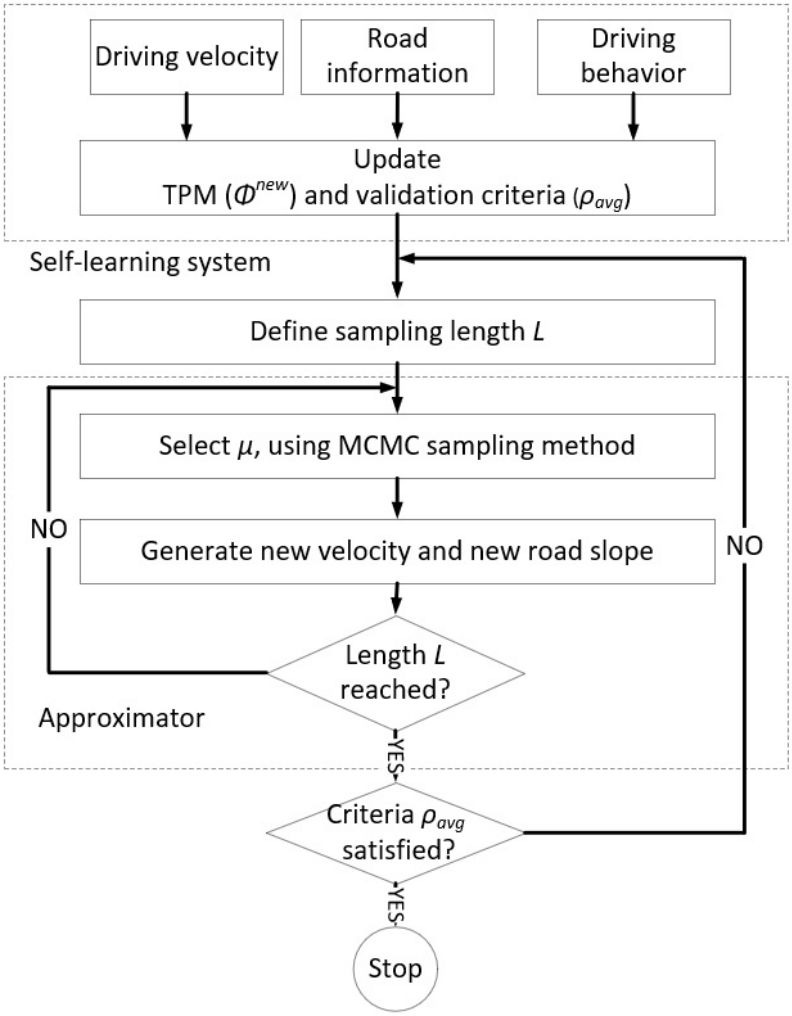

Figure 3.8. Flow chart of the average-reward filter process

3.3.2 Optimisation

The objective function F_{co} to minimise the equivalent fuel consumption cost is

$$F_{co} = \beta_{h2} \cdot \sum_{k=1}^{N} P_{h2}(k) \cdot \Delta t + \beta_b \cdot \sum_{k=1}^{N} P_{bin}(k) \cdot \Delta t \tag{3.36}$$

where β_{h2} is the price of hydrogen, β_b is the price of electricity, Δt is the time step, and N is the length of the generated cycle at every time step.

The optimisation problem is solved under the constrained convex optimisation framework.

$$\min_{u} \; F_{co} \tag{3.37}$$

subject to

$$P_{fcs} + P_{bo} - P_{eloss} - P_{dcdc} - P_a \geq P_v \tag{3.38}$$

$$P_{h_2}(t) \geq b_0 \cdot P_{fcs}^2(t) + b_1 \cdot P_{fcs}(t) + b_2 \tag{3.39}$$

$$P_{bloss}(t) = \frac{R \cdot P_{bin}(t)^2}{2c_0 \cdot \varepsilon_{soc} + \gamma \cdot c_1^2} \tag{3.40}$$

$$P_{bo}(t) = P_{bin}(t) - P_{bloss}(t) \tag{3.41}$$

$$P_{eloss} \geq a_0(\omega(t))\tau^2(t) + a_1(\omega(t))\tau(t) + a_2(\omega(t)) \tag{3.42}$$

$$\frac{d\varepsilon_{soc}}{dt} = -\frac{P_{bin}(t)}{C_n} \tag{3.43}$$

$$P_{soc} \geq i_{min} \cdot \gamma \cdot \sqrt{\frac{2 \cdot c_0 \cdot \varepsilon_{soc}}{\gamma} + c_1^2} \tag{3.44}$$

$$P_{soc} \leq i_{max} \cdot \gamma \cdot \sqrt{\frac{2 \cdot c_0 \cdot \varepsilon_{soc}}{\gamma} + c_1^2} \tag{3.45}$$

$$\varepsilon_{min} \leq \varepsilon_{soc} \leq \varepsilon_{max} \tag{3.46}$$

$$P_{fcs}(min) \leq P_{fcs} \leq P_{fcs}(max) \tag{3.47}$$

$$\triangle P_{fcs,min} \leq \triangle P_{fcs}(t) \leq \triangle P_{fcs,max} \tag{3.48}$$

$$\varepsilon_{soc}(t_f) = \varepsilon_{soc}(target) \tag{3.49}$$

where $\triangle P_{fcs}(t)$ is the increase rate of the output power of the PEMFCS. We impose this limitation to extend the durability of the fuel cell stack. Specifically, the convex programming is applied on the cycle generated by the approximator at each time step, and then the optimal action is selected via the rollout algorithm (Bertsekas and Castanon 1998). The optimisation process of the proposed EMS at each time step is as follows

- Step 1: Update ρ_{avg} and $\mathbf{\Phi}^{new}$ based on new observations V_c, α_{avg}
- Step 2: Generate a cycle by the approximator based on $\mathbf{\Phi}^{new}$ and ρ_{avg}
- Step 3: Calculate the posterior average-reward distribution δ_p based on the generated cycle according to (3.4), (3.7) and (3.8)
- Step 4: Solve the convex optimisation problem in (3.37) on the average-reward distribution and obtain optimal action u_1
- Step 5: Send the command u_1 to the DC-DC converter to control the energy flow

To deal with the errors of the model, first, we adopt the receding horizon principle for optimisation. That is, we take new measurements at each time step to compensate

for unmeasured disturbances and model inaccuracy, both of which cause the system output to be different from the distribution generated by the average-reward filter.

Second, we impose a hard constraint on the final value of battery SoC in the optimisation process at each time step. Namely, we enforce the final value of battery SoC to the reference value (see equation (3.49)) to maintain the battery's SoC.

The closed-loop performance is dependent on long-run average power demand in the energy management system design, which is represented by an average-reward distribution under the POMDP framework that we present in this section. Therefore, the dependence between the closed-loop performance and the predictive model of future power demand is decoupled.

3.4 Simulation results

3.4.1 Experiment and simulation

To verify the performance of the proposed EMS, we simulate the driving dynamics of a golf cart in MATLAB. Although the simulation result cannot entirely reflect the situation in real-world experiments, all the simulations and models in our design are based on the data collected from the trials of driving on the golf cart in a driving experiment on a campus by the same driver. Therefore, the simulation is provided with a realistic driving environment for verifying the proposed EMS design.

The experimental conditions are set as follows:

- A fuel cell hybrid golf cart prototype (Tolj *et al.* 2013) is used for the driving experiments.
- All the experiments are operated by the same driver.
- The golf cart is operated with a predefined route, which is shown in Fig. 3.9.
- Six-lap driving experiments are conducted, and the driving data are shown in Fig. 3.10.
- The initial value of the residual battery energy in each lap is set to the end value of the previous driving cycle.

Figure 3.9. Route of the experimental drive

To compare the performance of the proposed EMS, three other EMSs are used as the benchmarks. They are

- CD-CS. The standard charge-depleting charge-sustaining EMS used in FCVs.
- IMPC1. The method provides the globally optimal solution on each driving cycle. The optimisation problem in (3.37) is solved by convex programming by assuming the future power demand in each driving cycle is known in advance.
- IMPC2. The method is similar to IMPC1 for providing the global optimal solution on each driving cycle except that IMPC2 takes $\varepsilon_{soc}(t)$ as the final target value of the battery's final residual battery energy in (3.49), where $\varepsilon_{soc}(t)$ denotes the real final residual battery energy by implementing the proposed EMS.

We show an example of the cycle generated by the approximator (yellow line) and the future driving velocity (dotted line in blue) in 300 time steps in Fig.3.11. Since the generated cycle represents the driver's average driving performance by a vector of random variables instead of predicting the future power demand, we observe that

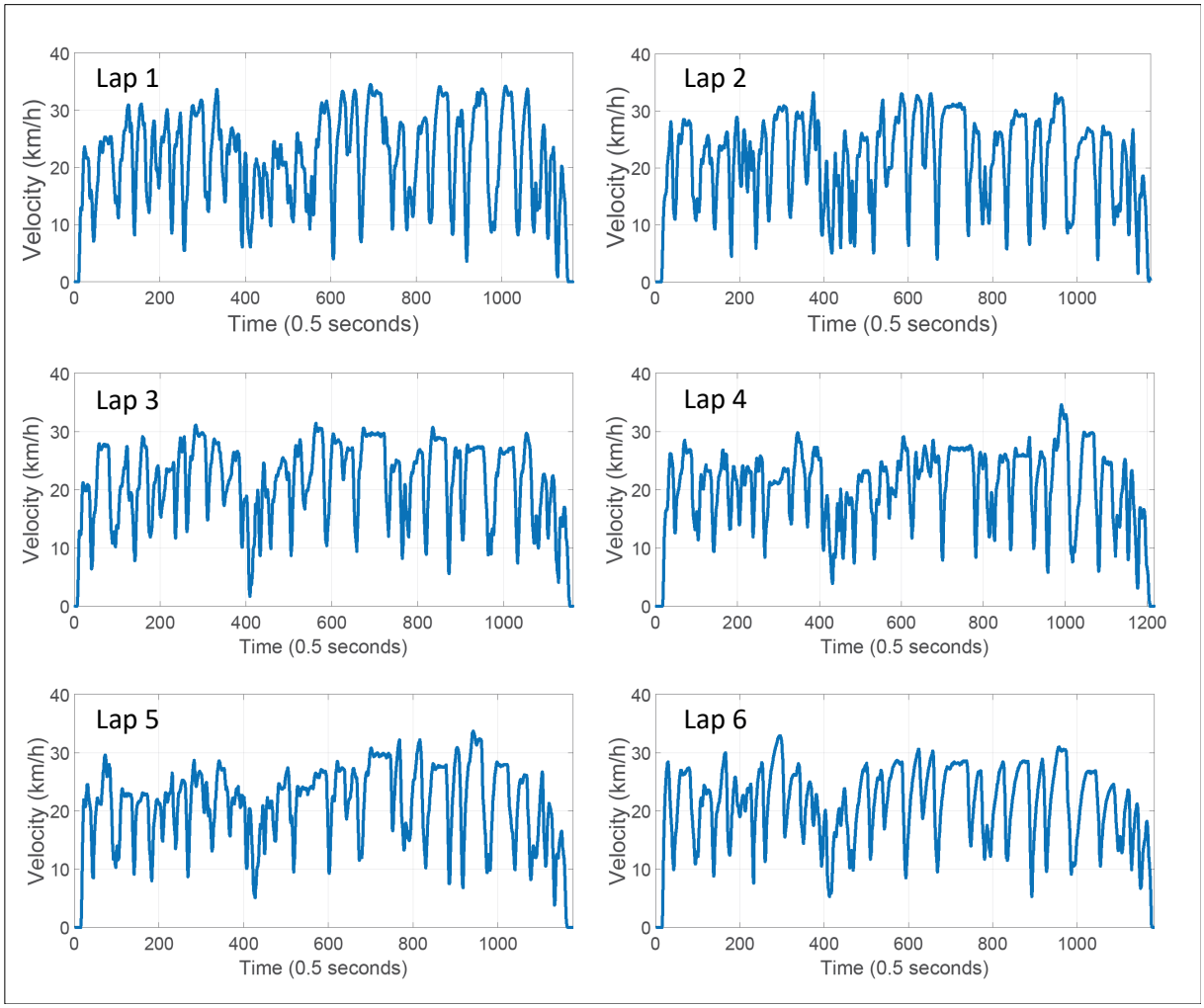

Figure 3.10. Route of the experimental drive

the cycle generated by the approximator does not match the plot of the future driving velocity.

Table 3.2 shows the specifications of the power sources used in this simulation study. Although the capacity of power sources influences the efficiency of the system performance, our focus is on the performance of the new EMS on a predefined propulsion system.

The data collected from the driving experiment Lap 1 is used for training our approximator and the driving experiments of the following five laps are used for the performance verification. Although Lap 1 is not long enough for the training data of MCMC since Lap 1 cannot reflect the long-run average power demand well, the self-learning

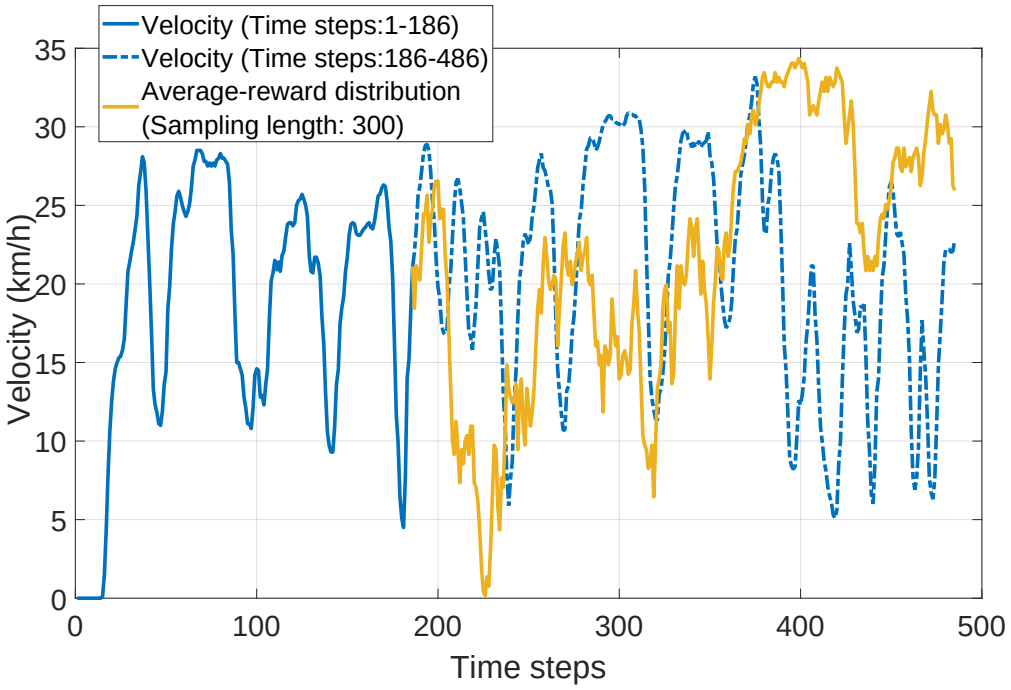

Figure 3.11. Average-reward distribution at time step 186 in Lap 2 driving experiment

system provides an update mechanism to train the unobservable measurements recursively.

The results are shown in Table 3.3, including the norm of the hydrogen consumption (H_2 cons.(g)), the difference of the residual battery energy from the target value ($\Delta(Energy)$), the equivalent fuel consumption cost ($Equiv.\ cost$), and the improvement of the equivalent fuel consumption cost based on CD-CS.

The results show that IMPC1, IMPC2 and our EMS (called E_{new}) offer better fuel economy than CD-CS in five driving cycles. Since the future power demand is known in advance, IMPC1 and IMPC2 are the top two in terms of performance among all the EMSs. Compared with CD-CS, IMPC1 provides 12 % to 15 % improvement in the five driving experiments, and IMPC2 shows 8 % to 11 % improvement. As for E_{new}, we observe that the performance is close to IMPC2 in all the experiments. In other words, E_{new} provides an approximated globally optimal solution in the experiments.

Figs. 3.12 - 3.13 show the power demand of the real driving and simulation data, and the performance comparison of the four EMSs in terms of battery residual energy in five driving experiments. We observe that E_{new} presents good performance in Lap 2 driving experiment, while the trajectories of the battery residual energy between E_{new}

Table 3.2. Specifications of the power sources

Parameter	Value
PEMFCS maximum power [kW]	15
PEMFCS maximum increase power [kW/s]	1
Average DC-DC efficiency [%]	95
Cell capacity [Ah]	20
Cell maximum discharging current [A]	100
Cell maximum charging current [A]	80
Initial battery SoC [%]	50
Maximum battery SoC [%]	80
Target battery SoC [%]	50
Minimum battery SoC [%]	20
Number of battery in series	14
Number of battery in parallel	2

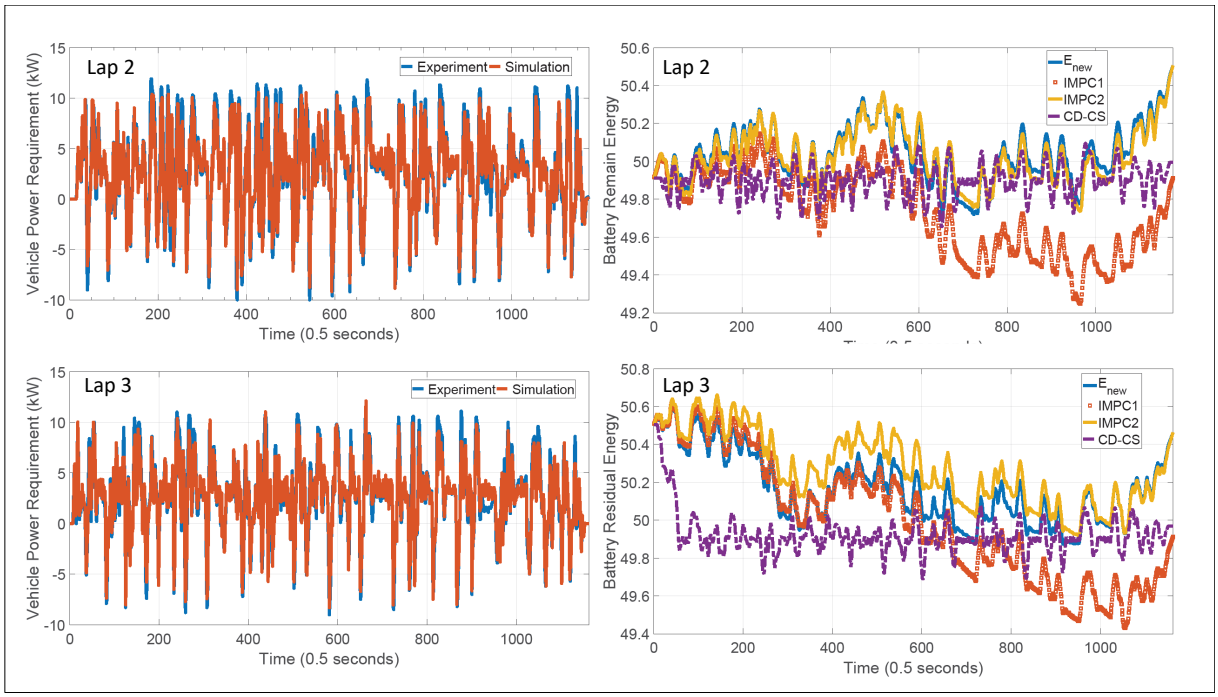

Figure 3.12. Results of Laps 2-3 driving experiments: the power demand of the real driving and the simulation data (left), and the performance of four EMSs in terms of battery residual energy (right)

and IMPC2 show some differences in Laps 3 - 6 driving experiments. The reason is that E_{new} is based on the average-reward approximator described in Section 3.3.1. The

Table 3.3. Simulation results of five laps driving experiments

	H_2 cons. (g)	$\Delta(Energy)$	Equiv. cost ($)	Improvement (%)
Lap 2 driving experiment (588s)				
CD-CS	109.0097	0.0817	1.4126	0
IMPC1	92.7469	0	1.2028	14.85
IMPC2	97.6726	0.5901	1.2584	10.92
E_{new}	97.8699	0.5901	1.2609	10.74
Lap 3 driving experiment (581s)				
CD-CS	97.0254	0.0572	1.2659	0
IMPC1	84.1004	0	1.0991	13.18
IMPC2	88.6117	0.5504	1.1498	9.17
E_{new}	88.7976	0.5504	1.1522	8.98
Lap 4 driving experiment (609s)				
CD-CS	96.6017	0.059	1.2079	0
IMPC1	80.5447	0	1.0523	12.88
IMPC2	85.2378	0.5797	1.105	8.52
E_{new}	85.4768	0.5797	1.1081	8.26
Lap 5 driving experiment (589s)				
CD-CS	97.4852	0.056	1.2717	0
IMPC1	84.0596	0	1.0983	13.64
IMPC2	87.336	0.401	1.1352	10.73
E_{new}	87.596	0.401	1.1385	10.47
Lap 6 driving experiment (592s)				
CD-CS	102.1035	0.0821	1.3287	0
IMPC1	89.0186	0	1.1601	12.69
IMPC2	91.8863	0.3483	1.1924	10.26
E_{new}	92.044	0.3483	1.1945	10.1

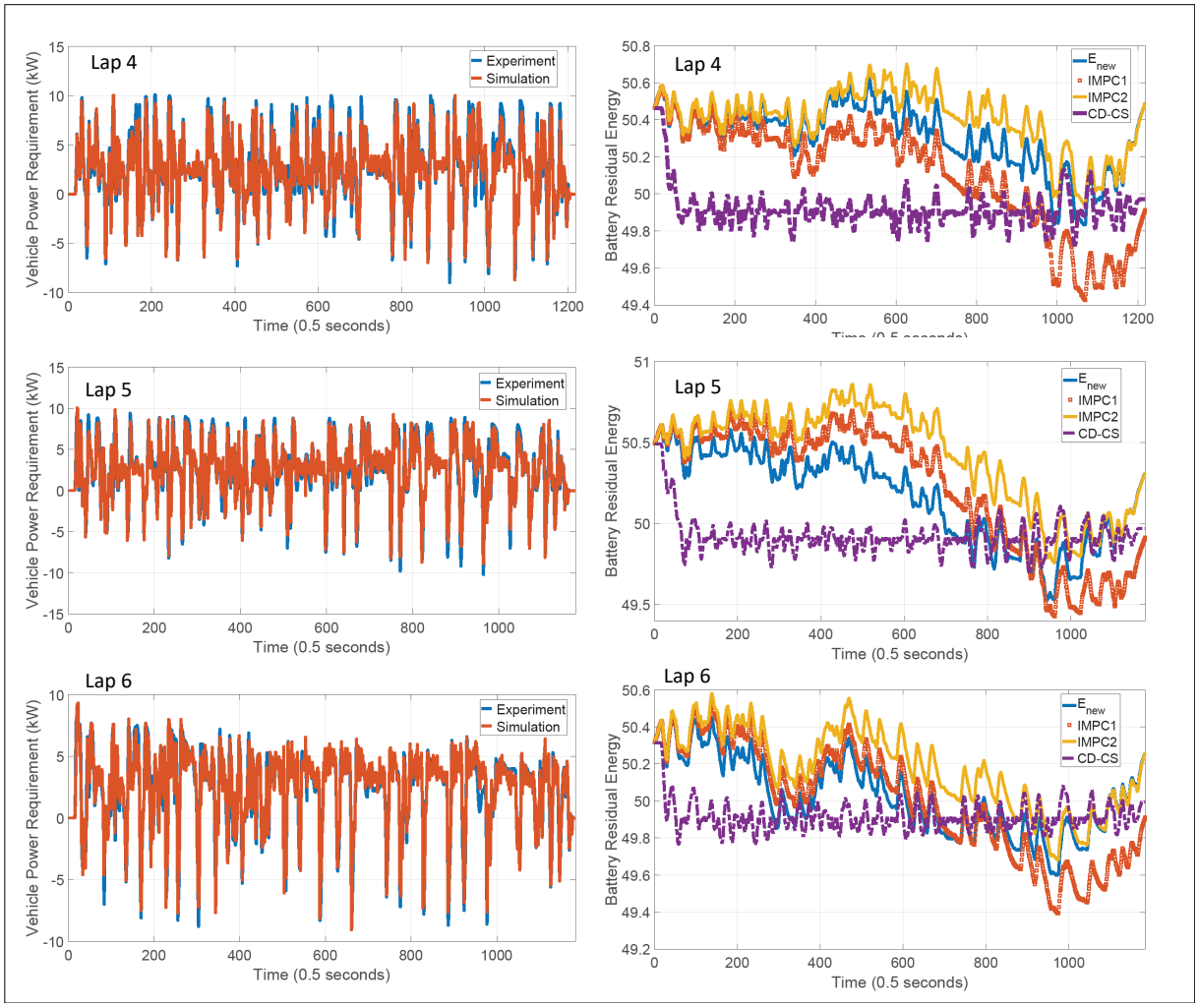

Figure 3.13. Results of Laps 4-6 driving experiments: the power demand of the real driving and the simulation data (left), and the performance of four EMSs in terms of battery residual energy (right)

hidden state δ_p in the driving experiments is estimated by the driver's historical data. From Fig. 3.10, we observe that the driving behaviors in Lap 1 (our initial training model) and Lap 2 are similar, whereas the driving behaviors in Laps 3 - 6 are somehow different from the driver's previous behavior.

3.4.2 Computational consideration

Computational time is one central issue for practical implementations. In the proposed EMS design, the MCMC sampling method used in the approximator and the convex

Table 3.4. Computational time of IMPC1 and IMPC2

	Total CPU time(s)	CPU time per iteration(s)
Lap 2 driving experiment		
IMPC1	11.33	0.28
IMPC2	10.08	0.27
Lap 3 driving experiment		
IMPC1	18.30	0.44
IMPC2	18.25	0.43
Lap 4 driving experiment		
IMPC1	18.52	0.43
IMPC2	17.12	0.4
Lap 5 driving experiment		
IMPC1	20	0.47
IMPC2	13.98	0.36
Lap 6 driving experiment		
IMPC1	18.89	0.44
IMPC2	17.49	0.41

programming in the optimisation process are computationally intensive. We can reduce the computational need by implementing a short horizon optimisation via the MCMC technique.

The average computational time required to solve the optimisation problem with IMPC1, IMPC2 and E_{new} are shown in Table 3.4 and Table 3.5. The data are collected from the simulation studies in a Windows 7 Enterprise PC with Intel® i7-6700 3.40GHz processor, 16GB RAM and MATLAB R2016b. We use CVX toolbox with SDPT3 solver (Grant and Boyd 2020) to solve the convex programming problem.

Tables 3.4-3.5 show that the processing times for IMPC1 and IMPC2 are significantly higher than E_{new}. The higher computational time is due to the fact that IMPC1 and IMPC2 are required to find a unique optimal solution over the entire driving length horizon.

In addition to using the short time horizon optimisation process, the computational time of E_{new} can be further decreased by reducing the sampling length. For example, using a length of 200 instead of 500 samples can reduce computational time by 37%.

Table 3.5. Computational time of E_{new}

Sample length	Total CPU time(s)	CPU time per iteration(s)	Success
100	0.42	0.01	N
200	0.478	0.02	Y
300	0.545	0.02	Y
400	0.628	0.02	Y
500	0.762	0.02	Y

Note that the sampling length cannot be too short - the approximator may fail to generate required cycle if it cannot meet the validation criteria in a short time horizon.

3.5 Chapter summary

This chapter presents a novel energy management system. The energy management problem is cast as a convex optimisation problem. An average reward approximator is developed to optimise the long-term average cost without forecasting future power demand under a partially observable Markov decision process framework. The proposed method shows good performance in simulation using data obtained from real-world driving experiments over a known driving path. However, since the proposed energy management system is based on an average-reward model, the main disadvantage of the method is that it is not applicable to the situation with highly varied driving conditions.

The next chapter will present a mixed H_2/H_∞ control based energy management system to increase the applicability of the energy management system over various driving scenarios.

Chapter 4

Mixed H2/H-infinity Control for Energy Management System Design

THIS chapter presents a real-time energy management system to guarantee system stability and optimality over various driving scenarios and could implement in a real vehicle. A mixed H_2/H_∞ control technique is used to design the energy management controller under the T-S fuzzy modelling framework. Then, the proposed control law is implemented in a vehicle simulator, and the performance of the energy management system is shown in simulation against the dynamic programming based benchmark solution. From the result, the proposed energy management system provides the capability of reducing fuel consumption, smoothing fluctuation of the power delivered from the fuel cell stack, and maintaining the battery charge in an admissible range in various driving scenarios.

4.1 Introduction

Driver's future driving behaviour is a primary uncertainty in energy management system design, which affects the charge-sustaining function of batteries as well as optimal energy flow control in fuel cell vehicles. The charge-sustaining function of batteries is related to stability robustness which can be measured by H_∞ norm, while optimal energy flow control is related to fuel economy which is appropriately measured by H_2 norm. Therefore, it is natural to cast the energy management problem in FCVs into a mixed H_2/H_∞ control problem. Mixed H_2/H_∞ control design has been studied by researchers over the past decades (Chen *et al.* 2000, Orukpe *et al.* 2007, Tseng and Chen 2003, El-Sousy and Abuhasel 2016). The primary purpose of the mixed H_2/H_∞ control problem is to achieve a desired H_2 optimal control when the upper bound of the disturbance is implemented under an H_∞ disturbance attenuation constraint (Chen *et al.* 2000). This control design has the advantages of achieving both the H_2 optimal performance and the H_∞ robustness specifications within a unified framework.

In practice, the powertrain in fuel cell vehicles is nonlinear, which increases the difficulty of incorporating optimal energy management system design into a mixed H_2/H_∞ objective. Takagi-Sugeno (T-S) fuzzy model, which uses a local linear system description for each rule, is appealing for nonlinear systems. By employing the T-S fuzzy model to approximate a nonlinear plant, we can devise a control methodology using the linear control designs that range from optimal control to robust control paradigms (Nguang and Shi 2003, Shi *et al.* 2016a, Shi *et al.* 2016b, Lu *et al.* 2015).

Motivated by the mixed H_2/H_∞ control design and T-S fuzzy model approach, we present a new method in this paper to design a real-time energy management system for fuel cell vehicles. The EMS guarantees optimality and stability for any driving cycle and easily implements in a real vehicle. Specifically, the T-S fuzzy model is used to approximate the nonlinear power system in fuel cell vehicles. Then, a fuzzy mixed H_2/H_∞ energy management controller is developed to achieve the suboptimal H_2 control performance under the H_∞ disturbance rejection constraints.

The chapter is organised as follows: the problem of regulating energy flow in a fuel cell vehicle is described in Section 4.2. The design of the new energy management system for fuel cell vehicles, where a control law is developed, based on mixed H_2/H_∞ control performance is illustrated in Section 5.3. The effectiveness and potential of the proposed design technique are illustrated by various driving scenarios in Section 4.4.

4.2 Problem formulation

A fuel cell hybrid vehicle uses hydrogen as fuel to power vehicles. The vehicle's energy management system performs the function of regulating the energy flow from multiple power sources in some optimal fashion, such that the total fuel consumption is minimized, the battery state of charge (SoC) is maintained in a certain level for any driving cycle, and the durability of the fuel cell system is considered.

We first present the control system model, operational constraints and objective function to formulate the EMS design problem.

4.2.1 System dynamics model

A fuel cell hybrid vehicle with parallel structure is used in this study. At sample time k, we have

$$P_{dc} + P_{bout} \geq P_{drive} \tag{4.1}$$

where P_{dc} is the output power from the fuel cell boost converter, P_{bout} is the power delivered from the battery pack, and P_{drive} is the power demand from the driver. The dynamic behaviors of the battery pack, fuel cell stack and DC-DC converter are simulated as follows.

Battery model

The battery is described by the RC-Branch equivalent circuit in Fig. 4.1. The battery's SoC is estimated by coulomb counting, that is

$$SoC(k+1) = SoC(k) - \frac{\eta_f \cdot i_b(k)}{3600 C_n} \Delta t \tag{4.2}$$

where k is the discrete time step, $i_b(k)$ is the instantaneous battery current (we denote positive for discharge and negative for charge), Δt is the sampling period, $SoC(k)$ is the battery's SoC at time k, C_n is the battery nominal capacitor, and η_f is the battery Faraday efficiency.

Diffusion resistor current i_{R_1} is expressed as

$$i_{R_1}(k+1) = \exp(\frac{-\Delta t}{R_1 C_1}) i_{R_1}(k) + (1 - \exp(\frac{-\Delta t}{R_1 C_1})) i_b(k) \tag{4.3}$$

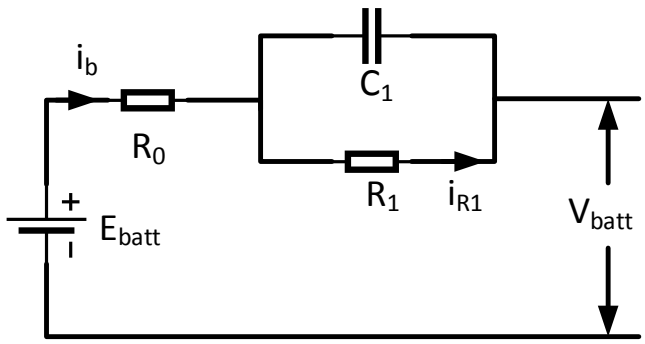

Figure 4.1. Equivalent circuit of the battery with one distinct time constants, internal resistance, and open circuit voltage

where R_1 and C_1 are the value of the resistor and capacitor in the RC-branch in Fig. 4.1, respectively

Moreover, provided the battery SoC is bounded from 20% to 80%, the relationship between the cell's SoC and open circuit voltage E_{batt} is approximated by the following linear equation,

$$E_{batt}(SoC) = b_0 SoC + b_1 \tag{4.4}$$

where b_0 and b_1 are the fitting parameters. Thus, we have

$$V_{batt}(k+1) = b_0 SoC(k) + b_1 - R_0 i_b(k) - R_1 i_{R_1}(k) \tag{4.5}$$

$$P_{bout}(k) = n_s \cdot n_p \cdot V_{batt}(k) \cdot i_b(k) \tag{4.6}$$

where V_{batt} is the battery terminal voltage, R_0 is the internal resistance, and n_s and n_p are the number of cells in series and in parallel in the battery pack, respectively.

Fuel cell model

The dynamic behavior of the fuel cell is described by considering activation losses and ohmic losses (Larminie *et al.* 2003). Provided the fuel cell stack is operated under normal temperature and pressure, the fuel cell dynamic is described by

$$V_{fc}(k) = E_{fc} - A_{fc} \ln\left(\frac{i_{fc}(k)}{i_0}\right) - i_{fc}(k) R_{fc} \tag{4.7}$$

$$P_{fcs}(k) = n_{fcs} \cdot V_{fc}(k) \cdot i_{fc}(k) \tag{4.8}$$

$$m_{H_2}(k) = \theta \cdot i_{fc}(k) \cdot n_{fcs} \tag{4.9}$$

where V_{fc} is the output voltage of a single fuel cell, E_{fc} is the fuel cell open-circuit voltage, A_{fc} is the Tafel slope, i_{fc} is the fuel cell output current, i_0 is the exchange current density, R_{fc} is the internal ohmic, n_{fcs} is the number of cells in the fuel cell stack, P_{fcs} is the power delivered from the fuel cell stack, m_{H_2} is the hydrogen consumption in slpm, and θ is a constant parameter.

DC-DC converter

The boost converter is modelled by its efficiency map. From (Hegazy *et al.* 2012, Chiu and Lin 2006, Pahlevaninezhad *et al.* 2012), we observe that the boost converter operates efficiently when $P_{dc}(k)$ is greater than a certain level ν, and it is reasonable to assume the efficiency of the boost converter to be a constant in the situation. Therefore, we describe the efficiency map of the boost converter as

$$\eta_{dc}(k) = \begin{cases} \bar{\eta}_{dc}, & \text{if } P_{dc}(k) \geq \nu \\ f_{dc}(P_{dc}(k)), & \text{otherwise} \end{cases} \tag{4.10}$$

where $f_{dc}(P_{dc})$ is a nonlinear function that associates P_{dc}.

4.2.2 Objective function and constraints

To achieve energy efficacy, the system performance index is defined to optimise the following objective function $J(k)$

$$J(k) = \sum_{k=0}^{T_n} m_{H_2}(k) \tag{4.11}$$

where T_n is the finite driving time.

Meanwhile, the battery SoC should be maintained at a certain level over the trip

$$SoC(k + T_n|k) \in \Omega_b \tag{4.12}$$

where Ω_b is the terminal set of the battery SoC.

For the power sources, instantaneous constraints are imposed on the battery and fuel cell due to their physical operation limitations, that is, at all time $k >= 0$

$$P_{bout,min} \leq P_{bout}(k) \leq P_{bout,max} \tag{4.13}$$

$$SoC_{min} \leq SoC(k) \leq SoC_{max} \tag{4.14}$$

$$i_{fcs,min} \leq i_{fcs}(k) \leq i_{fcs,max} \tag{4.15}$$

where $(\cdot)_{min}$ and $(\cdot)_{max}$ denote the minimum and maximum limitations of power delivered from the battery pack, battery SoC, and fuel cell output current, respectively.

The operational limitations of the power sources are highly dependent on component size in the vehicle. In this study, we assume that the fuel cell vehicle has capable of driving in the battery-only mode. Thus, we only consider the constraints (4.14) and (4.15).

4.2.3 T-S fuzzy modelling framework

To formulate the energy management problem in FCVs, the states, control input, and disturbance acting on the system are defined as follows

$$x_1(k) = SoC(k) - SoC_{ref}, \qquad x_2(k) = V_{batt} - b_0 SoC_{ref} - b_1, \qquad x_3(k) = i_{R_1}(k)$$
$$u(k) = i_{fc}(k), \qquad w(k) = P_{drive}(k)$$

From (4.1) - (4.10), we have

$$x(k+1) = Ax(k) + B(k)f_u(u(k))u(k) + C(k)w(k) \tag{4.16}$$

where $x = [x_1, x_2, x_3]^T$

$$A = \begin{bmatrix} 1 & 0 & 0 \\ b_0 & 0 & -R_1 \\ 0 & 0 & \exp(-\Delta t/R_1C_1) \end{bmatrix}$$

$$B(k) = \frac{\eta_{dc}(k)}{n_s n_p} \begin{bmatrix} \eta_f \Delta t/(3600 C_n f_{x_2(k)}) \\ R_0/f_{x_2(k)} \\ (-1+\exp(-\Delta t/R_1C_1))/f_{x_2(k)} \end{bmatrix}$$

$$C(k) = \frac{1}{n_s n_p} \begin{bmatrix} -\eta_f \Delta t/3600 C_n f_{x_2(k)} \\ -R_0/f_{x_2(k)} \\ (1-\exp(-\Delta t/R_1C_1))/f_{x_2(k)} \end{bmatrix}$$

$$f_{x_2(k)} = x_2(k) + b_0 SoC_{ref} + b_1$$
$$f_u(u(k)) = n_{fcs} \cdot (E_{fc} - A_{fc}\ln(u(k)/i_0) - R_{fc}u(k))$$

To approximate the nonlinear system, the T-S fuzzy modelling approach (Tanaka and Wang 2004) is adopted to guarantee the mixed H_2/H_∞ control performance index can be expressed in terms of stability, control performance and robustness.

First, we define premise variable $z(k) = 1/f(x_2(k))$ and the maximum and minimum value of $z(k)$ are z_{max} and z_{min} under the constraint on $z(k)$, respectively.

From z_{max} and z_{min}, $z(k)$ is represented by

$$z(k) = 1/f_{x_2(k)} = M_1(z(k))z_{max} + M_2(z(k))z_{min} \tag{4.17}$$

where $M_1(z(k))$ and $M_2(z(k))$ are the membership functions and can be calculated by

$$M_1(z(k)) = \frac{1/f_{x_2(k)} - z_{min}}{z_{max} - z_{min}}, M_2(z(k)) = 1 - M_1(z(k))$$

Then, the following nonlinear model is constructed by interpolating local linear models with the fuzzy membership functions:

Rule 1:

If $z(k)$ is "big",

Then $x(k+1) = Ax(k) + B_1(U(k) + v(k)) + C_1 w(k)$

Rule 2:

If $z(k)$ is "small",

Then $x(k+1) = Ax(k) + B_2(U(k) + v(k)) + C_2 w(k)$

where $U(k) = f(u(k))u(k)$,

$$B_1 = \frac{\bar{\eta}_{dc}}{n_s n_p} \begin{bmatrix} \eta_f \Delta t z_{max}/(3600 C_n) \\ R_0 z_{max} \\ (-1 + \exp(-\Delta t/(R_1 C_1)) z_{max} \end{bmatrix}$$

$$B_2 = \frac{\bar{\eta}_{dc}}{n_s n_p} \begin{bmatrix} \eta_f \Delta t z_{min}/(3600 C_n) \\ R_0 z_{min} \\ (-1 + \exp(-\Delta t/R_1 C_1)) z_{min} \end{bmatrix}$$

$$C_1(k) = \frac{1}{n_s n_p} \begin{bmatrix} -\eta_f \Delta t z_{max}/(3600 C_n) \\ -R_0 z_{max} \\ (1 - \exp(-\Delta t/R_1 C_1)) z_{max} \end{bmatrix}$$

$$C_2(k) = \frac{1}{n_s n_p} \begin{bmatrix} -\eta_f \Delta t z_{min}/(3600 C_n) \\ -R_0 z_{min} \\ (1 - \exp(-\Delta t/R_1 C_1)) z_{min} \end{bmatrix}$$

The defuzzification is carried out as

$$x(k+1) = \sum_{i=1}^{2} h_i(z(k))(A_i X(k) + B_i(U(k) + v(k)) + C_i w(k)) \tag{4.18}$$

where $h_1(z(k)) = M_1(z(k))$ and $h_2(z(k)) = M_2(z(k))$.

Remark 4.1. *We introduce a bounded disturbance $v(k) \leq \nu$ on the control input. Since the disturbance is considered in the controller design, we can set a saturation on control input to enforce P_{dc} to ν when $P_{dc} < \nu$. Therefore, we can guarantee that the boost converter operates efficiently, and the boost converter efficiency can be estimated by $\bar{\eta}_{dc}$, that is, $\eta_{dc}(k) = \bar{\eta}_{dc}$.*

The input nonlinearity is given by

$$U(k) = f(u(k)) \cdot u(k) \tag{4.19}$$

where $f(u(k))$ is the operational fuel cell voltage.

To address the input nonlinearity, we construct q local regions of local lower bounds $\underline{S}_r$ and upper bounds $\bar{S}_r$ of $f(u(k))$ by using T-S fuzzy model approach

$$\textbf{Rule } r\text{: IF } u(k) \text{ is } L^r\text{, THEN } \underline{S} = \underline{S}_r, \bar{S} = \bar{S}_r$$

where L^r is the fuzzy term that associates $u(k)$ in rule r.

Therefore, the global sector for control input can be aggregated as one summation

$$\underline{S} = \sum_{r=1}^{q} v_r(u(k))\underline{S}_r, \qquad \bar{S} = \sum_{r=1}^{q} v_r(u(k))\bar{S}_r$$

where $v_r(u(k))$ is the fuzzy membership function of rule r.

The input nonlinearity $U(k)$ is described by

$$U(k) = \sum_{r=1}^{11} v_r(u(k))(S_r + \Delta S_r) \cdot u(k) \tag{4.20}$$

where $S_r = (\underline{S}_r + \bar{S}_r)/2$ and ΔS_r represents the uncertainty of the operational fuel cell voltage.

Substituting (4.20) to (4.18), we have

$$x(k+1) = \sum_{i=1}^{2} h_i(z(k)) \sum_{r=1}^{11} v_r(u(k))(A_i x(k) + B_i((S_r + \Delta S_r)u(k) + v(k)) + C_i w(k)) \tag{4.21}$$

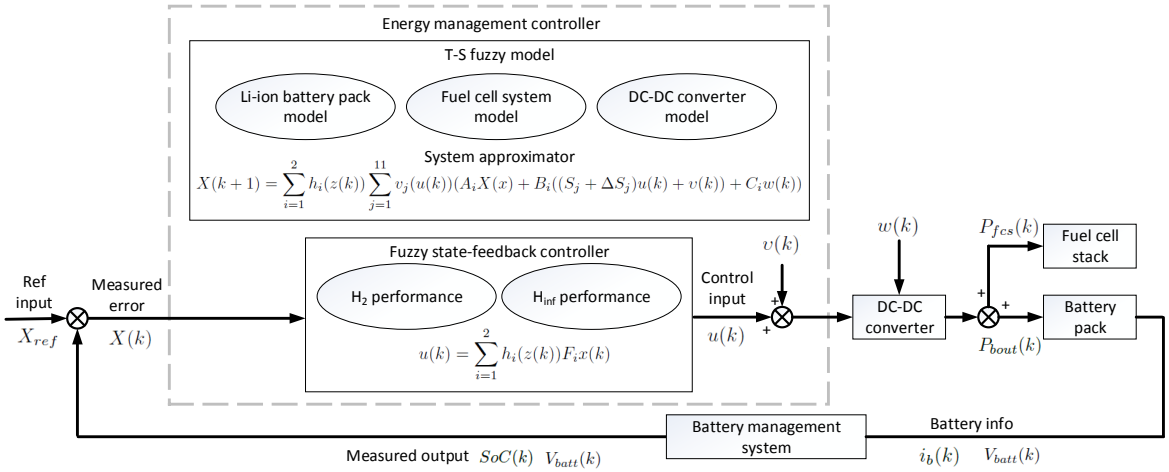

Figure 4.2. Block diagram of the energy management control system

Consider the fuzzy state-feedback controller

$$u(k) = \sum_{i=1}^{2} h_i(z(k))K_i x(k) \tag{4.22}$$

the closed-loop system becomes

$$x(k+1) = \sum_{i=1}^{2} h_i(z(k)) \sum_{r=1}^{11} v_r(u(k)) \sum_{j=1}^{2} h_j(z(k))) \times ((A_i + B_i(S_r + \Delta S_r)K_j)x(k) + B_i v(k) + C_i w(k)) \tag{4.23}$$

Remark 4.2. *The fuel cell dynamic is intricate which is affected by operating conditions of the stack, such as inlet stoichiometry, inlet pressure, humidity, and temperature. To handle the fuel cell dynamic, we introduce the time-varying parameter ΔS_j on S_j to describe the uncertainty of the fuel cell stack operational voltage response.*

4.3 New energy management design

In this section, we present a novel control law design with a desired H_2/H_∞ control performance to address the energy management problem in FCVs. The block diagram of the energy management controller design is shown in Fig. 4.2.

The H_2 and H_∞ performance indexes are defined as follows

$$J_{H_\infty} = \sum_{k=0}^{T_n} (z^T(k)z(k) - \alpha^2(w^T(k)w(k) + v^T(k)v(k))) \tag{4.24}$$

$$J_{H_2} = \sum_{k=0}^{T_n-1} (u^T(k)W_c u(k)) + x^T(T_n)Px(T_n) \tag{4.25}$$

where $z(k) = x_1(k) = C_z X(k)$, α^2 is the H_∞ attenuation level to reject the disturbance on battery SoC, W_c is the weighting scalar on control input, and P is the terminal cost on states.

The input constraint is defined as follows

$$u^T(k)u(k) \leq \mu^2 \tag{4.26}$$

To address the fuel cell dynamic uncertainty, we first define

$$\Delta S_r = HF(k)E_r$$

where H and E_r are known matrices with appropriate dimensions and $F(k)$ is an unknown matrix but satisfies

$$F(k) \in \Omega := \{F(k)|F^T(k)F(k) \leq I\}$$

Then, we rewrite the state-space representation of the closed-loop system (4.23) as

$$x(k+1) = A_c x(k) + B_h e(k) + B_v v(k) + C_w w(k) \tag{4.27}$$

$$e(k) = F(k)g(k) \tag{4.28}$$

$$g(k) = C_g X(k) \tag{4.29}$$

where

$$A_c = \sum_{i=1}^{2} h_i(z(k)) \sum_{r=1}^{11} v_r(u(k)) \sum_{j=1}^{2} h_j(z(k))(A + B_i S_r K_j)$$

$$B_h = \sum_{i=1}^{2} h_i(z(k))B_i H \qquad B_v = \sum_{i=1}^{2} h_i(z(k))B_i$$

$$C_w = \sum_{i=1}^{2} h_i(z(k))C_i \qquad C_g = \sum_{r=1}^{11} v_r(u(k)) \sum_{j=1}^{2} h_j(z(k))E_r K_j$$

Now, we present the main result in this paper as follows.

Theorem 4.1. *Consider the system of (4.23). Assume that system initial condition is zero, H_∞ attenuation level α^2 is specified, $Q = Q^T > 0$, $\lambda \in (0, 1]$, and $\|x(k)\| \leq \phi^2$. Then there exists a unique, admissible robust fuzzy controller (4.22), where*

$$K_i = Y_i Q^{-1} \tag{4.30}$$

that stabilizes system (4.23) with H_∞ attenuation level α^2, minimizes the upper bound of the H_2 control performance index (4.25) and subjects to the constraint $u^T(k)u(k) \leq \mu^2$ at all time $k \geq 0$. Q and M_i are obtained by solving the following optimisation problem:

$$\underset{Q,M_1,M_2}{minimize}\ \beta^2$$

subject to

$$Q = Q^T > \phi^2 I \tag{4.31}$$

$$\begin{bmatrix} Q & \star & \star & \star & \star & \star & \star \\ 0 & \lambda I & \star & \star & \star & \star & \star \\ 0 & 0 & \beta^2 I & \star & \star & \star & \star \\ 0 & 0 & 0 & \beta^2 I & \star & \star & \star \\ \Phi_{51} & \Phi_{52} & \Phi_{53} & \Phi_{54} & Q & \star & \star \\ \Phi_{61} & 0 & 0 & 0 & 0 & W_c & \star \\ \Phi_{71} & 0 & 0 & 0 & 0 & 0 & 1/\lambda \end{bmatrix} \geq 0 \tag{4.32}$$

$$\begin{bmatrix} Q & \star & \star & \star & \star & \star & \star \\ 0 & \lambda I & \star & \star & \star & \star & \star \\ 0 & 0 & \alpha^2 I & \star & \star & \star & \star \\ 0 & 0 & 0 & \alpha^2 I & \star & \star & \star \\ \Phi_{51} & \Phi_{52} & \Phi_{53} & \Phi_{54} & Q & \star & \star \\ C_z Q & 0 & 0 & 0 & 0 & I & \star \\ \Phi_{71} & 0 & 0 & 0 & 0 & 0 & 1/\lambda \end{bmatrix} \geq 0 \tag{4.33}$$

$$\begin{bmatrix} Q & Y_i^T \\ Y_i & \mu^2 I \end{bmatrix} \geq 0 \tag{4.34}$$

$$i \leq j \text{ subject to } h_i \cap h_j \neq \emptyset$$

where $\star$ denotes terms readily inferred from symmetry and

$$\Phi_{51} = AQ + \frac{B_i S_r Y_j + B_j S_r Y_i}{2} \qquad \Phi_{52} = \frac{B_i + B_j}{2} H \qquad \Phi_{53} = \frac{B_i + B_j}{2}$$
$$\Phi_{54} = \frac{C_i + C_j}{2} \qquad \Phi_{61} = W_c \frac{Y_i + Y_j}{2} \qquad \Phi_{71} = E_r \frac{Y_i + Y_j}{2}$$

Proof. The proof is given in the Appendix A. □

Remark 4.3. *Zero initial condition is feasible in practice. We can adjust reference battery SoC (SoC_{ref}) to be initial SoC ($SoC(0)$) in each vehicle.*

Remark 4.4. *In the mixed H_∞ / H_2 control design, J_{H_∞} performance index places importance on sustaining battery charge while J_{H_2} performance index concerns fuel consumption. The main advantage of this methodology is that the proposed EMS can be used in any driving cycle without explicit prediction of future power demand.*

Remark 4.5. *Unlike the emphasis on heuristics and reasoning in fuzzy logic control, fuzzy model based control in this study is used to approximate the nonlinear power system. Therefore, control specifications that can be expressed in terms of stability, performance, robustness to modelling error can be guaranteed. The desired mixed H_2 / H_∞ control performance index works as an objective function to improve fuel economy and guarantee charge sustainability.*

4.4 Verification examples

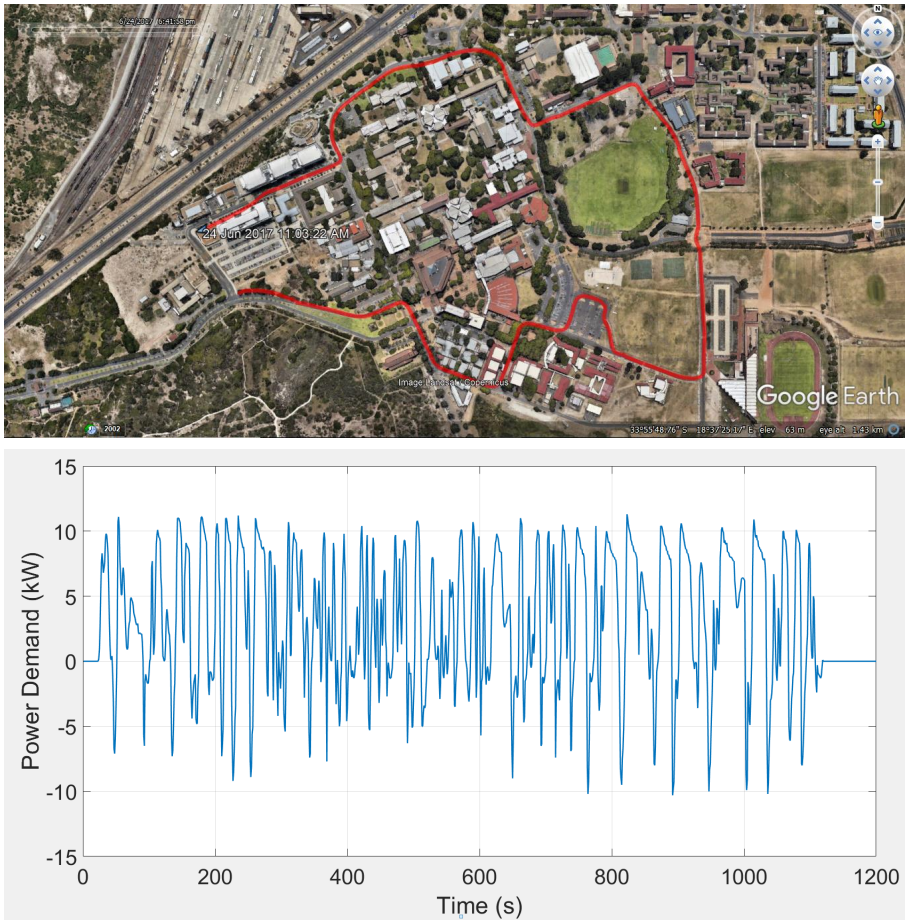

Figure 4.3. Driving route and corresponding power demand used in the simulation

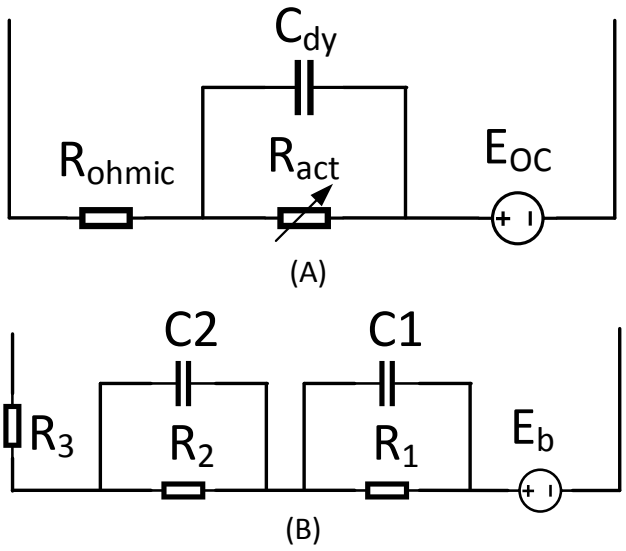

Figure 4.4. (a) Fuel cell equivalent circuit model (b) Battery equivalent circuit model

4.4.1 Experiments and simulation environment

To verify our new energy management controller for FCHVs, we use a closed-loop simulation in the MATLAB/Simulink environment with Powertrain Blockset™and LMI (Gahinet *et al.* 1994) toolbox with SDPT3 solver (Tütüncü *et al.* 2003). Although the simulation environment cannot entirely reflect the real-world situation, the models in our system are based on a golf cart prototype (Tolj *et al.* 2013), and the data of power demand is collected from the trials of driving on the golf cart. Shown in Fig. 4.3 are the driving route used.

Equivalent circuit models, as shown in Fig 4.4, are used to represent battery and fuel cell in the simulator. To estimate parameters of the equivalent circuit models, we conducted the following experiments based on a 15kW Ballard FCvelocity-9SSL fuel cell stack and a 20Ah lithium-ion Polymer battery:

- Fuel cell: Load current from 0A to 100A are applied to the fuel cell stack and the corresponding terminal voltage response data is collected.
- Battery: Discharge current pulses from 40A down to 0A are applied to the battery prototype and the corresponding terminal voltage response data is collected.

Based on the results, the parameters that used in the controller design are set as follows:

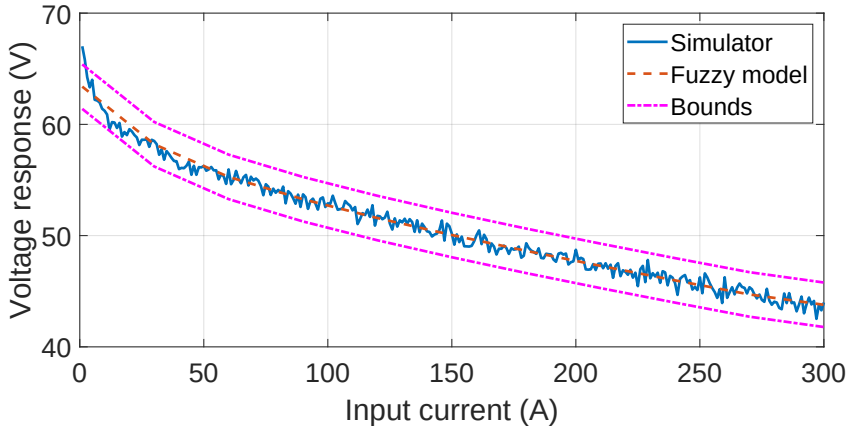

Figure 4.5. Voltage response from the model in the simulator and the fuzzy model in our controller design

- Battery: $b_0 = 0.6526$, $b_1 = 3.402$, $n_s = 28$, $n_p = 2$, $C_n = 20$, $R_0 = 0.0091$, $R_1 = 0.0017$, $C_1 = 3.0027e04$, $SoC_{ref} = 0.5$
- Fuel cell: $n_{fcs} = 75$, $E_{fc} = 0.9277$, $A_{fc} = 0.0325$, $R_{fc} = 4.3341e-4$, $i_0 = 0.3665$
- Others: $\Delta t = 1$, $\phi = 0.005$, $\bar{\eta}_{dc} = 0.9$, $\lambda = 0.3$, $Er = 2$, $H = 1$, $\alpha^2 = 0.003$, $C_z = \begin{bmatrix} 1 & 0 & 0 \end{bmatrix}$.

Moreover, the fuel cell boost converter is described by its efficiency map, and a uniform random number ($\rho \in [-2\%, +2\%]$) is added to simulate the efficiency uncertainty. To simulate fuel cell dynamic that affected by operating conditions, we add a random noise that follow a Gaussian distribution $N(\mu = 0, \sigma = 0.5)$ on the fuel cell operational voltage response in the fuel cell model.

4.4.2 Effectiveness of the fuzzy modelling framework

To verify the effectiveness of the fuzzy model, we apply load current from 0A to 300A to the fuel cell model in the simulator and the fuzzy model in our controller design, respectively. We then compare the voltage response from the models. The results are shown in Fig. 4.5. It is clear that by considering the uncertainty of the fuel cell stack operational voltage response ΔS_r, the fuzzy model has capable of handling the fuel

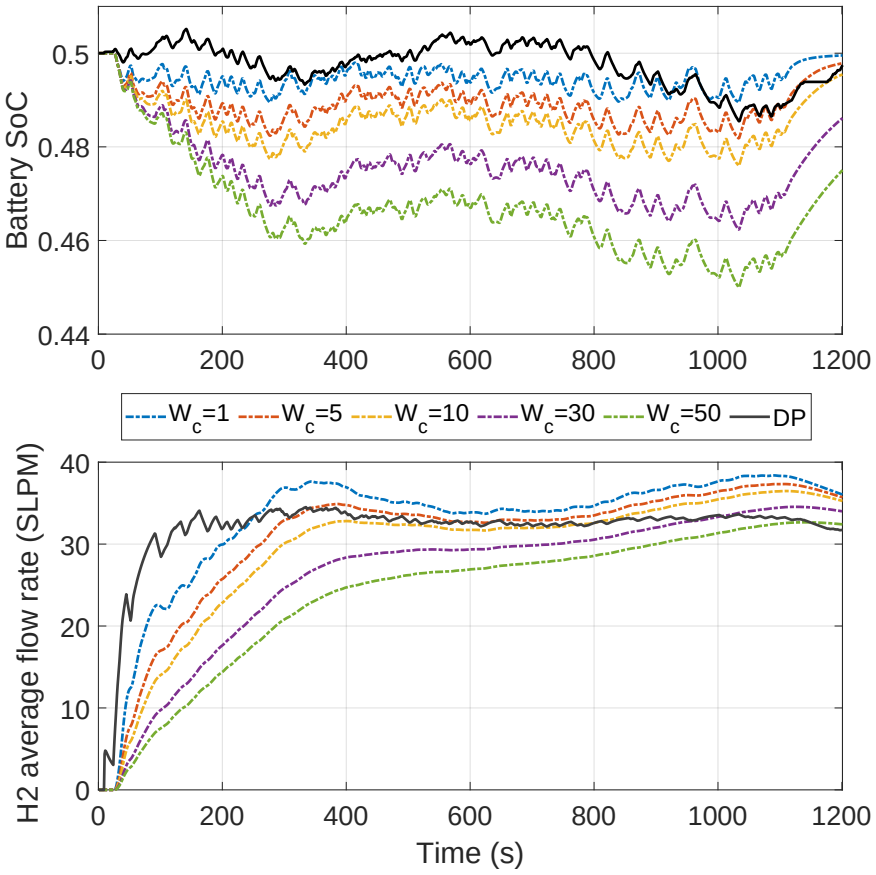

Figure 4.6. Battery SoC and hydrogen flow rate in average under five difference values of W_c and DP

cell dynamic that can affect the robust stability of the whole system. Therefore, the conclusion given in Remark 4.2 is verified.

4.4.3 Energy management controller performance

In this controller design, Weight W_c is a parameter that can be tuned in the simulation. It measures the contribution of the control input (hydrogen consumption) cost by comparing with the terminal cost on the state (battery SoC). Fig. 4.6 shows the system response (battery SoC and hydrogen average flow rate) by implementing five different W_c in the controller design. We observe that weight W_c can be increased in order to achieve better fuel economy, but it also brings the decline of the disturbance rejection ability to maintain the battery SoC under unknown power demand.

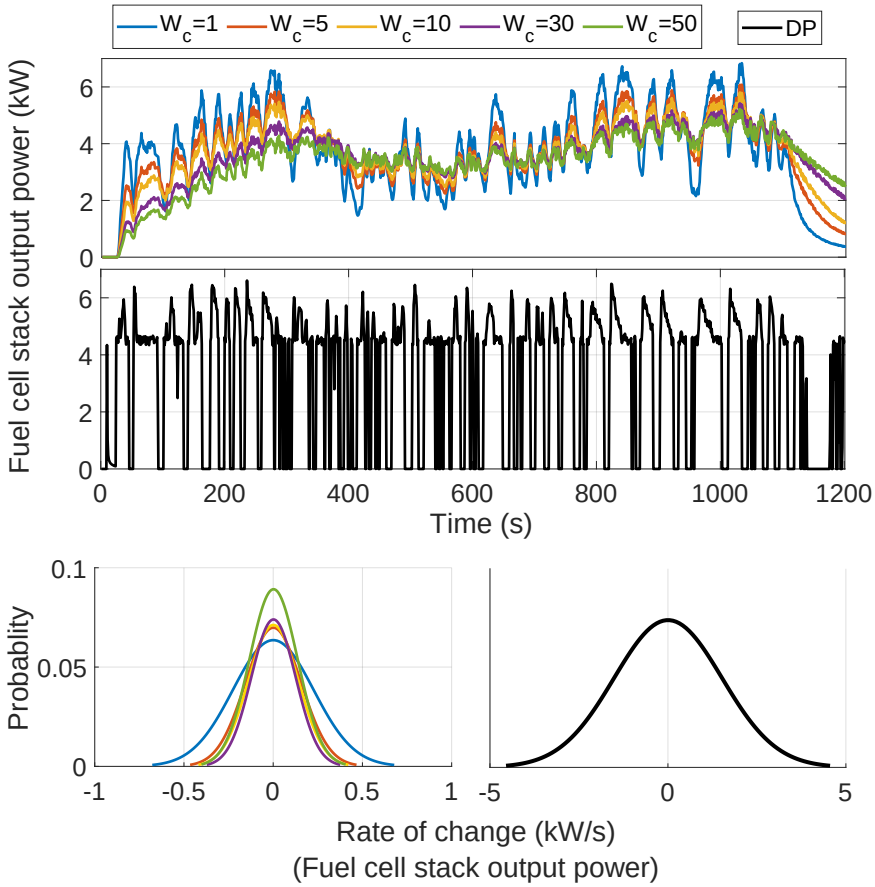

Figure 4.7. Output power delivered from the fuel cell stack and the normal distribution fit of the rate of power change under different W_c and DP

Furthermore, the performance of the controller is evaluated against the optimal global solution obtained from dynamic programming (DP) (Sundstrom and Guzzella 2009). The numeric results are shown in Table 4.1. Since we assume that DP knows the future power demand in advance, it shows the best control performance under the driving cycle as expected. It should be highlighted that the hydrogen flow rate on average under the proposed controller can consume only 2% more than the DP based EMS by relaxing the SoC variation. Since we introduce the noise on fuel cell stack and DC-DC converter in the simulator, we observe that the battery SoC doesn't exactly reach the reference value (50%) under the DP based EMS in the simulation.

The dynamic behavior of the fuel cell stack is highly affected by various operating conditions such as temperature, humidity, gas stoichiometry and pressure. Smoother fluctuation of the load will reduce the work of the fuel cell controller to deal with potential complex phenomena, such as water flooding and air starvation.

Table 4.1. Numeric results of battery SoC and hydrogen flow rate in average under different energy management systems

Strategy	SoC (%)	H_2 flow rate (SLPM)
DP	49.74	31.7324
$W_c = 1$	49.95	36.0438
$W_c = 5$	49.79	35.7013
$W_c = 10$	49.55	35.2653
$W_c = 30$	48.61	33.9931
$W_c = 50$	47.50	32.4085

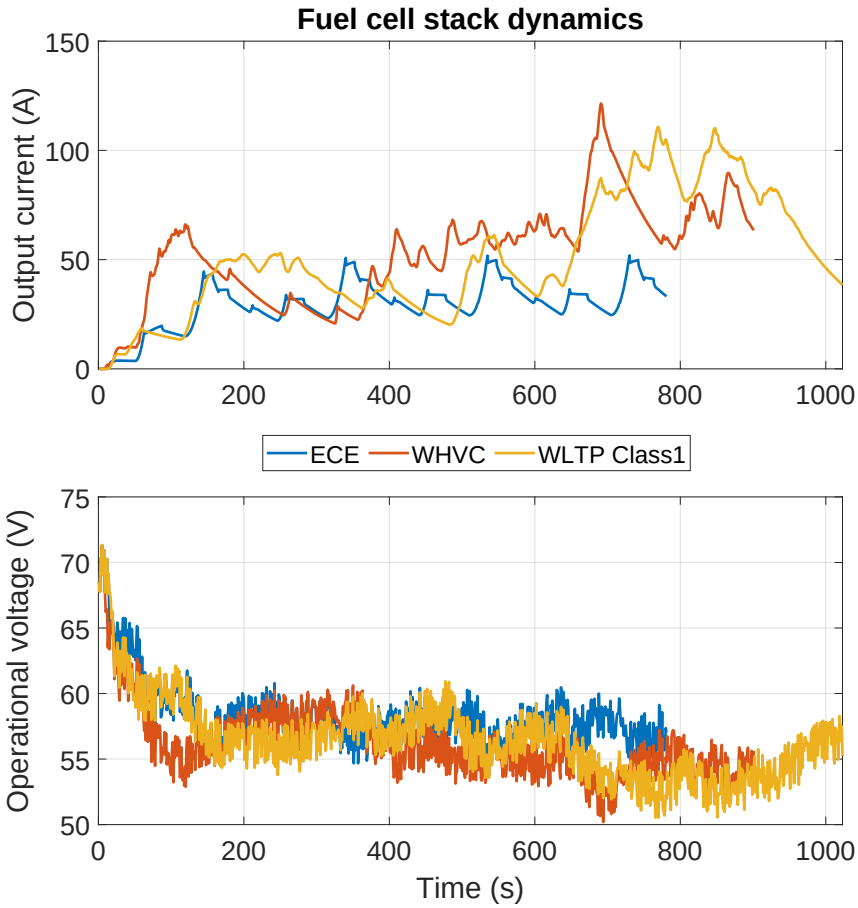

Figure 4.8. Fuel cell stack dynamic response with the proposed controller with $W_c = 30$ under three standard driving cycles

In this study, we propose a state-feedback energy management controller that mainly associates the battery SoC. Since the battery SoC is a slowly time-varying state compared to the power demand from drivers, the controller has capable of reducing the rate of power change from the fuel cell stack during the operation. In Fig. 4.7, we

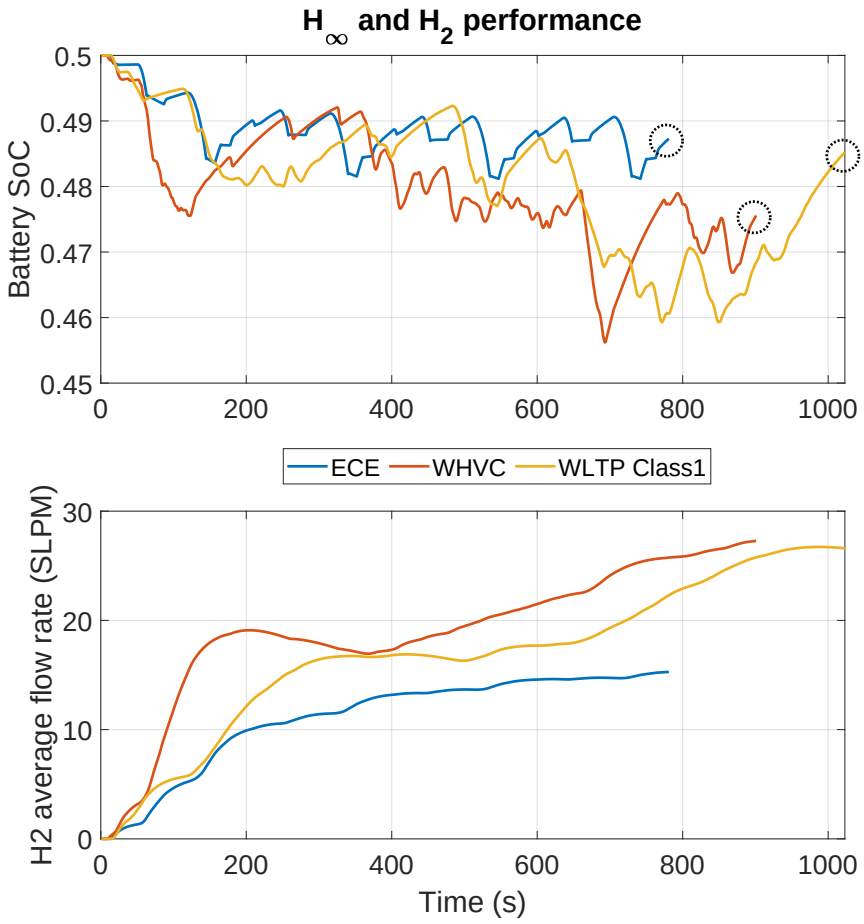

Figure 4.9. H_∞ and H_2 performance of proposed controller with $W_c = 30$ under three standard driving cycles

present the output power delivered from the fuel cell stack and the normal distribution fit of the rate of power change under different W_c and DP. It is clear that our proposed energy management controller demonstrates smoother fluctuation of the power delivered from the fuel cell stack compared to DP.

To further verify the effectiveness of the controller, we implement the controller with $W_c = 30$ in the simulator under the following standard driving cycles:

- Four-lap European driving cycle ECE-15
- One-lap World Harmonized Vehicle Cycle (WHVC)
- One-lap Worldwide Harmonised Light Vehicle Test Procedure (WLTP): Class 1

where Powertrain Blockset™in Simulink is used for the vehicle dynamic simulation and power demand calculation.

Figs. 4.8-4.9 show the fuel cell stack dynamic response and the controller performance corresponding to H_∞ and H_2 performance indexes, respectively. Although the power demand in each driving cycle is different, the controller provides the functionality of disturbance rejection that stabilizes the battery SoC at a certain level in all driving cycles. Therefore, the conclusion given in Remark 4.4 is verified.

4.5 Chapter summary

This chapter describes a real-time energy management system for fuel cell vehicles over various driving scenarios. A T-S fuzzy model is used to approximate the nonlinear energy system and then a mixed H_2/H_∞ energy management controller is developed to achieve suboptimal H_2 control performance under the H_∞ disturbance rejection constraints. The energy management controller offers good control performance to improve the fuel economy while maintaining the battery SoC in an admissible range over various driving scenarios. The potential of the new design technique developed is demonstrated by various real-world driving scenarios.

In the next chapter, we will further investigate how to incorporate traffic condition into the energy management controller design to further improve optimisation performance.

Chapter 5

Robust Model Predictive Control for Energy Management System design

In this chapter, we present a new approach for energy management in fuel cell vehicles. Robust model predictive control technique is used for the energy management system design to achieve the desired system performance in terms of reducing hydrogen consumption while maintaining battery state of charge under practical operating constraints and uncertain future power demand. The optimisation problem is cast into a convex optimisation problem in the form of linear matrix inequalities and solved online. Furthermore, traffic condition is incorporated into the energy management controller design to further improve fuel economy. MATLAB/Simulink based simulation serves to illustrate the effectiveness of the control scheme.

5.1 Introduction

The partially observable Markov decision process based control approach in Chapter 3 shows significant potential for fuel cell vehicle's energy management system design, especially in fixed driving scenarios (such as the bus driving route). Nevertheless, several challenges remain before their practical use in automotive applications. These practical challenges include:

- The control system may perform very poorly when the future power demand is not well described by the model. In fuel cell vehicles, the future power demand is determined by the driver's driving behaviour. From an energy point of view, it is challenging to predict human's behaviour even the external driving conditions are given.
- How to further mitigate the computational burden in the nonlinear optimisation?
- How to blend theoretical development and practical issues to guarantee stability, robustness and optimality of energy management design in fuel cell vehicles?

Motivated by these practical challenges, we propose a novel robust fuzzy model predictive control (MPC) based approach in this chapter to design an energy management system in fuel cell vehicles. Unlike previous fuzzy logic based control strategies (Sorrentino *et al.* 2011, Schouten *et al.* 2003, Tanaka and Wang 2004), Takagi-Sugeno (T-S) fuzzy approach (Tanaka and Wang 2004, Rhee and Won 2006) is used as a systematic modelling methodology to approximate the nonlinear power system in fuel cell vehicles. The approach enables the use of most linear control design tools to address stability analysis, systematic design and performance analysis. In addition, the T-S fuzzy approach renders itself naturally to Lyapunov based system analysis with linear matrix inequalities (LMIs)(Boyd *et al.* 1994, Lian *et al.* 2020, Lian *et al.* 2019), where LMIs are used to express constraints in convex optimisation, and the optimisation problem can be solved in polynomial time.

Furthermore, the robust model predictive control (RMPC) technique is employed in this study for the power control unit design. Compared with the stochastic model predictive control based approaches from the preceding review, advantageous features of robust model predictive control are twofold: the control technique has capable of addressing uncertainties and disturbances in the application, and the optimisation performance of the approach is decoupled from the predictive model as the optimisation

is to minimise the upper bound of the performance index instead of minimising the objective function over the prediction horizon. In the literature, there have been many research findings on robust model predictive control and fuzzy systems. A review of robust model predictive control approaches is given in (Kothare *et al.* 1996, Bemporad and Morari 1999). The features of recent research on robust and stochastic model predictive control are discussed in (Mayne 2016, Mesbah 2016). In (Yang *et al.* 2014, Xia *et al.* 2010), model predictive control based approaches with T-S fuzzy modelling framework are discussed.

The chapter is organised as follows. In Section 5.2, the energy management problem in fuel cell vehicles is formulated as an optimisation problem under a fuzzy modelling framework. In Section 5.3, the robust fuzzy model predictive control based control scheme is presented to design the power control unit for fuel cell vehicles. We then extend the control scheme to incorporate traffic condition for further improving the fuel consumption. Simulation result is given in Section 5.4 to illustrate the effectiveness of the control schemes.

5.2 Problem formulation

5.2.1 System dynamics of the power system in fuel cell vehicles

Fig. 5.1 shows the typical parallel structure of the power plant in the current FCV market (Nonobe 2017) and Fig. 5.2 presents the power flow in the system. At sampling time k, we have

$$P_{motor}(k) = P_{batt}(k) + P_{boost}(k) \tag{5.1}$$
$$P_{fcs}(k) = i_{fcs}(k) \cdot V_{fcs}(k) \tag{5.2}$$
$$P_{boost}(k) = i_{dc}(k) \cdot V_{bus}(k) \tag{5.3}$$
$$P_{batt}(k) = i_b(k) \cdot V_{bus}(k) \tag{5.4}$$
$$\eta_{boost}(k) = P_{boost}(k)/P_{fcs}(k) \tag{5.5}$$
$$\eta_{fcs}(k) = P_{fcs}(k)/P_{h2}(k) \tag{5.6}$$

where P_{motor} is the power demand from the motor, P_{boost} is the output power of the boost converter, P_{h2} is the output power of the hydrogen tank, P_{batt} is the power delivered from the battery pack, P_{fcs} is the power delivered from the fuel cell system, i_{fcs}

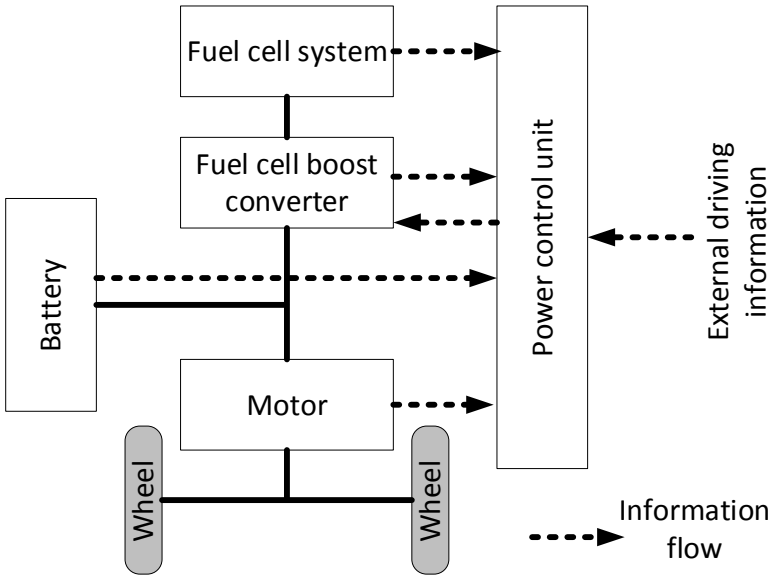

Figure 5.1. Fuel cell vehicle with parallel hybrid system configuration

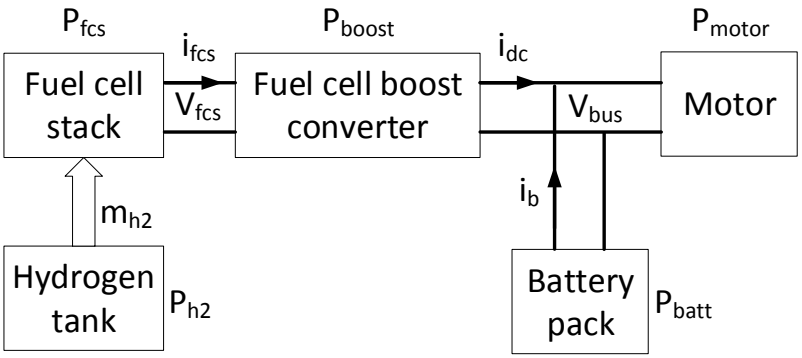

Figure 5.2. Power flow in a fuel cell vehicle with parallel energy configuration

is the output current of the fuel cell stack, V_{fcs} is the terminal voltage of the fuel cell stack, i_{dc} is the output current of the boost converter, i_b is the output current of the battery pack, V_{bus} is the terminal voltage of the battery pack, η_{boost} is the boost converter efficiency, and η_{fcs} is the fuel cell system efficiency.

Hydrogen consumption increases with current and is dependent on the number of fuel cells in the stack, which can be calculated by

$$m_{h2}(i_{fc}) = co_{fc} \cdot i_{fc} \cdot N_{fc} \tag{5.7}$$

where m_{h2} is the hydrogen consumption in standard liter per minute, co_{fc} is the corresponding constant coefficient and N_{fc} is the number of fuel cells.

Now, we are ready to present the system dynamic model in this study.

Battery model

Fig. 5.3(a) shows the battery model in this study due to the simplicity and the focus of energy-efficient driving. V_{bus} is, thus, defined as

$$V_{bus}(k) = n_{sb} \cdot (E_{batt}(k) - \frac{i_b(k)}{n_{pb}} \cdot R_b) \tag{5.8}$$

where n_{sb} is the number of cells in serial and n_{pb} is the number of cells in parallel.

The battery state of charge (SoC) is estimated by the coulomb counting method

$$S_{batt}(k+1) = S_{batt}(k) - \frac{\eta_i \cdot \Delta t}{C_n \cdot n_{pb}} i_b(k) \tag{5.9}$$

where η_i is the faraday efficiency of the cell, S_{batt} is the cell SoC, Δt is the sampling time period, C_n is the cell capacity, and $i_b(k)$ is the instantaneous current delivered from the battery.

Furthermore, the battery open-circuit voltage E_{batt} is assumed to be a linear dependence of the SoC with parameters p_a and p_b when the battery SoC is between 20% and 80%

$$E_{batt}(S_{batt}) = p_a \cdot S_{batt} + p_b, \quad \text{for } S_{batt} \in [0.2, 0.8] \tag{5.10}$$

Fuel cell model

The fuel cell model is shown in Fig. 5.3(b) where we assume that the fuel cell stack operating under normal temperature and pressure. In the model, V_{fc} is the terminal voltage of the fuel cell, E_{oc} models the open-circuit voltage of the fuel cell, R_{ohmic} models the ohmic losses, and R_{act} models the activation losses. The voltage drop ΔV_{act} caused by activation overvoltage is given by

$$\Delta V_{act} = A_{fc} \cdot \ln(\frac{i_{fc}}{i_0}) \tag{5.11}$$

where i_0 is the exchange current density on a proton exchange membrane, A_{fc} is the Tafel slope, and i_{fc} is the current delivered from the fuel cell.

To summarise, the voltage response of the fuel cell stack is described by

$$V_{fcs}(k) = N_{fc} \cdot (E_{oc} - A_{fc} \cdot \ln(\frac{i_{fc}(k)}{i_0}) - i_{fc}(k) \cdot R_{ohmic}) \tag{5.12}$$

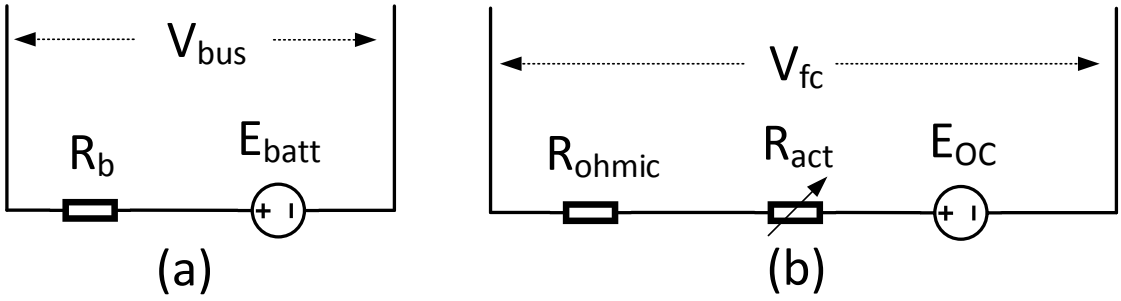

Figure 5.3. (a) Equivalent circuit model for a battery cell; (b) Equivalent circuit model for a fuel cell

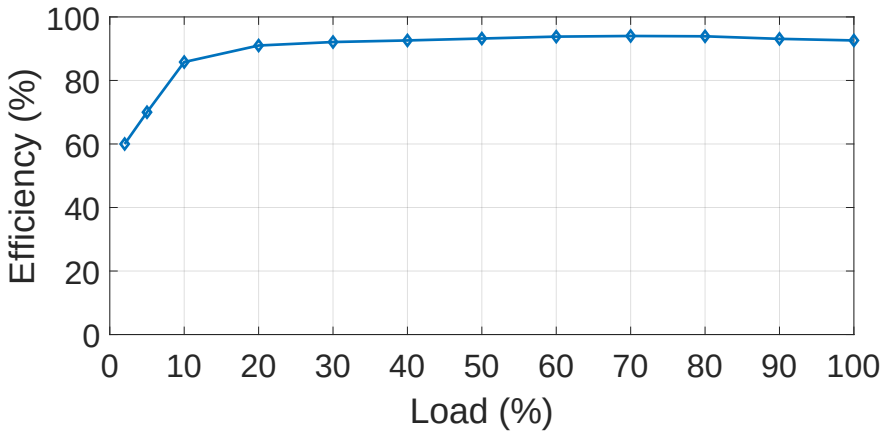

Figure 5.4. Efficiency map of a fuel cell boost converter

Fuel cell boost converter model

Since we focus on energy-efficient driving, the fuel cell boost converter is modelled by its efficiency map. Based on (Hegazy *et al.* 2012), a typical efficiency map of a fuel cell boost converter can be described by Fig. 5.4. The boost converter efficiency is given by

$$\eta_{boost}(k) = f(P_{boost}(k)) \tag{5.13}$$

where $f(P_{boost})$ is the relationship function between the load and the boost converter efficiency.

The optimality of the power distribution in FCVs is defined by minimising hydrogen consumption, which is represented by the following performance index $J(k)$

$$J(k) = \sum_{k=0}^{T_n} m_{h2}(i_{fc}(k)) \tag{5.14}$$

where T_n is the travel time.

The stability of the power plant is defined by maintaining the battery SoC at a certain level over the trip

$$S_{batt}(k + T_n|k) \in \Omega_b \tag{5.15}$$

where Ω_b is the terminal constraints set of the battery SoC.

5.2.2 Fuzzy modelling framework of fuel cell vehicles

To build a fuzzy modelling framework, we reformulate the energy management problem in FCVs to minimise the output power from the hydrogen tank during a driving mission. The objective function consists of two parts: The first part represents the control input efforts over the driving mission. The practical meaning of the part is the total energy consumed from the fuel cell stack over a driving mission. The second part represents the cost of the states at the terminal point only. Consequently, the performance index $J(k)$ is rewritten by

$$J(k) = \sum_{i=0}^{T_n-1} P_{h2}^T(k+i|k) L_{h2} P_{h2}(k+i|k) + \nu_t(x(k+T_n|k)) \tag{5.16}$$

$$\nu_t(x(k+T_n|k)) = x(k+T_n|k)^T P x(k+T_n|k) \tag{5.17}$$

where L_{h2} is the weighting scalar, P is the weighting matrices, and ν_t is the terminal cost on states.

We define the states, control input, and disturbance acting on the system as follows.

$$\begin{aligned} x_1(k) &= S_{batt}(k) - S_{batt\cdot ref} \\ x_2(k) &= V_{bus}(k) - V_{bus\cdot ref} \\ u(k) &= P_{fcs}(k) \\ w(k) &= P_{motor}(k) \end{aligned}$$

where $S_{batt\cdot ref}$ and $V_{bus\cdot ref}$ are the reference values of the cell SoC and DC-BUS voltage, respectively.

Substituting (5.6) to (5.16), we have

$$J(k) = \sum_{i=0}^{T_n-1} u^T(k+i|k) L_u u(k+i|k) + \nu_t(x(k+T_n|k)) \tag{5.18}$$

where $L_u = (1/\eta_{fcs})^2 \cdot L_{h2}$.

The objective $J(k)$ consists of finding the control $u(k)$ that leads to the minimisation of the fuel consumed over the driving mission while maintaining the battery SoC within certain admissible range at the terminal point T_n.

Remark 5.1. *From an energy point of view, the power demand is determined by the driver's driving behaviour. Poor control performance may occur if the future power demand is not well predicted. However, it is challenging to predict human behaviour even if the external driving route is given. A compromise is to use a fixed reference value for the final states to deal with all driving scenarios. It will lead to sub-optimal results, but the setting increases the controller's applicability to handle all driving conditions found in the real application.*

Combining (5.1) - (5.13), we have the following system dynamic model

$$x_1(k+1) = x_1(k) - \frac{\eta_i \cdot \Delta t}{C_n \cdot n_{pb}} \cdot \frac{w(k) - \eta_{boost} u(k)}{x_2(k) + V_{bus\cdot ref}} \tag{5.19}$$

$$x_2(k+1) = n_{sb}(p_a x_1(k) - \frac{R_b}{n_{pb}} \cdot \frac{w(k) - \eta_{boost} u(k)}{x_2(k) + V_{bus\cdot ref}}) \tag{5.20}$$

In this study, the fuzzy model is constructed by the approach of the local sector nonlinearity in fuzzy partition spaces (Tanaka and Wang 2004). Shown in Fig. 5.5 is a local sector nonlinearity. To find a local sector for a nonlinear system

$$x(k+1) = f(x(k)) \in \begin{bmatrix} a_1 & a_2 \end{bmatrix} x(k)$$

where $x(k) \in \begin{bmatrix} d_1 & d_2 \end{bmatrix}$, we approximate the nonlinear function by the local sector using fuzzy membership functions.

The steps to construct the fuzzy model is as follows.

Equations (5.19) and (5.20) can be written as

$$x(k+1) = \begin{bmatrix} 1 & 0 \\ n_{sb}p_a & 0 \end{bmatrix} x(k) + \begin{bmatrix} \frac{\eta_i \Delta t \eta_{boost}}{C_n n_{pb}(x_2(k)+V_{bus\cdot ref})} \\ \frac{R_b \eta_{boost}}{n_{pb}(x_2(k)+V_{bus\cdot ref})} \end{bmatrix} u(k) - \begin{bmatrix} \frac{\eta_i \Delta t}{C_n n_{pb}(x_2(k)+V_{bus\cdot ref})} \\ \frac{R_b}{n_{pb}(x_2(k)+V_{bus\cdot ref})} \end{bmatrix} w(k) \tag{5.21}$$

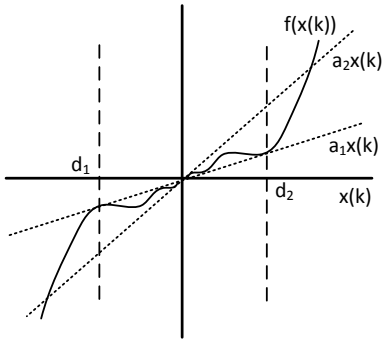

Figure 5.5. Local sector nonlinearity

where $x(k) = [x_1(k), x_2(k)]^T$.

Since $n_{sb}, p_a, \eta_i, \Delta t, C_n, n_{pb}, R_b$ are known constants, the only nonlinear term in the system is $1/(x_2(k) + V_{bus\cdot ref})$ if η_{boost} can be assumed as a constant. For the nonlinear term, define $z(k) = 1/(x_2(k) + V_{bus\cdot ref})$. Then, we have

$$x(k+1) = \begin{bmatrix} 1 & 0 \\ n_{sb}p_a & 0 \end{bmatrix} x(k) + \begin{bmatrix} \frac{\eta_i \Delta t \eta_{boost}}{C_n n_{pb}} z(k) \\ \frac{R_b \eta_{boost}}{n_{pb}} z(k) \end{bmatrix} u(k) - \begin{bmatrix} \frac{\eta_i \Delta t}{C_n n_{pb}} z(k) \\ \frac{R_b}{n_{pb}} z(k) \end{bmatrix} w(k) \tag{5.22}$$

Next, we calculate the maximum and minimum values of $z(k)$ under $x_2(k) \in [x_{2\cdot min}, x_{2\cdot max}]$, that is,

$$z_{max} = 1/(x_{2\cdot min} + V_{bus\cdot ref})$$
$$z_{min} = 1/(x_{2\cdot max} + V_{bus\cdot ref})$$

For their maximum and minimum values, $z(k)$ is represented by

$$z(k) = 1/(x_2(k) + V_{bus\cdot ref}) = M_1(z(k)) \cdot z_{min} + M_2(z(k)) \cdot z_{max} \tag{5.23}$$

where $M_1(z(k)) + M_2(z(k)) = 1$.

From (5.23), the membership functions can be defined as

$$M_1(z(k)) = (z(k) - z_{max})/(z_{min} - z_{max})$$
$$M_2(z(k)) = (z(k) - z_{min})/(z_{max} - z_{min})$$

We denote the membership functions "Large" and "Small". Then, the nonlinear system (5.21) is represented by the following 2-rule fuzzy model

RULE A:

IF $z(k)$ is "Small"

$$x(k+1) = Ax(k) + B_1u(k) + E_1w(k) \tag{5.24}$$

RULE B:

IF $z(k)$ is "Large"

$$x(k+1) = Ax(k) + B_2u(k) + E_2w(k) \tag{5.25}$$

where

$$A = \begin{bmatrix} 1 & 0 \\ n_{sb}p_a & 0 \end{bmatrix} B_1 = \begin{bmatrix} \frac{\eta_i \Delta t \eta_{boost}}{C_n n_{pb}(x_{2\cdot max}+V_{bus\cdot ref})} \\ \frac{R_b \eta_{boost}}{n_{pb}(x_{2\cdot max}+V_{bus\cdot ref})} \end{bmatrix} B_2 = \begin{bmatrix} \frac{\eta_i \Delta t \eta_{boost}}{C_n n_{pb}(x_{2\cdot min}+V_{bus\cdot ref})} \\ \frac{R_b \eta_{boost}}{n_{pb}(x_{2\cdot min}+V_{bus\cdot ref})} \end{bmatrix}$$

$$E_1 = \begin{bmatrix} \frac{-\eta_i \Delta t}{C_n n_{pb}(x_{2\cdot max}+V_{bus\cdot ref})} \\ \frac{R_b}{n_{pb}(x_{2\cdot max}+V_{bus\cdot ref})} \end{bmatrix} E_2 = \begin{bmatrix} \frac{-\eta_i \Delta t}{C_n n_{pb}(x_{2\cdot min}+V_{bus\cdot ref})} \\ \frac{R_b}{n_{pb}(x_{2\cdot min}+V_{bus\cdot ref})} \end{bmatrix}$$

From Fig. 5.4, we observe that the boost converter operates efficiently when the output power of the boost converter is higher than a certain level ε_{p1} (around 10% of its maximum power). In this situation, it is reasonable to assume the boost converter efficiency η_{boost} a constant. In addition, a fuel cell system (Staunton *et al.* 2006, Wipke *et al.* 2012, Gemmen and Johnson 2006) shows the similar efficiency characteristic, that is, a fuel cell system operates efficiently and η_{fcs} can be assumed as a constant when the power delivered from the fuel cell system is higher than a certain value ε_{p2}.

Therefore, we introduce a bounded uncertainty $\Delta u \leq \max(\varepsilon_{p1}, \varepsilon_{p2})$ on the input part to guarantee that the fuel cell system and the boost converter operate efficiently. By considering the uncertainty Δu in the system, we can enforce P_{boost} to ε_{p1} when $P_{boost} < \varepsilon_{p1}$ and P_{fcs} to ε_{p2} when $P_{fcs} < \varepsilon_{p2}$. We rewrite the T-S fuzzy model in (5.24) - (5.25) by

$$x(k+1) = \sum_{i=1}^{r} h_i(z)(Ax(k) + B_i(u(k) + \Delta u) + E_i w(k)) \tag{5.26}$$

where r is the number of fuzzy rules ($r = 2$ in our case) and

$$h_1(z) = M_1(z(k)) \qquad h_2(z) = M_2(z(k))$$

In addition, the constraint on control input is considered

$$u(k+i|k) \in \mathbb{U}, \quad i = 0, 1, ..., T_n - 1 \tag{5.27}$$

where $\mathbb{U}$ is a constraint set of the power delivered from the fuel cell stack.

Remark 5.2. *To employ T-S fuzzy approach as the approximator for the power system in FCVs, an intuitive solution is to take i_{fc} as the control input, S_{batt} as the state, and then linearise the control system under a T-S fuzzy modelling framework. However, the solution suffers from computational burden since the premise variables have to be the functions of the input variables which introduces a complicated defuzzification process of fuzzy controllers (Tanaka and Wang 2004). Therefore, we adopt the alternative approach (5.24)-(5.26) to build the fuzzy modelling framework.*

Remark 5.3. *Battery SoC is normally estimated and monitored by a battery management system in an FCV. Its estimated state is sent to the power control unit via CAN bus. In this study, we follow this concept and assume the battery SoC is observable.*

In summary, the energy management problem in this study is to minimise the cost function $J(k)$ in (5.18), subject to the system dynamic model in (5.26) and constraints in (5.15) and (5.27).

5.3 Control scheme of fuzzy model predictive control

In this section, we describe our proposed control scheme to address the energy management problem posed in Section 5.2. A robust MPC based approach is proposed to minimise the upper bound of the cost function $J(k)$ in (5.18) with a state-feedback controller

$$u(k) = \sum_{i=1}^{r} h_i(z(k))K_i x(k) \tag{5.28}$$

5.3.1 Recursive feasibility

The first issue that we address is the recursive feasibility of the control scheme in the presence of disturbance and uncertainties. In this study, we adopt the concept of robust positively invariant (RPI) set (Blanchini 1999, Mayne *et al.* 2006, Valmorbida and Anderson 2017) to design the control law, which provides sufficient conditions to guarantee the recursive feasibility.

Definition 5.1 (RPI for discrete-time systems (Blanchini 1999))**.** *For the system $x(k+1) = f(x(k), w(k))$, a set $\mathrm{Y} \subset \mathbb{R}^n$ is robust positively invariant if for all $x(0) \in \mathrm{Y}$ and all $w(k) \in \mathbb{W}$, the solution is such that $x(k) \in \mathrm{Y}$ for $k > 0$.*

For the fuzzy system in (5.26), we define the candidate invariant set Y as follows.

$$\mathrm{Y} = \{x \in \mathbb{R}^n : x^T P x \leq \xi\} \tag{5.29}$$

Derived from the results in (Alessandri *et al.* 2004), the set in (5.29) is an RPI set if

$$\frac{1}{\xi} x(k)^T P x(k) \geq \frac{w(k)^T w(k) + \Delta u(k)^T \Delta u(k)}{\gamma^2 + \delta^2} \tag{5.30}$$

implies

$$\frac{1}{\xi} x(k+1)^T P x(k+1) \leq \frac{1}{\xi} x(k)^T P x(k) \tag{5.31}$$

where γ and δ are known constants that, for all $k \geq 0$,

$$w(k)^T w(k) \leq \gamma^2 \tag{5.32}$$

$$\Delta u(k)^T \Delta u(k) \leq \delta^2 \tag{5.33}$$

Using the S-procedure technique (Yakubovich 1992, Iwasaki *et al.* 2000), (5.31) holds if there exists $\lambda \in (0, 1]$ such that

$$\begin{aligned} &\frac{1}{\xi}(x(k+1)^T P x(k+1) - x(k)^T P x(k)) \\ &\quad - \lambda(\frac{w(k)^T w(k) + \Delta u(k)^T \Delta u(k)}{\gamma^2 + \delta^2} - \frac{1}{\xi} x(k)^T P x(k)) \leq 0 \end{aligned} \tag{5.34}$$

The following theorem shows that the conditions in (5.34) can be cast in the form of LMIs to guarantee Y is a robust positively invariant set for the system in (5.26).

Theorem 5.1. *The state feedback matrices K_i in (5.28) to ensure* Y *being an RPI for the system in (5.26) are given by*

$$K_i = M_i Q^{-1} \tag{5.35}$$

where $\lambda \in (0, 1]$, $Q > 0$ and M_i are obtained from the following matrix inequality

$$\begin{aligned} &\begin{bmatrix} (1-\lambda)Q & \star & \star & \star \\ 0 & \lambda/(\gamma^2+\delta^2) & \star & \star \\ 0 & 0 & \lambda/(\gamma^2+\delta^2) & \star \\ AQ + \frac{B_i M_j + B_j M_i}{2} & \frac{B_i + B_j}{2} & \frac{E_i + E_j}{2} & Q \end{bmatrix} \geq 0 \\ &\text{for } i \leq j \text{ subject to } h_i \cap h_j \neq \emptyset \end{aligned} \tag{5.36}$$

where $\star$ denotes terms readily inferred from symmetry.

Proof. See Appendix B.1. □

Remark 5.4. *The feedback matrices K_i computed from Theorem 5.1 are capable of ensuring that the candidate invariant set Υ is an RPI set for the system in (5.26). According to Definition 5.1, the path constraints on the states are imposed by the RPI set.*

Moreover, we impose the following conditions on the terminal cost ν_t to achieve stability:

$$\begin{aligned}&\nu_t(x(k+1+i|k)) - \nu_t(x(k+i|k)) \\ &\leq \alpha^2(w(k+i|k)^T w(k+i|k) + \Delta u(k+i|k)^T \Delta u(k+i|k)) - u^T(k+i|k) L_u u(k+i|k)\end{aligned} \tag{5.37}$$

where α is a positive scalar. The stability and optimality analysis of the control system will be given in the following sections.

5.3.2 Optimality and constraints

Summing (5.37) from $i = 0$ to $i = T_n - 1$,

$$\begin{aligned}J(k) &= \sum_{i=0}^{T_n-1} u^T(k+i|k) L_u u(k+i|k) + \nu_t(x(k+T_n|k)) \\ &\leq \nu_t(x(k|k)) + \alpha^2 \sum_{i=0}^{T_n-1} (w(k+i|k)^T w(k+i|k) + \Delta u(k+i|k)^T \Delta u(k+i|k))\end{aligned} \tag{5.38}$$

From (5.32) and (5.33), we have

$$\sum_{i=0}^{T_n-1} (w(k+i|k)^T w(k+i|k) + \Delta u(k+i|k)^T \Delta u(k+i|k)) \leq T_n(\gamma^2 + \delta^2) \tag{5.39}$$

Thus, we obtain

$$J(k) \leq \nu_t(x(k|k)) + \alpha^2 T_n(\gamma^2 + \delta^2) \tag{5.40}$$

Consider

$$\nu_t(x(k)) = x(k)^T P x(k) \leq \xi \tag{5.41}$$

the upper bound of the cost function $J(k)$ is minimised by solving

$$\min \xi, \text{ subject to } \nu_t(x(k)) \leq \xi \tag{5.42}$$

and the input constrain is defined as follows.

$$u^T(k)u(k) \leq \mu^2 \tag{5.43}$$

The following theorem gives us LMIs conditions for existence of the appropriate P satisfying (5.37) and input constraint (5.43), and the corresponding state feedback matrices K_i.

Theorem 5.2. *The state feedback matrices K_i in (5.28) that minimise the upper bound of the performance function $J(k|k)$ at time step k and subject to the constraint $u^T(k)u(k) \leq \mu^2$ at all time $k \geq 0$ are given by (5.35), where $Q > 0$ and M_i are obtained by solving the following optimisation problem*

$$\min \xi$$

subject to

$$\begin{bmatrix} Q & \star & \star & \star & \star \\ 0 & \xi\alpha^2 & \star & \star & \star \\ 0 & 0 & \xi\alpha^2 & \star & \star \\ AQ + \frac{B_iM_j + B_jM_i}{2} & \xi\frac{B_i+B_j}{2} & \xi\frac{E_i+E_j}{2} & Q & \star \\ \frac{M_i+M_j}{2}L_u & 0 & 0 & 0 & \xi L_u \end{bmatrix} \geq 0$$

for $i \leq j$ subject to $h_i \cap h_j \neq \emptyset$ (5.44)

$$\begin{bmatrix} Q & M_i^T \\ M_i & \mu^2 I \end{bmatrix} \geq 0 \tag{5.45}$$

and

$$\begin{bmatrix} 1 & x^T(k) \\ x(k) & Q \end{bmatrix} \geq 0 \tag{5.46}$$

Proof. See Appendix B.2 □

Fig. 5.6 shows the block diagram of the RMPC based control scheme, and the procedure for the control scheme is shown as follows.

- Step 1: At time step k, control law (5.28) is yielded by the solution of the following optimisation problem with the fuzzy membership values h_i:

$$\min \xi \tag{5.47}$$
$$\text{subject to (5.36), (5.44), (5.45), (5.46)}$$

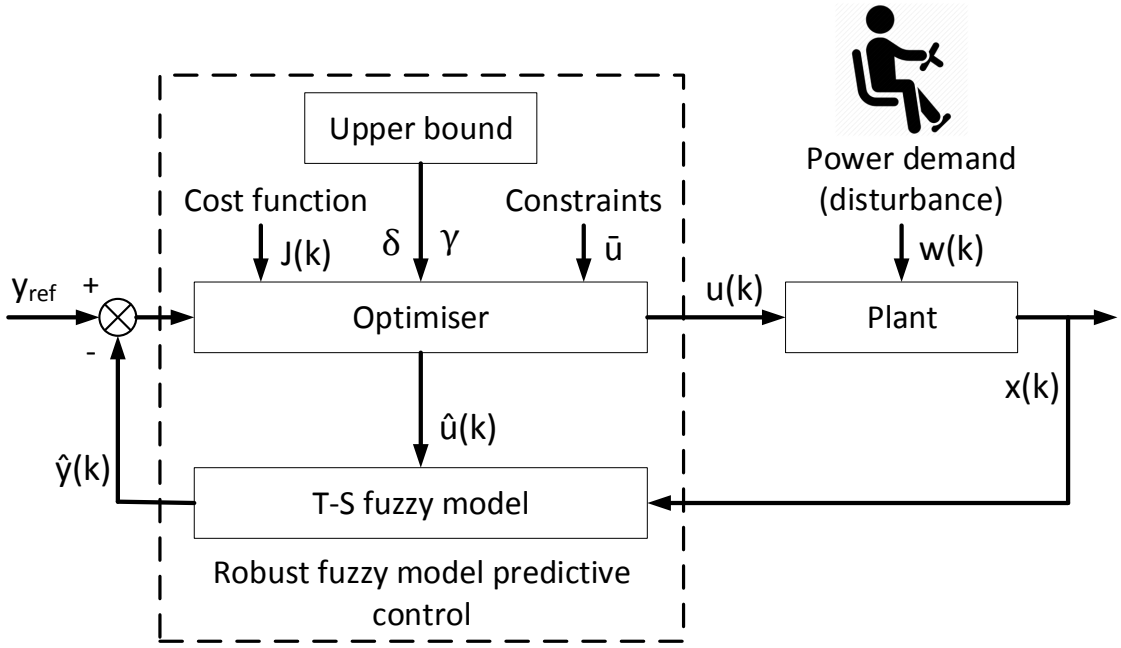

Figure 5.6. Block diagram of the robust fuzzy model predictive control based control scheme

- Step 2: At time step $k+1$, the new measurement $x(k+1)$ is taken, and Step 1 is repeated.

Remark 5.5. *The range of the RPI set* Υ *can be calculated off-line from (5.47). Since the path constraints on the states are imposed by* Υ*, if the maximum range of* Υ *does not exceed the battery SoC limitation, then the battery will not be fully depleted or overloaded over the trip.*

5.3.3 Stability analysis

In this section, we adopt the input-to-state stability framework (Sontag and Wang 1995, Jiang and Wang 2001, Magni *et al.* 2006) for analysing the stability of the proposed RMPC based control scheme. First, we give the following definitions:

Definition 5.2. *If a function* $\kappa : \mathbb{R} \geq 0 \rightarrow \mathbb{R} \geq 0$ *is continuous, strictly increasing, it is called a* $\mathscr{K}$ *function; If a function* $\kappa : \mathbb{R} \geq 0 \rightarrow \mathbb{R} \geq 0$ *is a* $\mathscr{K}$ *function and* $\kappa(k) = \infty$ *as* $k \rightarrow \infty$*, it is called a* $\mathscr{K}_\infty$ *function.*

Definition 5.3. *Consider the discrete-time system*

$$x(k+1) = f(x(k), u(k), w(k)) \tag{5.48}$$

Provided that the disturbance is bounded by $w \in \mathbb{W}$. *A function* $V(*) : \mathbb{R}^n \to \mathbb{R} \geq 0$ *is an input-to-state practical stability Lyapunov function if it satisfies*

$$\theta_1(\|x\|) \leq V(k) \leq \theta_2(\|x\|) \tag{5.49}$$

$$V(x(k+1)) - V(x(k)) \leq -\theta_3(\|x\|) + \phi(\|w\|) \tag{5.50}$$

where $\theta_1, \theta_2, \theta_3$ *are* $\mathcal{K}_\infty$ *functions,* ϕ *is a* $\mathcal{K}$ *function, and* $\|x\|$ *and* $\|w\|$ *are norms of given vectors* x *and* w*, respectively.*

Lemma 5.1 (Input-to-state practical stable (Limón *et al.* 2006))**.** *If there exists an input-to-state practical stability Lyapunov function* $V(k)$ *that satisfies (5.49) and (5.50) for system (5.48), then the system is called input-to-state practical stable.*

Lemma 5.2. *If there exists a feasible solution of the optimisation problem in (5.47) at sampling time* $t = k$*, then the solution is also feasible for all time* $t > k$.

Proof. Since (5.46) is the only matrix inequality in the optimisation problem that depends on the state, we only need to prove that (5.46) is feasible for all time $t > k$.

The feasibility of (5.46) implies $x(k|k)^T P x(k|k) \leq \xi$. Thus, for any time $t > k$, we must prove

$$x(k+i|k)^T P x(k+i|k) \leq \xi \text{ for all } i > 0 \tag{5.51}$$

As shown in (5.31), the matrix inequality in (5.36) implies

$$x(k+i|k)^T P x(k+i|k) \leq x(k|k)^T P x(k|k) \text{ for all } i > 0$$

Thus, (5.51) is guaranteed for any time $t > k$ and the proof is completed. □

Theorem 5.3. *Provided that a feasible solution exists for the optimisation problem in (5.47) at time* $k = 0$*, then the system in (5.26) is input-to-state practical stable.*

Proof. First, from Lemma 5.2, we can guarantee the recursive feasibility of the control law. Then, to guarantee input-to-state practical stable of the system in (5.26), we only need to find an input-to-state practical stability Lyapunov function $V(k)$ that satisfies (5.49) and (5.50).

Consider optimal control gain $K^*(k)$ and $P^*(k)$ at sampling time k, we have

$$v_t^* = x^T(k) P^*(k) x(k) \tag{5.52}$$

$$\lambda_{min}\|x\|^2 \leq v_t^* \leq \lambda_{max}\|x\|^2 \tag{5.53}$$

where λ_{min} and λ_{max} represent minimal and maximal eigenvalues of $P^*(k)$, respectively.

Moreover, from (5.37), we obtain

$$\begin{aligned} v_t^*(x(k+1|k)) - v_t^*(x(k|k)) \leq & \alpha^2(w(k|k)^T w(k|k) + \Delta u(k|k)^T \Delta u(k|k)) \\ & - x^T(k|k)K^*(k|k)L_u K^*(k|k)x(k|k) \end{aligned} \tag{5.54}$$

which satisfies (5.50).

Thus, v_t is an input-to-state practical stability Lyapunov function of the system, and the proof is completed. □

5.3.4 Controller design by incorporating traffic condition

The major disadvantage of using the above RMPC based control scheme for energy management systems is its conservatism since the control law intents to minimise the upper bound of the performance index in (5.40) where γ defined in (5.32) should cover the maximum power that the vehicle can provide.

In some driving scenarios, the upper bound of the power demand is much smaller than the maximum power that the vehicle can provide. For example, in the scenario when the vehicle is stuck in a traffic jam, the upper bound of the power demand is passively limited by the poor traffic condition.

Motivated by the potential feasibility to relax the conditions of the RMPC based control scheme, we incorporate traffic condition into the energy management controller design to further improve the fuel consumption.

To process, we make the following assumption.

Assumption 5.1. *There exists a power upper bound mapping system such that traffic conditions are capable of mapping to the different upper bound of the vehicle power demand by several associative rules.*

An example of the power upper bound mapping from a set of rules is as follows.

- Rule1: If traffic condition is 'excellent', then $\gamma(k) = \theta_1$
- Rule2: If traffic condition is 'good', then $\gamma(k) = \theta_2$
- Rule3: If traffic condition is 'bad', then $\gamma(k) = \theta_3$
- Rule4: If traffic condition is 'poor', then $\gamma(k) = \theta_4$

Given that the mapping between the traffic conditions and the upper bound of the vehicle power demand can be analysed off-line, and that live traffic information service is widely available in many countries, it is reasonable and practical to make Assumption 5.1.

Extended from Fig. 5.6, the block diagram of the new control scheme is shown in Fig. 5.7. Since the upper bound γ is adjustable based on different traffic conditions, the performance index $J(k)$ in (5.38) becomes:

$$J(k) \leq \nu_t(x(k|k)) + \alpha^2(\gamma^*(k)^2 + \delta^2) \tag{5.55}$$

where $\gamma^*(k)$ is the upper bound of the power demand at sampling step k based on the traffic condition.

Intuitively, since $\gamma^*(k) \leq \gamma$, the new control scheme is capable of achieving better control performance in terms of the performance expressed in (5.38) than the RMPC based control scheme with constant γ, but how could we guarantee robust stability and feasibility in the new control scheme?

We first give the procedure for the design of the new control scheme:

Since the upper bounds γ and δ only appear in the matrix inequality in (5.36) of the optimisation problem in (5.47) in the RMPC based control scheme, we only need to rewrite the matrix inequality in (5.36) by

$$\begin{bmatrix} (1-\lambda)Q & \star & \star & \star \\ 0 & \frac{\lambda}{\gamma^*(k)^2+\delta^2} & \star & \star \\ 0 & 0 & \frac{\lambda}{\gamma^*(k)^2+\delta^2} & \star \\ AQ + \frac{B_iM_j+B_jM_i}{2} & \frac{B_i+B_j}{2} & \frac{E_i+E_j}{2} & Q \end{bmatrix} \geq 0 \tag{5.56}$$

Therefore, the procedure for the new control scheme is summarised as follows.

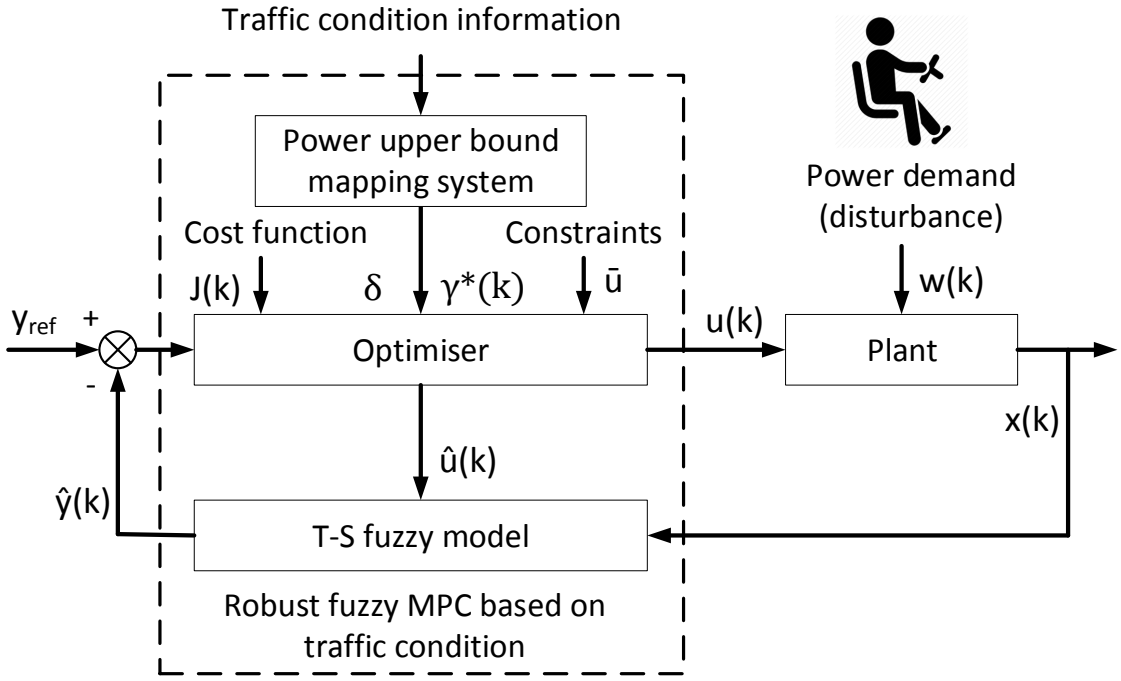

Figure 5.7. Block diagram of the robust fuzzy model predictive control with driving scenario recognition

- Step 1: At sampling step k, control law (5.28) is obtained by solving the following optimisation problem with the fuzzy membership values h_i:

$$\min \xi \tag{5.57}$$
$$\text{subject to (5.44), (5.45), (5.46), (5.56)}$$

- Step 2: At time step $k+1$, new measurement $x(k+1)$ and measurements $\gamma^*(k+1)$ are taken, and go to Step 1 again.

To prove recursive feasibility and stability of the new control scheme, the following useful lemma is given.

Lemma 5.3. *For the system in (5.26), if there exists a solution to the optimisation problem in (5.47) at sampling time $t = k$, the solution of the optimisation problem in (5.57) is also feasible for all $t \geq k$.*

Proof. Suppose that the solution of the optimisation problem in (5.47) is feasible, condition (5.34) must be satisfied. Since γ is defined as the upper bound of $w(k)$ for all

$k \geq 0$, we must have

$$\gamma^*(k)^2 + \delta^2 \leq \gamma^2 + \delta^2 \tag{5.58}$$

Substituting (5.58) into (5.34) yields

$$\begin{aligned}\frac{1}{\xi}[x(k+1)^T P x(k+1) - x(k)^T P x(k)] &\leq \lambda[\frac{w(k)^T w(k) + \Delta u(k)^T \Delta u(k)}{\gamma^2 + \delta^2} - \frac{1}{\xi} x(k)^T P x(k)] \\ &\leq \lambda[\frac{w(k)^T w(k) + \Delta u(k)^T \Delta u(k)}{\gamma^*(k)^2 + \delta^2} - \frac{1}{\xi} x(k)^T P x(k)] \end{aligned} \tag{5.59}$$

As shown in Theorem 5.1, the condition in (5.59) can be cast in the form of LMIs (5.56) to guarantee that Y in (5.29) is a robust positively invariant set for the system. The rest of proof is similar to that of Lemma 5.2 and thus is omitted. □

Theorem 5.4. *The feasible control law obtained by solving the optimisation problem in (5.57) robustly stabilises the T-S fuzzy system in (5.26).*

Proof. Lemma 5.3 states the recursive feasibility of the optimisation problem (5.57). The rest of proof is similar to that of Theorem 5.3 and thus is omitted. □

Remark 5.6. *Since (5.59) implies that (5.56) relaxes the condition of (5.36), the RMPC with varied γ shows less conservative LMI conditions of the close-loop system than the RMPC based control scheme with constant γ. Therefore, by incorporating traffic condition, the RMPC based energy management controller is capable of achieving better control performance with regard to minimising the performance index $J(k)$ in (5.18).*

5.4 Case study

5.4.1 Simulation environment

To illustrate the effectiveness of the proposed control schemes, MATLAB Powertrain Blockset^{TM} is used in the simulation studies. Since the software has not supported LMI toolbox and provided fuel cell models, it is used mainly to simulate the power demand from the driver and then develop a power plant model based on real-world experimental data for verifying the effectiveness of our control schemes. The data acquisition and processing time resolution is set to one second.

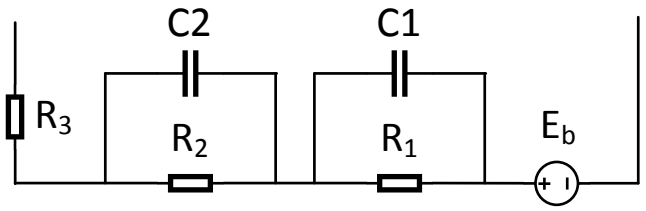

Figure 5.8. Two RC-branch equivalent circuit model in the vehicle simulator

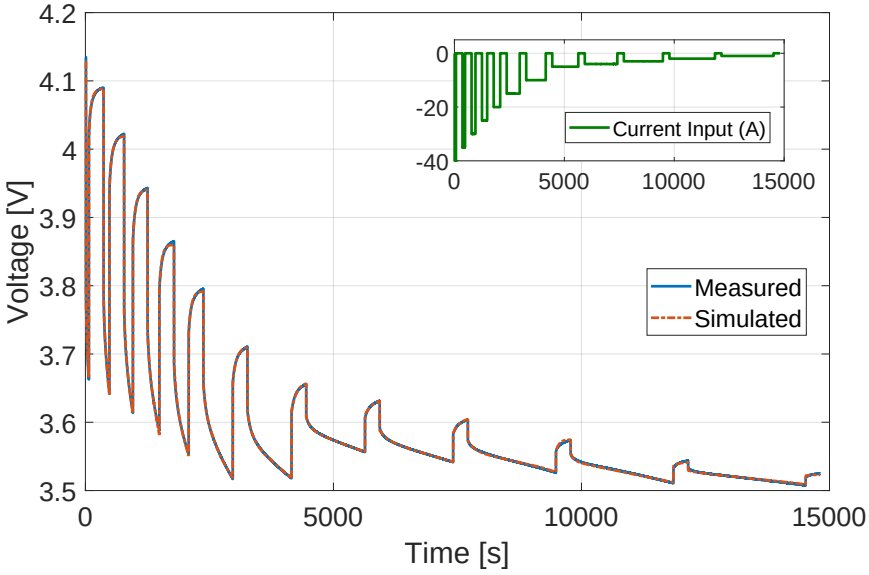

Figure 5.9. Parameters estimation and verification of the battery model

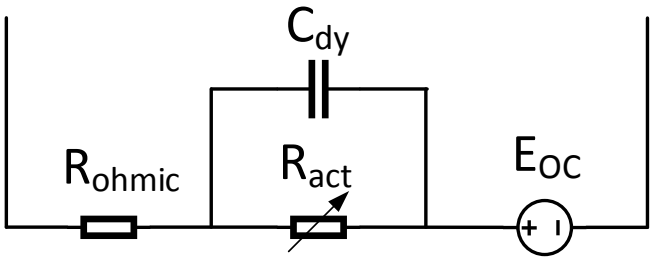

Figure 5.10. Equivalent circuit model in the vehicle simulator

In order to build a high-fidelity model of the fuel cell vehicle system, the following experiments are conducted to build the battery model and fuel cell model in the simulator:

The battery in the vehicle simulator is modelled by a two RC-branch equivalent circuit as shown in Fig. 5.8. A 20Ah prototype lithium-ion Polymer battery is used to estimate and verify the parameters of the model. Discharge current pulses from 40A down to 0A are applied to the prototype, and the corresponding terminal voltage response data is then collected.

The fuel cell is modelled by the equivalent circuit model in Fig. 5.10, by assuming fuel cells operate at optimal condition. A Ballard FCvelocity-9SSL fuel cell stack is used for model verification. Similar to the battery experiment, load current from 0A to 100A are applied to the fuel cell stack, and the corresponding terminal voltage response data is collected.

The results of simulated data from the models and measured data from the prototypes are shown in Fig. 5.9 and Fig. 5.11, respectively. We observe that the battery model and the fuel cell model are capable of capturing the dynamic characteristics of two prototypes well.

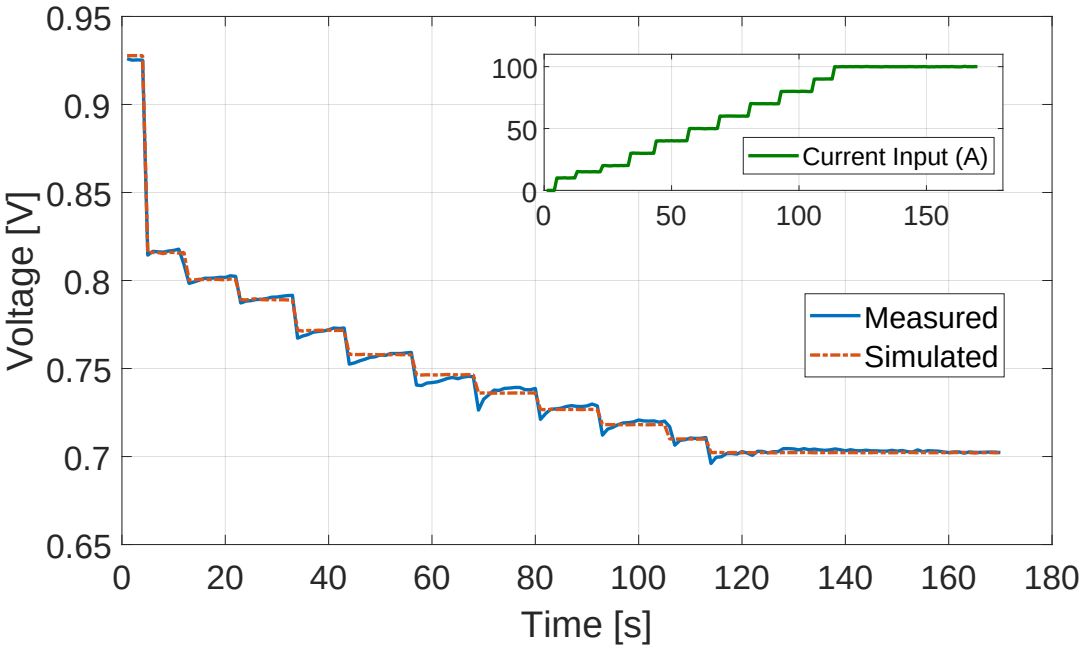

Figure 5.11. Parameters estimation and verification of the fuel cell model

The YALMIP toolbox (Lofberg 2004) with SDPT3 solver (Tütüncü *et al.* 2003) is used to solve the optimisation problems. In the power plant, The battery pack contains 78

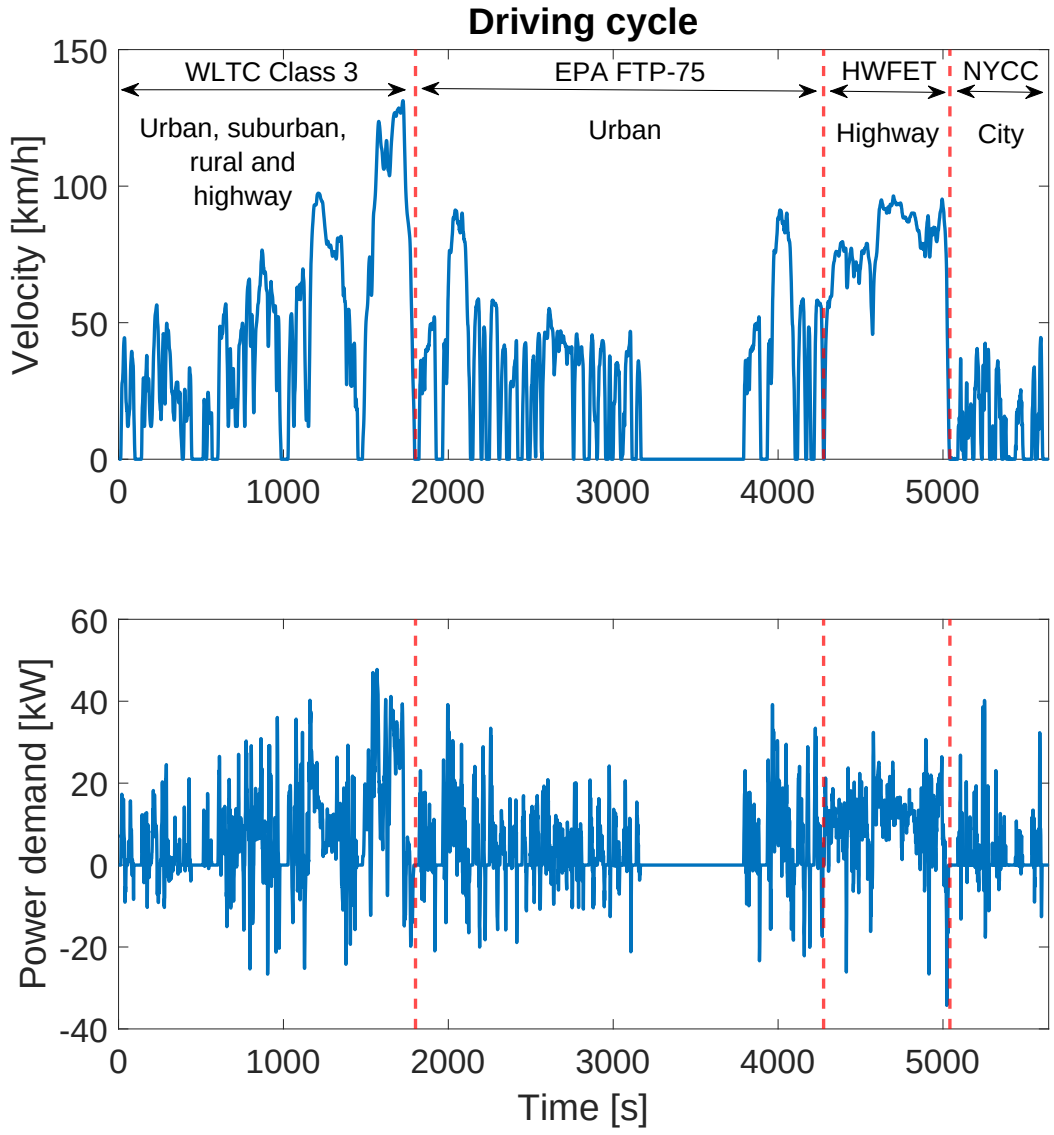

Figure 5.12. Driving cycle used in the case study (top) and power demand of the vehicle in the simulation (bottom)

cells (20Ah) in series then 5 strings in parallel and the fuel cell stack includes 210 cells in series.

In the RMPC based control scheme, the term γ represents the upper bound of the maximum power of the vehicle propulsion system. The term δ represents the upper bound of the uncertainty Δu on the control input to enforce the fuel cell system and the boost converter operate efficiently. Based on the physical constraints of the system, we set $\gamma = 60$ kW and $\delta = 2$ kW.

Moreover, the term λ is the parameter in Theorem 5.1 to ensure Y is an RPI set. The term L_u is the weighting scalar on control input to balance the control effort (fuel consumption) and the terminal cost on the state (battery charge-sustaining). The term α^2 is a parameter before the disturbance part in (5.37) which plays a role to determine the disturbance rejection level of the control system. The primary principle to select λ, L_u and α^2 is to ensure that LMIs (5.44)-(5.46) have a feasible solution while λ is in $(0, 1]$ and α^2 is desired to be small to maintain high-disturbance rejection level. In the case study, we set $\alpha^2 = 9e-5$, $L_u = 1.2e-9$ and $\lambda = 0.06$.

To assess the performance of the proposed control strategy over different driving scenarios, we set a combined driving cycle consisting of one Worldwide Harmonised Light Vehicles Test Procedure (WLTP) Class 3b that was developed by the United Nations Economic Commission for Europe, one Federal Test Procedure 75 (FTP-75) that was defined by US Environmental Protection Agency (EPA), one EPA Highway Fuel Economy Driving Schedule (HWFET), and one EPA New York City Cycle (NYCC). By using the vehicle dynamic model in MATLAB Powertrain Blockset^{TM}, the power demand of the vehicle is simulated. Fig. 5.12 shows the driving velocity and the power demand of the vehicle over a duration of 5641 seconds covering the total distance of 59.44 km. For benchmarking the effectiveness of the proposed control strategies, a dynamic programming (DP) based algorithm, in which the driving cycle is assumed to be a priori known, is used.

5.4.2 Effectiveness of the fuzzy model

To verify the accuracy of the fuzzy model, we compare the battery SoC response (corresponding to state x_1) and DC-BUS voltage response (corresponding to state x_2) between the fuzzy model and the simulator over the driving cycle in the battery-driven mode. Since MPC has the ability to take new measurements (x_1 and x_2) at each sampling time, we further compare the effectiveness of the off-line fuzzy model and fuzzy MPC model in the case study.

The results of the fuzzy model performance are shown in Fig. 5.13. We observe that both the off-line fuzzy model and the fuzzy MPC model work effectively to approximate the nonlinear system. The fuzzy MPC model offers better control performance than that of the off-line fuzzy model. The reason being that new measurements (x_1 and

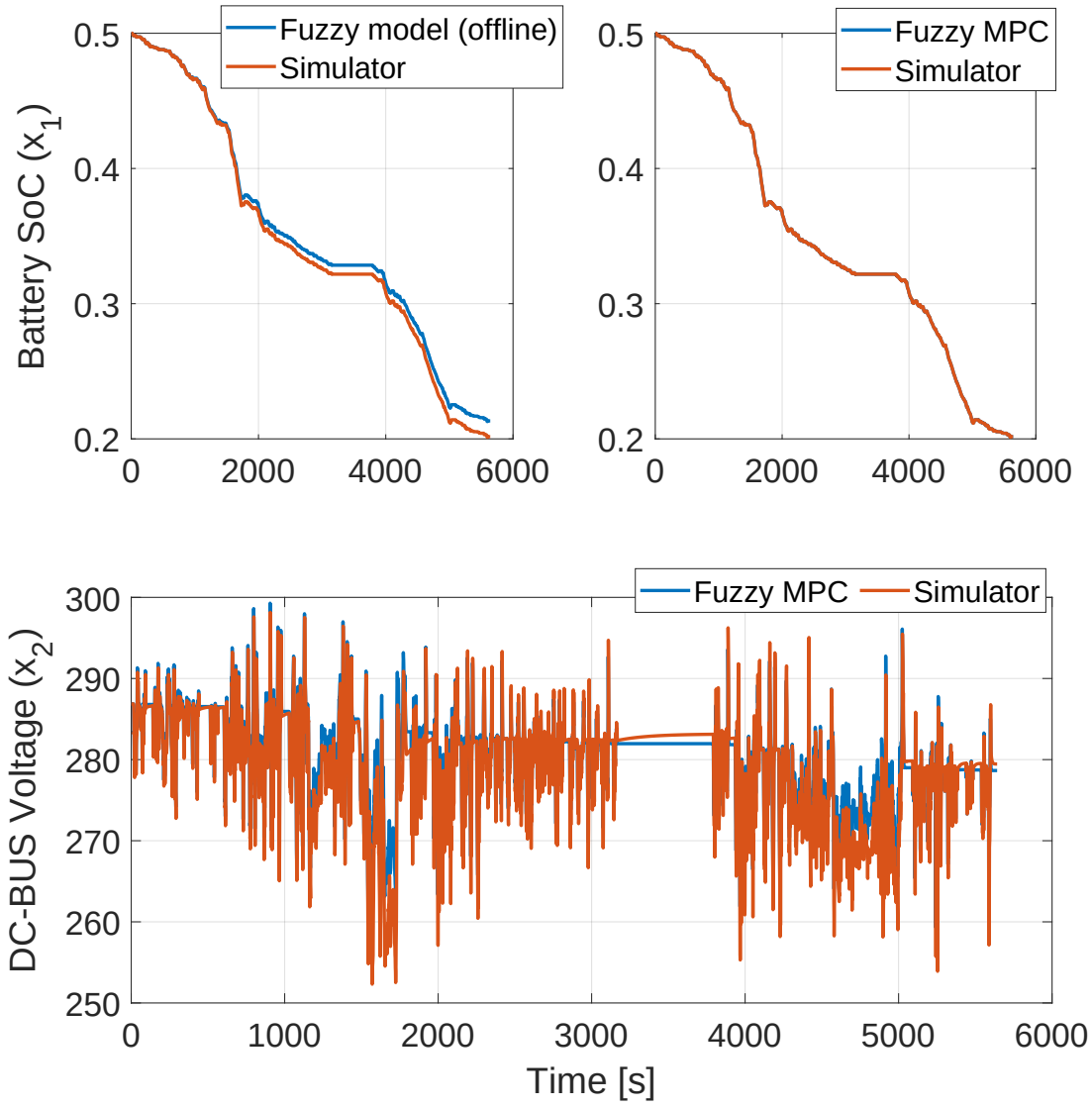

Figure 5.13. Battery SoC output comparison between the off-line fuzzy model and the simulator (top-left), battery SoC output comparison between the fuzzy MPC model and the simulator (top-right), and DC-Bus voltage output comparison between the fuzzy MPC model and the simulator (bottom)

x_2) taken at each sampling time in the fuzzy MPC model enables further model inaccuracy correction and disturbance compensation, where else there is no similar capability in the off-line fuzzy model.

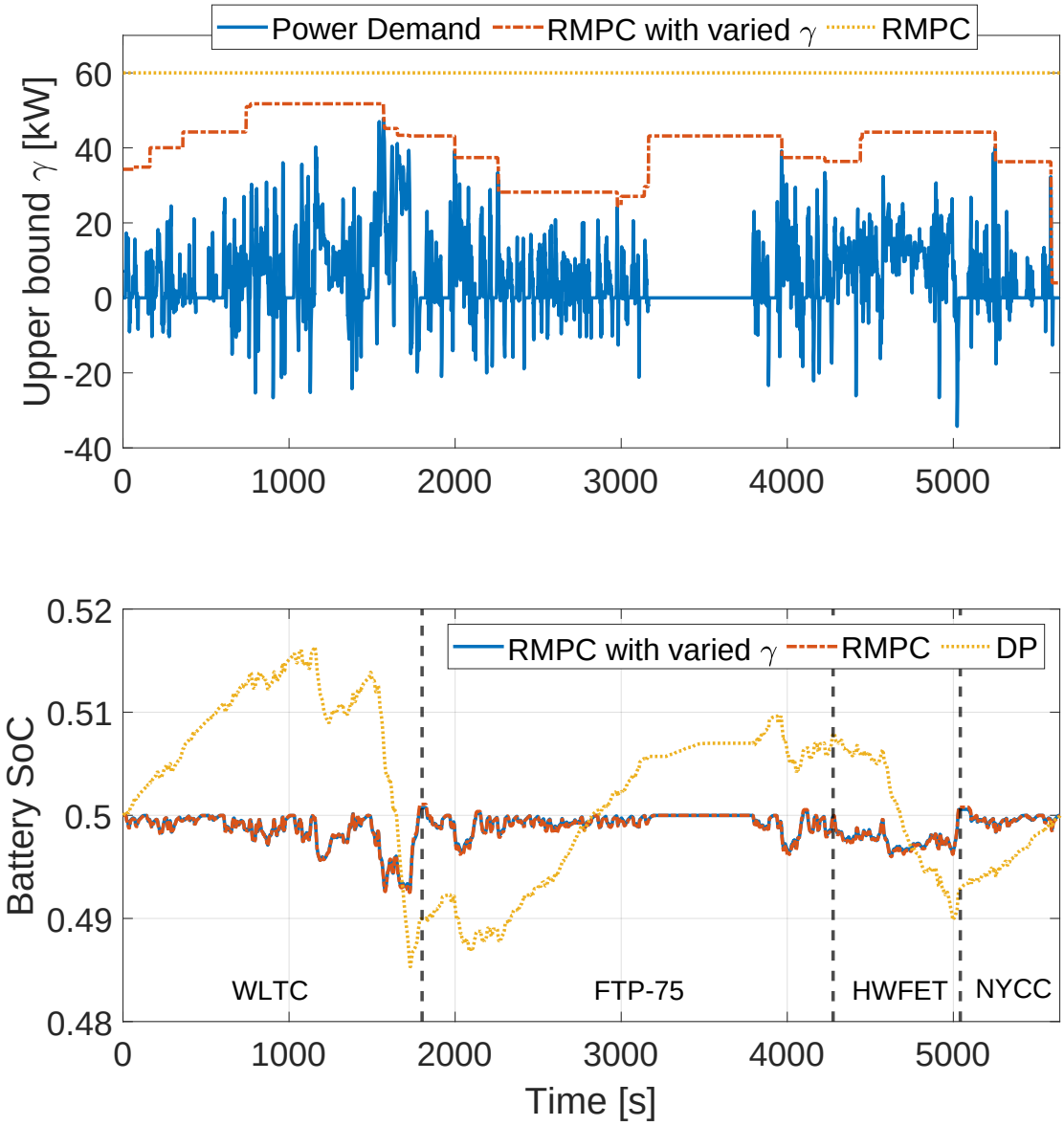

Figure 5.14. Power demand of the vehicle in the case study and upper bound estimation of the power demand under RMPC and RMPC with varied γ (top) and battery state of charge response under RMPC, RMPC with varied γ, and DP (bottom)

5.4.3 Control performance

Shown in Fig. 5.14(a) are two scenarios considered in the case study: a) RMPC with constant $\gamma = 60$ (called "RMPC"), and b) RMPC with vaired γ.

Table 5.1. Numerical results of three control schemes over the driving cycle

WLTC		
Control scheme	Terminal SoC [%]	MPGe
DP	49.00	61.16
RMPC	50.11	54.33
RMPC (varied γ)	50.07	54.66
WLTC+FTP-75		
Control scheme	Terminal SoC [%]	MPGe
DP	50.78	57.46
RMPC	49.99	58.27
RMPC (varied γ)	49.99	58.55
WLTC+FTP-75+HWFET		
Control scheme	Terminal SoC [%]	MPGe
DP	49.29	62.13
RMPC	50.08	59.13
RMPC (varied γ)	50.06	59.38
WLTC+FTP-75+HWFET+NYCC		
Control scheme	Terminal SoC [%]	MPGe
DP	50.00	59.79
RMPC	50.00	58.57
RMPC (varied γ)	50.00	58.79

Fig. 5.14(b) shows the battery SoC response of the system in the presence of disturbance (power demand). We observe that the battery SoC is maintained to the reference value at the end of the driving cycle under all control schemes.

To assess the optimisation performance of the control schemes, we use miles per gallon gasoline equivalent (MPGe) that defined by US EPA to measure the average distance travelled per unit of energy consumed. The formulation to calculate MPGe is

$$\frac{(\text{total mile driven}) \times (\text{energy of one gallon of gasoline})}{\text{total energy consumed}}$$

Fig. 5.15 shows the result of the optimisation performance. We observe that the proposed control schemes are capable of achieving good performance compared to the

global optimal solution that DP provided. While RMPC with varied γ demonstrates the ability to outperform RMPC, which verifies the statement given in Remark 5.6.

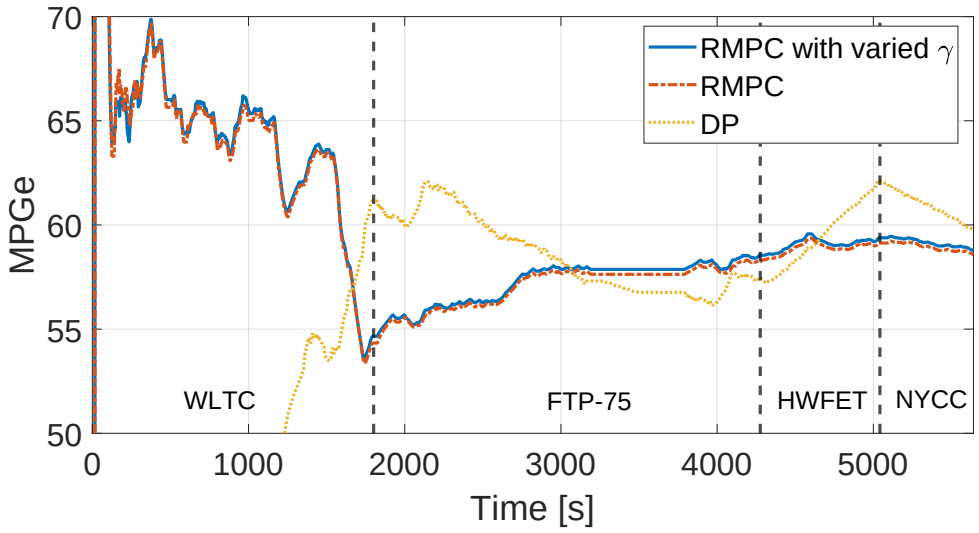

Figure 5.15. Energy consumption comparison among RMPC, RMPC with varied γ, and DP

Furthermore, the numerical results of battery SoC at the terminal points and MPGe of the FCV under three control schemes over the driving cycle are shown in Table 5.1. Since the optimization horizon is the whole driving cycle under the DP based approach, it is clear that battery SoC is maintained at the terminal point for the whole driving cycle, but not at the terminal point of each separate driving cycle.

When comparing with MPGe of DP, we observe that the proposed controllers achieve sub-optimal results. The results in Table 5.1 show that the controllers are applicable for all driving cycles to maintain battery SoC within certain admissible range near the scheduled reference SoC with competitive MPGe performance.

5.4.4 Computational time

Computational burden at each sampling step is a critical limiting factor for a real-time EMS design. Fig. 5.16 shows the computational time of RMPC with varied γ required to calculate the control law $u(k)$ at each sampling time over the driving cycle on a PC with Intel® i7-6700 3.40GHz CPU processor, 16GB RAM, using Simulink R2019a. We observe that the average time to solve the LMI optimisation problem at each sampling

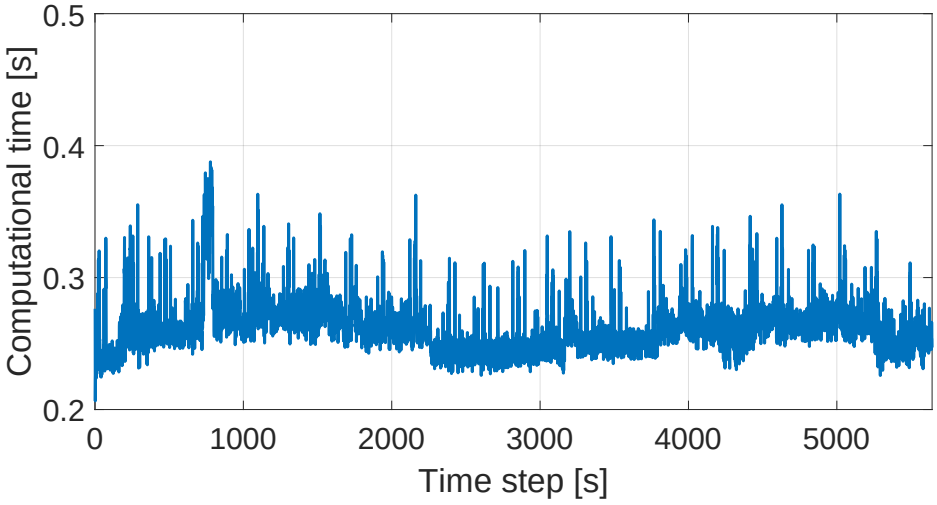

Figure 5.16. Computational time of the RMPC (varied γ) based control scheme in the case study

step is 0.2621s and the maximum time is 0.3877s. The low computational cost shows its applicability in practice.

For the dynamic programming based approach, it takes 83.3116s to solve the optimisation problem since the whole driving cycle is required to consider in the computation. Although the dynamic programming based approach is capable of providing the global optimal solution, the heavy computational burden and the requirements of the prior information of the future power demand limit its ability in a real application.

5.5 Chapter summary

This chapter blends the theoretical analysis and practical issue to develop a new approach for energy management in fuel cell vehicles. The approach is formulated by the T-S fuzzy modelling framework and robust model predictive control technique to leverage real-time driving condition for the energy management controller design. The energy management problem is cast as a convex optimisation problem where the state-feedback control law is obtained online by minimising the upper bound of the cost function, subject to real-time traffic condition system constraints. The advantages of the proposed control scheme have been illustrated by a simulator developed based on real-world experimental data.

In the next chapter, the fuel cell optimisation will be introduced in the energy management system design for prolonging fuel cell lifespan.

Chapter 6

Energy Management Design with Fuel Cell Lifespan Optimisation

In this chapter, we present a novel control scheme for energy management design in fuel cell vehicles. The energy management problem is transformed to a nonlinear optimisation problem with multi-objectives in order to improve fuel economy, maintain battery state of charge, and reduce the incidence of factors affecting the fuel cell performance degradation. A robust model-predictive-based fuzzy control method is employed to design the nonlinear control law. The energy management system is capable of coordinating with a sigma-point Kalman filter based fuel cell stack state of health estimator and an energy storage system scheduler to achieve the optimisation objectives in the presence of uncertainty of the driver's power demand. Furthermore, we conduct a comparative experiment and simulation study under three typical urban/highway driving scenarios to verify the effectiveness and potential of the control scheme.

6.1 Introduction

The robust fuzzy model predictive control based control technique is Chapter 5 shows promising potential for real-time energy management system design in fuel cell vehicles. The remaining practical challenge, fuel cell system optimisation, is not considered in the control scheme. Developing an effective energy management controller to concurrently optimise fuel economy and fuel cell lifespan has been one primary motivation of this study.

To design an effective energy management system in fuel cell vehicles, there are two primary challenging control system requirements:

How to increase the fuel cell system operating efficiency and maintain the battery charge level in an admissible range under various driving scenarios and uncertain fuel cell system state of health?

How to reduce the computational cost of the energy management system in order to respond instantaneously to the power demand input?

To address the challenges, we present a novel energy management system for fuel cell vehicles in this chapter. An online fuel cell state of health estimation and an energy storage system scheduler are incorporated into the energy management system design to achieve optimal control in terms of battery state of charge maintenance, fuel cell durability protection and fuel economy in fuel cell vehicles. The energy management problem is elegantly cast into a trajectory tracking problem under adjustable control input constraints and the robust model predictive control technique under fuzzy modelling framework is employed to design the energy management controller.

The chapter is organised as follows. The energy management problem formulation in a fuel cell vehicle is described in Section 6.2. The design of the new energy management system for fuel cell vehicles is illustrated in Section 6.3. The effectiveness and potential of the proposed design technique are illustrated by various driving scenarios in Section 6.4.

6.2 Problem formulation

We first present the control system model, operational constraints and objective function to formulate the EMS design problem.

6.2.1 System dynamics model

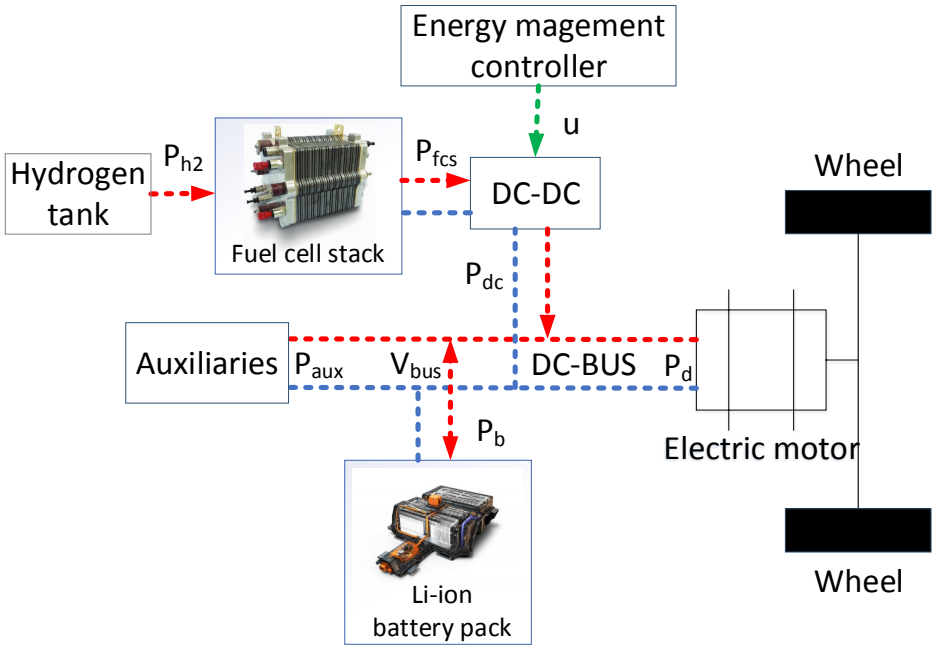

Figure 6.1. Block diagram of a fuel cell vehicle with parallel hybrid configuration

Fig. 6.1 shows the major components of the power system in an FCV where the fuel cell and the battery operate in parallel. At sample time k, we have

$$P_{dc,k} + P_{b,k} = P_{d,k} + P_{aux,k} \tag{6.1}$$

where P_{dc} is the output power from the fuel cell boost converter, P_b is the power delivered from the battery pack, P_d is the power demand from the driver, and P_{aux} is the power consumption for the drive train losses and supply of the auxiliary systems.

Battery dynamic model

The battery is described by an open-circuit voltage v_b in series with an internal resistance R_b as the energy management problem emphasises on energy system efficiency.

The battery's state of charge (SoC) is estimated by coulomb counting, that is

$$SoC_{k+1} = SoC_k - \frac{\eta_f i_{b,k}}{C_n}\Delta t \tag{6.2}$$

where i_b is the instantaneous battery current (we denote positive for discharge and negative for charge), $v_{b,k}$ is the cell's open-circuit voltage, Δt is the sampling period, SoC_k is the battery's SoC at time k, C_n is the battery nominal capacity, and η_f is the battery Faraday efficiency.

The relationship between the cell's SoC and open-circuit voltage v_b is represented by

$$v_{b,k}(SoC_k) = a_0 - \frac{a_1}{SoC_k} - a_2 SoC_k + a_3 \ln(SoC_k) + a_4 \ln(1 - SoC_k) \tag{6.3}$$

where a_0, a_1, a_2, a_3, a_4 are the parametric fitting coefficients. Since the battery pack is passively connected on the DC-BUS, the battery pack output current $I_{b,k}$ is calculated by

$$I_{b,k} = \frac{P_{d,k} + P_{aux,k} - P_{dc,k}}{V_{bus,k}} \tag{6.4}$$

where V_{bus} is the battery terminal voltage. The battery terminal voltage is updated by

$$V_{bus,k+1} = n_s(v_{b,k}(SoC_k) - R_b \frac{P_{d,k} + P_{aux,k} - P_{dc,k}}{n_p V_{bus,k}}) \tag{6.5}$$

where n_s and n_p are the numbers of cells in series and in parallel in the battery pack, respectively.

Fuel cell model

To develop an effective health estimator, the following empirical model is used to describe the fuel cell's V-I characteristic

$$V_f = E_f - b_f \ln \frac{I_f + i_l}{i_l} - r_f I_f - b_0(e^{b_1 I_f} - 1) \tag{6.6}$$

where V_f is the fuel cell stack voltage, I_f is the stack output current, E_f is the open-circuit voltage, b_f is the Tafel constant, r_f is the overall resistance of the cell, i_l is the exchange current density, and the term $b_0(e^{b_1 I_f} - 1)$ represents the mass transfer loss with two parametric fitting coefficients b_0 and b_1.

According to (Bressel *et al.* 2016) regarding the effect of the performance degradation on the electrochemical parameters' value, overall resistance r_f exhibits significant variations when the performance degradation occurs during the operation compared with

Table 6.1. Primary factors for fuel cell performance degradation

Operational condition	Proportion [%]
Sudden load changes	56.8
Frequent start-stop	33
Long-time idling	4.7
Continuous high-power delivery	5.8

other parameters. We thus use the overall resistance as the indicator for the fuel cell's state of health.

Furthermore, based on the fuel cell lifetime evaluation studies in (Pei and Chen 2014, Yu *et al.* 2012), we identify four operational conditions that are contributing to the performance degradation of the fuel cells. Table 6.1 shows these four conditions and their effects on the degradation.

The design of a fuel cell system is complex. A fuel cell system consists of a fuel cell stack, a fuel processor, power conditioners, air compressors, and humidifiers. Based on the test result provided in (Höflinger *et al.* 2017), the efficiency characteristics of a fuel cell stack and the fuel cell system are described in Fig. 6.2. The peak efficiency of the whole fuel cell system occurs around one third of its maximum load. The air compressor, water pump and hydrogen recirculation pump are taken into account in the system's efficiency calculation.

6.2.2 Objectives and challenges

An effective EMS for FCVs should provide the following capabilities during driving operation in the presence of uncertain power demand from the driver and unobservable State of health (SoH) information of the fuel cell stack:

1. maintenance of battery SoC within the admissible range
2. reduction of the negative factors of fuel cell performance degradation shown in Table 6.1 that causes the fuel cell performance degradation
3. maximisation of the vehicle's fuel economy
4. real-time capability to respond instantaneously to the power demand input.

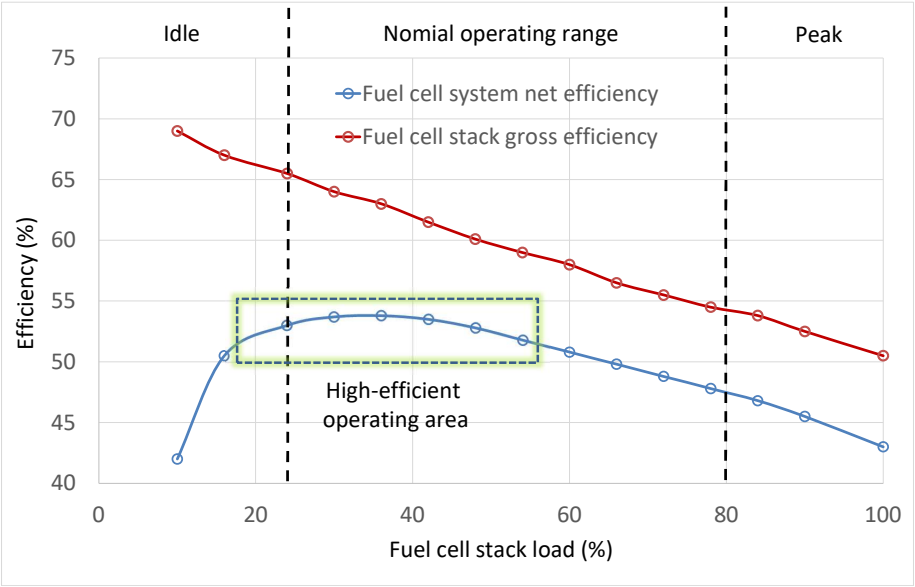

Figure 6.2. Efficiency characteristics of the fuel cell stack and the fuel cell system

Design an effective EMS for FCVs to achieve these objectives in the presence of the constraints is the focus of this study.

6.3 New energy management system design

The block diagram of the proposed energy management system is shown in Fig. 6.3. The system consists of a fuel cell stack SoH estimator, an energy management system scheduler, and an energy management controller.

6.3.1 Fuel cell stack state of health estimator

The fuel cell stack SoH estimator provides high-fidelity estimation of fuel cell stack health status to energy management controller for reducing the negative factors that cause the fuel cell performance degradation.

Recall from Section 6.2.1 that the overall fuel cell internal resistance r_f is defined as the health indicator for fuel cell performance degradation. We extract $E_f, b_f, i_l, r_f, b_0, b_1$

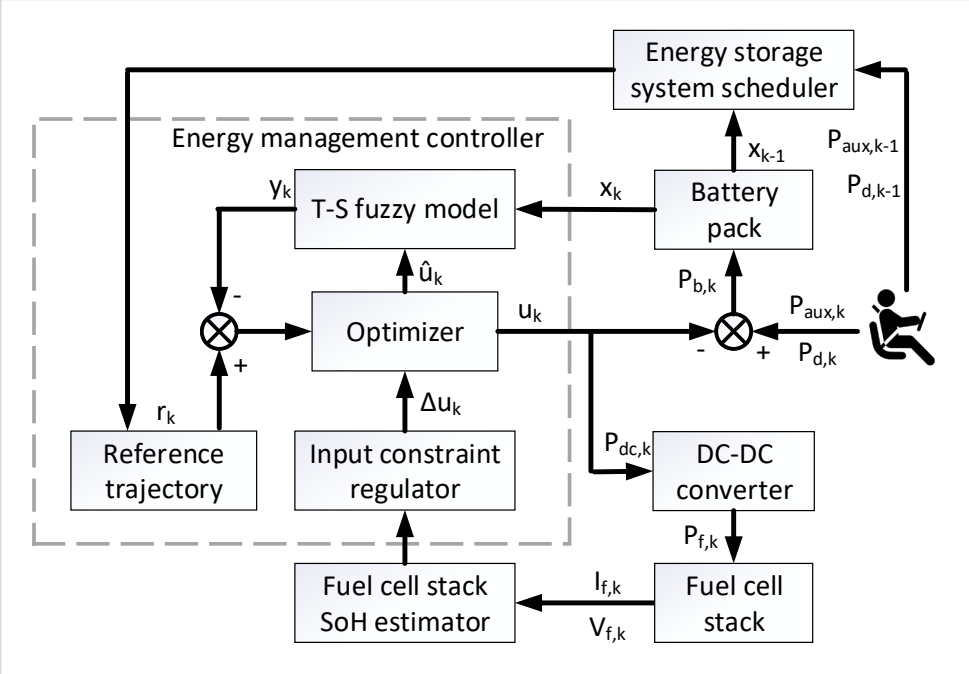

Figure 6.3. Block diagram of the energy management system for fuel cell vehicles

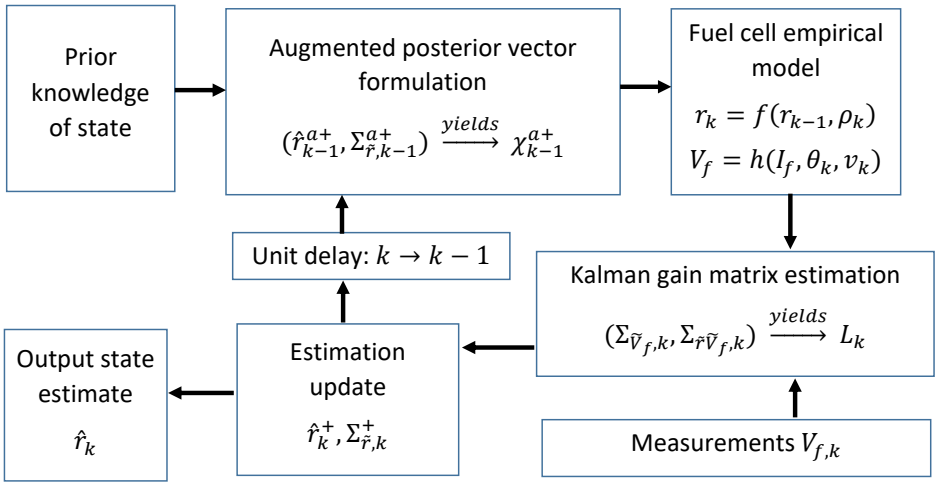

Figure 6.4. Block diagram of sigma-point Kalman filter based overall fuel cell internal resistance estimation

from the empirical model in (6.6) by parameters fitting according to the fuel cell polarisation curve provided in the stack user manual. The obtained r_f is used as the fuel cell overall resistance benchmark value.

To estimate r_f of the fuel cell stack in real time, we use the sigma-point Kalman filtering technique (Wan *et al.* 2001, Wan and Van Der Merwe 2000, Kandepu *et al.* 2008). Its

state estimation usually outperforms that of the extended Kalman filter (EKF), since the sigma-point Kalman filter is based on derivativeless statistical linearisation. Since the fuel cell overall resistance change slowly, we model r_f as a constant with some added small zero mean white noise perturbation ρ_k

$$r_{f,k+1} = f(r_k, \rho_k) = r_{f,k} + \rho_k \tag{6.7}$$

The output equation for the sigma-point Kalman filter is

$$V_{f,k} = h(I_{f,k}, r_{f,k}, v_k) = E_f - b_f \ln \frac{I_{f,k} + i_l}{i_l} - r_{f,k} I_{f,k} - b_0(e^{b_1 I_{f,k}} - 1) + v_k \tag{6.8}$$

where v_k models the sensor and modeling error.

Let p be the dimension of input x. We first form $2p+1$ augmented sigma points as the set χ_k^{a+}

$$\hat{r}_k^{a+} = \{\hat{r}_k^+, \bar{\rho}, \bar{v}\} \quad \Sigma_{\tilde{r},k}^{a+} = \mathrm{diag}(\Sigma_{\tilde{r},k}^+, \Sigma_{\tilde{\rho}}, \Sigma_{\tilde{v}}) \quad \chi_k^{a+} = \{\hat{r}_k^{a+}, \hat{r}_k^{a+} + \gamma\sqrt{\Sigma_{\tilde{r},k}^{a+}}, \hat{r}_k^{a+} - \gamma\sqrt{\Sigma_{\tilde{r},k}^{a+}}\}$$

where $\hat{r}_k^{a+}$ is the augmented a posteriori state estimate vector for the previous time step, $\Sigma_{\tilde{r},k}^{a+}$ is the augmented a posteriori covariance estimate, $\hat{r}_k^+$ is the posteriori estimated state for the previous time step, $\bar{\rho}$ and $\Sigma_{\tilde{\rho}}$ are the mean and covariance of the noise ρ_k, $\bar{v}$ and $\Sigma_{\tilde{r}}$ are the mean and covariance of the noise v_k, and γ is a scaling parameter.

Next, the a priori state estimate $\hat{r}_{k+1}^-$ and covariance estimate $\Sigma_{\tilde{r},k+1}^-$ are computed as

$$\hat{r}_{k+1}^- \approx \sum_{i=0}^{2p} \alpha_i f(\chi_{k,i}^{r+}, \chi_{k,i}^{\rho+}) = \sum_{i=0}^{2p} \alpha_i \chi_{k+1,i}^{r-}$$
$$\Sigma_{\tilde{r},k+1}^- = \sum_{i=0}^{2p} \beta_i (\chi_{k+1,i}^{r-} - \hat{r}_{k+1}^-)(\chi_{k+1,i}^{r-} - \hat{r}_{k+1}^-)^T$$

where α_i and β_i are the weighting scalars for each sigma point, and $\chi_{k,i}^{r+}$ and $\chi_{k,i}^{\rho+}$ are the state portion and process-noise portion in χ_k^{a+}, respectively.

Then, the output estimate $\hat{V}_{f,k}$ and the covariance estimate $\Sigma_{\tilde{v},k}$ are obtained from

$$\hat{V}_{f,k} \approx \sum_{i=0}^{2p} \alpha_i h(I_{f,k}, \chi_{k,i}^{r+}, \chi_{k,i}^{v+}) = \sum_{i=0}^{2p} \alpha_i \nu_{k,i}$$
$$\Sigma_{\tilde{v},k} = \sum_{i=0}^{2p} \beta_i (\nu_{k,i} - \hat{V}_{f,k})(\nu_{k,i} - \hat{V}_{f,k})^T$$

Table 6.2. Fuel cell SoH health rating level

	Excellent	Good	Average	Poor
$\hat{r}_k$	$\leq r_1$	$(r_1, r_2]$	$(r_2, r_3]$	$> r_3$

$r_{i\in[1,3]}$ is the reference value for each health rating level

The Kalman filter gain L_k is computed as

$$\Sigma^{-}_{\tilde{r}\tilde{v},k} = \sum_{i=0}^{2p} \beta_i (\chi^{r-}_{k+1,i} - \hat{r}^{-}_{k+1})(\nu_{k,i} - \hat{V}_{f,k})^T$$

$$L_k = \Sigma^{-}_{\tilde{r}\tilde{y},k} \times \Sigma_{\tilde{y},k}$$

Combining the fuel cell stack terminal voltage measurement and the output estimate yields the a posteriori state estimate and the error covariance

$$\hat{r}^{+}_k = \hat{r}^{-}_k + L_k(V_{f,k} - \hat{V}_{f,k}) \tag{6.9}$$

$$\Sigma^{+}_{\tilde{x},k} = \Sigma^{-}_{\tilde{x},k} - L_k \Sigma_{\tilde{v},k} L^T_k \tag{6.10}$$

With the numerical value $\hat{r}^{+}_k$ obtained from (6.9) at k, we classify the operation of the stack SoH into the following four health rating levels, in which "Excellent" represents the best health status and "Poor" is the lowest rating. The selection of $r_{i\in[1,3]}$ is based on the overall resistance benchmark value r_f extracted by parameters fitting from the fuel cell polarisation curve in the user manual.

To summarise, the estimation procedure for the operation of the fuel cell stack SoH is as follows.

- At time k, new measurements $V_{f,k}$ and $I_{f,k}$ are taken.
- The Kalman filter gain matrix L_k is updated and the overall fuel cell internal resistance $\hat{r}^{+}_k$ is estimated.
- By comparing $\hat{r}^{+}_k$ with $r_{i\in[1,3]}$ in Table 6.2, the fuel cell SoH health rating level is indicated.

6.3.2 Energy storage system scheduler

The energy storage system scheduler optimises the energy stored in the battery pack and indicates the desired SoC set-point of the battery pack to the energy management

controller for assisting the fuel cell stack to optimally track the high-efficient area of the fuel cell system. Fig. 6.3 illustrates their connection and data flow.

First, based on the efficiency characteristics of the fuel cell system in Fig. 6.2, we set the desired fuel cell system output power $P_{fcs,r}$ to one-third of its maximum load (peak efficiency) as

$$P_{fcs,r} = \frac{\eta_{dc}}{3} P_{fcs,max} \tag{6.11}$$

where $P_{fcs,max}$ is the fuel cell system admissible maximum load and η_{dc} is the efficiency of the fuel cell boost converter at the power point.

Substituting (6.11) into (6.1) yields

$$P_{b,k} = P_{d,k} + P_{aux,k} - P_{fcs,r} \tag{6.12}$$

Then, substituting (6.12) into (6.2) gives optimal battery SoC level reference $SoC_{r,k+1}$ as follows

$$SoC_{r,k+1} = SoC_k - \frac{\eta_f \Delta t}{C_n} \times \frac{P_{d,k} + P_{aux,k} - P_{fcs,r}}{V_{bus,k}} \tag{6.13}$$

The scheduler is constrained by

$$(SoC_{r,k+1} - SoC_{r,k}) \in \Delta SoC_r, \quad SoC_{r,k} \in [30\%, 70\%]$$

The main challenge to obtain the optimal battery SoC reference in (6.13) is the uncertainty of $P_{d,k}$. In practice, $P_{d,k}$ is determined by the driver's driving behaviour, but predicting human behaviour is always challenging.

To better explain the point, we conducted a real-world driving experiment in our previous work (Shen *et al.* 2020b). In the experiment environment, one driver took a four-lap driving with a golf cart prototype in a campus following a fixed route at a weekend (few students on campus). Fig. 6.5 shows the raw power demand data collected from the golf cart over the driving experiment. As shown from the result, the driver performed different driving behaviors in four laps even the exterior information is almost the same.

To address the issue, we proposed a frozen-time scheduler where power demand P_d and system bus voltage V_{bus} are assumed constant at adjacent sampling points. That is, in the optimal battery SoC reference calculation in (6.13), we have

$$\hat{P}_{d,k} + \hat{P}_{aux,k} \approx P_{d,k-1} + P_{aux,k-1}$$

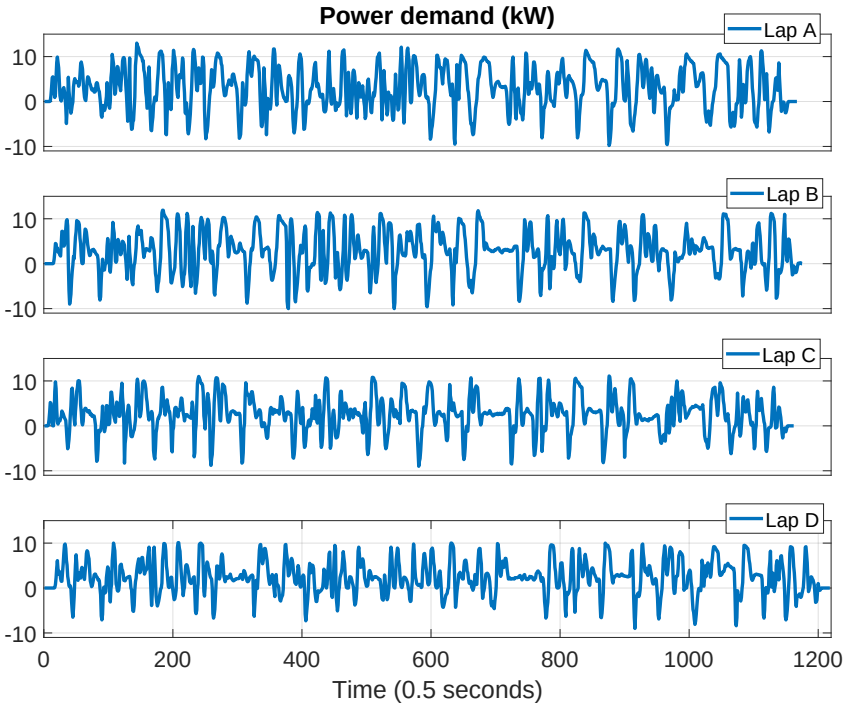

Figure 6.5. Power demand from the golf cart prototype in a four-laps driving experiment

$$\hat{V}_{bus,k} \approx V_{bus,k-1}$$

where $\hat{P}_{d,k} + \hat{P}_{aux,k}$, and $\hat{V}_{bus,k}$ are the prediction of the power demand and system bus voltage at time k, respectively.

Furthermore, by using receding horizon principle, new measurements are taken at each time step to compensate the predictive inaccuracy.

To validate the performance of the frozen-time scheduler, the following two energy storage system schedulers are proposed as the benchmark

- Proportional scheduler (P scheduler). The battery SoC reference $SoC_{r,k}$ is scheduled according to some proportionality to the difference between the desired set-point $P_{fcs,r}$ and the current measured power demand $P_{fcs,k}$, that is,
  If $P_{fcs,k} < P_{fcs,r}$, then we increase $SoC_{r,k}$ with an admissible increment $\Delta SoC_{r,k}$.
  If $P_{fcs,k} > P_{fcs,r}$, then we decrease $SoC_{r,k}$ with the admissible increment $\Delta SoC_{r,k}$.
- Constant scheduler. The battery SoC reference $SoC_{r,k}$ is set to a constant.

6.3.3 Energy management controller

The energy management controller is to regulate the power flow between the fuel cells and energy storage system in real-time during vehicle driving. The critical functions that an effective energy management controller are required to perform to meet the control objectives in Section 6.2.2 are (i) to track the generated battery SoC reference trajectory and (ii) to incorporate the fuel cell SoH estimation into the controller design to reduce the negative factors affecting fuel cell performance degradation.

To achieve the objectives, the following practical challenges remain:

- How to track the reference SoC trajectory effectively subject to online adjustable input constraint and uncertain power demand in various driving scenarios.

- The energy system dynamic is nonlinear which may cause the high computational cost to solve the energy management optimisation problem.

To address the challenges, we propose a novel robust-model-predictive based energy management controller under a fuzzy modelling framework.

In the controller design, we adopt the robust control technique to provide the functionality of disturbance rejection. Model predictive control technique is used to cover the adjustable control input constraint in the optimisation and compensate the predictive inaccuracy in the frozen-time scheduler. By using the T-S fuzzy model, we blend the local linear tasks to deliver the overall model. Consequently, we are able to devise a robust model predictive control methodology to address the challenges with low computational complexity.

In the following, we use the fuzzy modelling framework to approximate the nonlinear plant. Then, we incorporate the fuel cell SoH estimator and energy storage system scheduler into the control design. We complete this section by describing the nonlinear control law design and discussing theoretical analysis for stability and feasibility of the controller.

Fuzzy modelling framework

We first define the system states, control input and disturbances acting on the system as follows.

$$x_{1,k} = SoC_k \quad x_{2,k} = V_{bus,k} \quad u_k = P_{dc,k} \quad w_k = P_{d,k} + P_{aux,k}$$

From (6.2) - (6.5), we have,

$$x_{1,k+1} = x_{1,k} - \frac{\eta_f \Delta t}{n_p C_n} \frac{1}{x_{2,k}} (w_k - u_k) \tag{6.14}$$

$$x_{2,k+1} = n_s v_{b,k}(x_{1,k}) - \frac{n_s R_b}{n_p} \frac{1}{x_{2,k}} (w_k - u_k) \tag{6.15}$$

To approximate the nonlinear system, a T-S fuzzy model is constructed by using sector nonlinearity. The underlying idea of sector nonlinearity is as follows.

Consider a nonlinear function $f(x_k)$, where $f(x) \in [a_2, a_1]x$. At any x_k in the boundary, the nonlinear function is represented by

$$f(x_k) = h_1(x_k)a_1 + h_2(x_k)a_2$$

where $h_1(x_k) + h_2(x_k) = 1$. Therefore $h_1(x_k)$ and $h_2(x_k)$ can be calculated as

$$h_1(x_k) = \frac{f(x_k) - a_2}{a_1 - a_2} \quad h_2(x_k) = \frac{a_1 - f(x_k)}{a_1 - a_2} \tag{6.16}$$

In the system model in (6.14) and (6.15), the nonlinear terms are $v_{b,k}(x_{1,k})$ and $\frac{1}{x_{2,k}}$. Consequently, we define $h_{1,k} \equiv v_{b,k}(x_{1,k})$ and $h_{2,k} \equiv \frac{1}{x_{2,k}}$. Then, we have

$$x_{k+1} = \begin{bmatrix} 1 & 0 \\ n_s h_{1,k} & 0 \end{bmatrix} x_k + \begin{bmatrix} \frac{\eta_f \Delta t}{n_p C_n} h_{2,k} \\ \frac{n_s R_b}{n_p} h_{2,k} \end{bmatrix} u_k - \begin{bmatrix} \frac{\eta_f \Delta t}{n_p C_n} h_{2,k} \\ \frac{n_s R_b}{n_p} h_{2,k} \end{bmatrix} w_k$$

where $x = [x_1, x_2]^T$.

By considering operational limitations $x_{1,k} \in [20\%, 80\%]$ and $x_{2,k} \in n_s[v_b(0,2), v_b(0,8)]$, we calculate the boundary of $h_{1,k}$ and $h_{2,k}$ as

$$h_{1,k} \in [h_{1,min}, h_{1,max}]x_1, \quad h_{2,k} \in [h_{2,min}, h_{2,max}]$$

where h_{max} and h_{min} are the maximum and minimum values of h, respectively. Consequently, $h_{1,k}$ and $h_{2,k}$ are represented by

$$h_{1,k} = M_1(h_{1,k})h_{1,max} + M_2(h_{1,k})h_{1,min}$$

$$h_{2,k} = N_1(h_{2,k})h_{2,max} + N_2(h_{2,k})h_{2,min}$$

Following (6.16) yields

$$M_1(h_{1,k}) = \frac{h_{1,k} - h_{1,min}}{h_{1,max} - h_{1,min}} \quad M_2(h_{1,k}) = \frac{h_{1,max} - h_{1,k}}{h_{1,max} - h_{1,min}}$$
$$N_1(h_{2,k}) = \frac{h_{2,k} - h_{2,min}}{h_{2,max} - h_{2,min}} \quad N_2(h_{2,k}) = \frac{h_{2,max} - h_{2,k}}{h_{2,max} - h_{2,min}}$$

We name the membership functions "High" and "Low", "Big" and "Small" for M and N, respectively. The nonlinear system model is thus approximated by the following fuzzy model

Model Rule 1:

IF $h_{1,k}$ is "High" and $h_{2,k}$ is "Big"

THEN $x_{k+1} = A_1 x_k + B_1 u_k + C_1 w_k$

Model Rule 2:

IF $h_{1,k}$ is "High" and $h_{2,k}$ is "Small"

THEN $x_{k+1} = A_2 x_k + B_2 u_k + C_2 w_k$

Model Rule 3:

IF $h_{1,k}$ is "Low" and $h_{2,k}$ is "Big"

THEN $x_{k+1} = A_3 x_k + B_3 u_k + C_3 w_k$

Model Rule 4:

IF $h_{1,k}$ is "Low" and $h_{2,k}$ is "Small"

THEN $x_{k+1} = A_4 x_k + B_4 u_k + C_4 w_k$

Here,

$$A_1 = A_2 = \begin{bmatrix} 1 & 0 \\ n_s h_{1,max} & 0 \end{bmatrix}, A_3 = A_4 = \begin{bmatrix} 1 & 0 \\ n_s h_{1,min} & 0 \end{bmatrix}$$
$$B_1 = B_3 = \begin{bmatrix} \frac{\eta_f \Delta t}{n_p C_n} h_{2,max} \\ \frac{n_s R_b}{n_p} h_{2,max} \end{bmatrix}, B_2 = B_4 = \begin{bmatrix} \frac{\eta_f \Delta t}{n_p C_n} h_{2,min} \\ \frac{n_s R_b}{n_p} h_{2,min} \end{bmatrix}$$
$$C_1 = C_3 = -\begin{bmatrix} \frac{\eta_f \Delta t}{n_p C_n} h_{2,max} \\ \frac{n_s R_b}{n_p} h_{2,max} \end{bmatrix}, C_2 = C_4 = -\begin{bmatrix} \frac{\eta_f \Delta t}{n_p C_n} h_{2,min} \\ \frac{n_s R_b}{n_p} h_{2,min} \end{bmatrix}$$

The defuzzification is carried out as

$$x_{k+1} = \sum_{i=1}^{4} m(z_{i,k})(A_i x_k + B_i u_k + C_i w_k) \tag{6.17}$$

where

$$m(z_{1,k}) = M_1(h_{1,k}) \times N_1(h_{2,k}) \quad m(z_{2,k}) = M_1(h_{1,k}) \times N_2(h_{2,k})$$
$$m(z_{3,k}) = M_2(h_{1,k}) \times N_1(h_{2,k}) \quad m(z_{4,k}) = M_2(h_{1,k}) \times N_2(h_{2,k})$$

To track the battery SoC reference set-point, the fuzzy system output is defined as

$$y_k = Hx_k \quad H = [1, 0] \tag{6.18}$$

Remark 6.1. *The fuzzy model here is used as an approximator of nonlinear functions in which the membership function is constructed based on the nonlinear terms in the system. Consequently, the model-based fuzzy control can make use of a large number of powerful control tools available for linear systems.*

Problem reformulation

To incorporate the fuel cell SoH estimator and the energy storage system scheduler into the control design, we reformulate the system model in which the controlled object is the increment of the FCS output power instead of the original stack output power.

Define

$$\tilde{x}_k = x_k - x_{k-1}, \quad \tilde{u}_k = u_k - u_{k-1}, \quad \tilde{w}_k = w_k - w_{k-1},$$
$$\tau_{r,k} = SoCr, k, \quad \tilde{\tau}_{r,k} = \tau_{r,k} - \tau_{r,k-1}, \quad \tilde{\xi}_k = y_k - \tau_{r,k},$$
$$\psi_k = [\tilde{x}_k, \tilde{\xi}_{k-1}]^T, \quad \kappa_k = [\tilde{w}_k, \tilde{\tau}_{r,k}]^T$$

Then, the system model in (6.17) expressed in terms of the fuzzy system is as follows:

$$\begin{cases} \psi_{k+1} = \sum_{i=1}^{4} m(z_{i,k})(\mathcal{A}_i\psi_k + \mathcal{B}_i\tilde{u}_k + \mathcal{C}_i\kappa_k) \\ \tilde{\xi}_k = \mathcal{D}\psi_k + \mathcal{E}\kappa_k \end{cases} \tag{6.19}$$

where

$$\mathcal{A}_i = \begin{bmatrix} A_i & 0 \\ H & I \end{bmatrix}, \mathcal{B}_i = \begin{bmatrix} B_i \\ 0 \end{bmatrix}, \mathcal{C}_i = \begin{bmatrix} C_i & 0 \\ 0 & -I \end{bmatrix}, \mathcal{D} = \begin{bmatrix} H, I \end{bmatrix}, \mathcal{E} = \begin{bmatrix} 0, -I \end{bmatrix}$$

The energy management controller is designed as

$$\tilde{u}_k = \sum_{i=1}^{4} m(z_{i,k}) K_i \psi_k \tag{6.20}$$

where K_i are the feedback gains of the controller.

Note that controller (6.20) is called the fuzzy state-feedback controller and is nonlinear in general.

Thus, the control design problem is cast as a reference trajectory tracking problem subject to satisfying input constraint:

Design a real-time fuzzy state-feedback controller of form (6.20) for fuzzy system (6.19) such that the $\mathcal{H}_\infty$ attenuation level δ^2 is minimised to adapt to parametric changes. The optimisation problem is subject to the following control performance index

$$\sup_{\kappa_k \neq 0} \frac{||\xi_k||_{\mathcal{L}_2}}{||\kappa_k||_{\mathcal{L}_2}} \leq \delta^2 \tag{6.21}$$

and the control input constraint

$$\tilde{u}_k^T \tilde{u}_k \leq \bar{u}_k^2 \tag{6.22}$$

where $\bar{u}_k$ denotes the upper bound on the control input at sampling time k.

Remark 6.2. *In the problem formulation, the fuel cell stack SoH estimator is incorporated into the control input constraint (6.22) via setting the upper bound for the input constraint $\bar{u}_k$, while the energy storage system scheduler is taken into account in the system output $\xi_k = y_k - \tau_{r,k}$ which affects $\mathcal{H}_\infty$ control performance of the system in constraint (6.21).*

Remark 6.3. *The system operational cost is optimised by the energy storage system scheduler in terms of tracking the battery SoC reference set-point. Consequently, we only consider the problem of disturbance attenuation in the energy management controller design with no cost imposed on the control input.*

Energy management controller design

To address the formulated control problem given in (6.21), the model predictive control principle (Mayne 2014, Kwon and Han 2006) and robust positively invariant (RPI) set (Blanchini 1999, Mayne *et al.* 2006) concept are adopted in the controller design to provide sufficient conditions to guarantee the optimisation recursive feasibility and system stability.

The definition of RPI for discrete-time systems is given in Definition 5.1 in Chapter 3.

We define the candidate invariant set Ψ for the fuzzy model (6.19) as follows

$$\Psi = \{\psi \in \mathbb{R}^n : \psi^T P \psi \leq 1\} \tag{6.23}$$

where P is a positive definite matrix.

We then introduce the following RPI set lemma, which will be used in Theorem 6.1.

Lemma 6.1 ((Alessandri *et al.* 2004)). *The set Ψ in (6.23) is an RPI set if*

$$\psi_k^T P \psi_k \geq \frac{\kappa_k^T \kappa_k}{\sigma_0^2} \tag{6.24}$$

implies

$$\psi_{k+1}^T P \psi_{k+1} \leq \psi_k^T P \psi_k \tag{6.25}$$

where σ_0 is the known upper bound of κ_k for all time $k > 0$, that is

$$\kappa_k^T \kappa_k \leq \sigma_0^2 \tag{6.26}$$

Using the S-procedure technique (Iwasaki *et al.* 2000), the condition specified in (6.24) implies that (6.25) holds if there exists a constant $\lambda \in (0, 1]$ such that

$$\psi_{k+1}^T P \psi_{k+1} - \psi_k^T P \psi_k - \lambda(\frac{\kappa_k^T \kappa_k}{\sigma_0^2} - \psi_k^T P \psi_k) \leq 0 \tag{6.27}$$

Remark 6.4. *The upper bound σ_0 of the disturbance κ_k consists of two elements. The first element $\tilde{w}_k$ indicates the maximum increment of the power demand. The second element $\tilde{\tau}_{r,k}$ provides the maximum increment of the SoC reference ΔSoC_r in (6.13) for battery SoC reference scheduling.*

To incorporate the fuel cell SoH estimation into the controller design, we make the following assumption:

Assumption 6.1. *There exists a constant upper bound $\bar{u}_0$ on the control input such that such that for all time k, the following constraint is imposed*

$$\tilde{u}_k^T \tilde{u}_k \leq \bar{u}_0^2 \leq \bar{u}_k^2 \tag{6.28}$$

Remark 6.5. *In practice, Assumption 6.1 is feasible where $\bar{u}_0$ provides the baseline (minimal constraint) that we can impose on the increment of the fuel cell output power according to the estimated fuel cell performance degradation.*

Now, we present the first result of this chapter as follows. For notational convenience, the star in Theorem 6.1 denotes the transposed matrices for symmetric positions.

Theorem 6.1. *Consider the fuzzy system in (6.19). Suppose that the candidate invariant set for the fuzzy system is defined by (6.23) and a scalar λ satisfies $\lambda \in (0, 1]$, then the fuzzy state feedback matrices $K_{i\in[1,4]}$ in control law (6.20) that minimise the $\mathcal{H}_\infty$ attenuation level δ on the control performance function specified in (6.21) and ensure Ψ in (6.23) is an RPI set for the fuzzy system, are given by*

$$K_i = Y_i Q^{-1} \tag{6.29}$$

where the matrices Y_i and $Q > 0$ are obtained by solving the following linear objective minimisation problem

$$\min_{Q, Y_1, \ldots, Y_4} \delta^2$$

subject to:

$$\begin{bmatrix} Q & 0 & \star & (\mathcal{D}Q)^T \\ 0 & \delta^2 & (\frac{\mathcal{C}_i+\mathcal{C}_j}{2})^T & \mathcal{E}^T \\ \frac{\mathcal{A}_i Q+\mathcal{B}_i Y_j+\mathcal{A}_j Q+\mathcal{B}_j Y_i}{2} & \frac{\mathcal{C}_i+\mathcal{C}_j}{2} & Q & 0 \\ \mathcal{D}Q & \mathcal{E} & 0 & I \end{bmatrix} \geq 0 \tag{6.30}$$

$$\begin{bmatrix} (1-\lambda)Q & 0 & \star \\ 0 & \lambda/\sigma_0^2 & (\frac{\mathcal{C}_i+\mathcal{C}_j}{2})^T \\ \frac{\mathcal{A}_i Q+\mathcal{B}_i Y_j+\mathcal{A}_j Q+\mathcal{B}_j Y_i}{2} & \frac{\mathcal{C}_i+\mathcal{C}_j}{2} & Q \end{bmatrix} \geq 0 \tag{6.31}$$

$$\begin{bmatrix} Q & Y_i^T \\ Y_i & \bar{u}_0^2 \end{bmatrix} \geq 0 \tag{6.32}$$

$$\begin{bmatrix} 1 & \psi_k^T \\ \psi_k & Q \end{bmatrix} \geq 0 \tag{6.33}$$

for $i \geq j$ subject to $m(z_i, k) \cap m(z_j, k) \neq \emptyset$

Proof. The proof is given in Appendix C. □

Thus the energy management controller design has been redefined to repeatedly solving the optimal control problem in Theorem 6.1 over a receding horizon where the nonlinear fuzzy state-feedback control law to minimise the $\mathcal{H}_\infty$ attenuation level δ on the control performance function is obtained at each sampling time k.

We give the following corollary to prove the feasibility of the optimisation in Theorem 6.1 over the receding horizon manner.

Corollary 6.1. *Any feasible solution of the optimisation in Theorem 6.1 at sampling time k is also feasible for all times $t > k$. Consequently, if there exists a feasible solution of the optimisation problem in Theorem 6.1 at time k, then the problem is feasible for all times $t > k$.*

Proof. Provided the optimisation problem in Theorem 6.1 is feasible at time k, the LMI in the optimisation problem in Theorem 6.1 depends explicitly on the measured state ψ_k of the system is (6.33). Consequently, to prove the corollary, we only need to prove that this LMI is feasible for time $k+1$.

Using Lemma 6.1, LMI (6.31) ensures that (6.23) is an RPI set. Consequently, we must have

$$\psi_{k+1}^T P \psi_{k+1} \leq 1$$

which implies

$$\begin{bmatrix} 1 & \psi_{k+1}^T \\ \psi_{k+1} & Q \end{bmatrix} \geq 0$$

Hence, the optimisation problem is feasible at time $k+1$ and the corollary is proved. □

In Theorem 6.1, we consider the constant upper bound $\bar{u}_0$ on the control input (the increment of the fuel cell output power). Based on the estimated fuel cell stack health status, the control input constraint can be further relaxed by implementing varied upper bound $\bar{u}_k$ as in (6.28). With the relaxed constraint on the control input, the controller is capable of achieving better control performance in terms of the $\mathcal{H}_\infty$ control performance index in (6.21).

We now state the algorithm of the energy manage system, which concurrently incorporates the fuel cell SoH estimator and the energy storage system scheduler into the energy management controller design.

Algorithm 6.1 (Fuzzy model predictive control)**.** *Consider the fuzzy system in (6.19) subject to input constraint (6.1). The energy management control law is calculated at time step k as follows*

1. *The fuel cell stack SoH estimator evaluates the fuel cell stack health status and identifies the upper bound of the control input constraint ($\bar{u}_k$).*

2. *The energy storage system scheduler evaluates the fuel cell system operational efficiency and indicates the tracking reference ($\tau_{r,k}$).*

3. *The energy management controller computes the fuzzy state feedback matrices $K_{i\in[1,4]}$ by using Theorem 6.1 with the following input constraint to replace (6.32):*

$$\begin{bmatrix} Q & Y_i^T \\ Y_i & \bar{u}_k^2 \end{bmatrix} \geq 0 \tag{6.34}$$

The following corollary is used to prove the feasibility of the optimisation in Algorithm 6.1.

Corollary 6.2. *If a feasible solution of the minimisation problem in Theorem 6.1 exists at sampling step k, then the optimisation problem in Algorithm 6.1 is feasible for all times $t > k$.*

Proof. To prove the corollary, we need only to prove that (6.34) is feasible at time k under Assumption 1. Suppose that the optimisation problem in Theorem 6.1 is feasible at time k and Assumption 6.1 holds. Then, from (6.28), we have

$$\begin{aligned} &\sum_{i=1}^{4} m(z_{i,k}) \sum_{j=1}^{4} m(z_{j,k}) \psi_k^T \left(\frac{1}{\bar{u}_k^2} K_i^T K_j - P\right) \psi_k \\ &\leq \sum_{i=1}^{4} m(z_{i,k}) \sum_{j=1}^{4} m(z_{j,k}) \psi_k^T \left(\frac{1}{\bar{u}_0^2} K_i^T K_j - P\right) \psi_k \leq 0 \end{aligned} \tag{6.35}$$

Following the proof in Theorem 6.1, condition (6.35) implies (6.34). Thus, the corollary is proved. □

A critical problem encountered in the control law design is that asymptotic stability of the origin cannot be established when the disturbances are merely bounded, the best that can be achieved is robust asymptotic stability of a set Z (Mayne *et al.* 2005). The stability analysis of the controlled system follows.

Theorem 6.2. *The feedback control law given by Algorithm 6.1 drives the state ψ_k in fuzzy system (6.19) asymptotically to the invariant set Ψ.*

Proof. Suppose that the set Ψ in (6.23) is an RPI set for the controlled system. From (6.27), we have

$$\psi_{k+1}^T P \psi_{k+1} - \psi_k^T P \psi_k \leq \lambda(\kappa_k^T \kappa_k / \sigma_0^2 - \psi_k^T P \psi_k) \tag{6.36}$$

Since the disturbance is bounded by (6.26), we obtain

$$\kappa_k^T \kappa_k / \sigma_0^2 \leq 1 \tag{6.37}$$

In the case that the state ψ_k is out of the set Ψ, that is, $\psi_k^T P \psi_k > 1$, we must have

$$\kappa_k^T \kappa_k / \sigma_0^2 - \psi_k^T P \psi_k \leq 0 \tag{6.38}$$

Substituting (6.38) into (6.36) yields

$$\psi_{k+1}^T P \psi_{k+1} - \psi_k^T P \psi_k \leq 0$$

Consequently, $\psi_{k+1}^T P \psi_{k+1}$ is a Lyapunov function for the controlled system regarding to the set Ψ. Theorem 6.2 is thus proved. □

6.4 Case studies

To verify our EMS design for FCVs, we use a vehicle driving simulation in the MATLAB/Simulink environment with Powertrain Blockset™(MathWorks 2020) and LMI toolbox with SeDuMi solver (Lofberg 2004).

Fig. 6.6 shows the set of fully assembled reference electric vehicle system (provided by Powertrain Blockset™) used in the simulation. In the vehicle simulator, the energy system consists of a 90-cell proton-exchange membrane fuel cell stack where a Ballard FCvelocity®–9SSL fuel cell stack (Ballard 2020) is used as the prototype and a lithium-ion battery pack made up of 5 parallel packs and each containing 88 cells in series where the 2Ah, INR18650 lithium-ion cylindrical cell from (CALCE 2020) is used as the prototype. Table 6.3 shows the primary vehicle parameters in the vehicle simulator. The proposed EMS is then implemented into the controller block in the vehicle simulator for performance validation.

Although the simulation environment cannot entirely reflect the situation in real-world experiments, the vehicle simulator provides a realistic driving environment for verifying the proposed energy management system design.

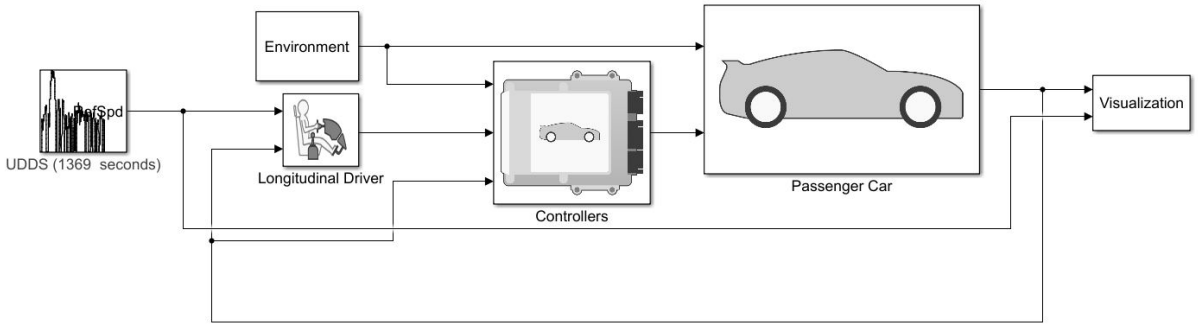

Figure 6.6. Electric vehicle system provided by Powertrain Blockset

Table 6.3. Primary vehicle parameters in the vehicle simulator

Parameters	Values
Vehicle mass [kg]	1850
Drag coefficient	0.28
Frontal area [m^2]	2.27
Lift coefficient	0.1
Center of gravity (CG) height above axles [m]	0.5
Horizontal distance from CG to front axle [m]	1.188
Horizontal distance from CG to rear axle [m]	1.512

By using the battery experimental data collect from (CALCE 2020) and the fuel stack performance benchmark given by the product manual (Ballard 2020), we first estimate the parameters in our battery OCV-SoC model (6.3) and fuel cell V-I model (6.6). Shown in Fig. 6.7 is the estimation results where the parameters used in the models are $a_0 = 2.3898, a_1 = 0.0922, a_2 = -1.8513, a_3 = -0.7924, a_4 = -0.0124, a_5 = 0.0200, E_f = 0.965, b_f = 0.0486, i_l = 1.9513, b_0 = 0.0001, b_1 = 0.02$.

Furthermore, the parameters used for the controller design in Theorem 6.1 is set as follows. The term $\lambda \in (0, 1]$ in (6.31) is set to 0.1, the upper bounds σ_0 of the disturbance in (6.31) is set to $[40, 0.001]$ where the first element denotes the maximum incremental power (kW/s) of the vehicle while the second provides the maximum SoC reference increment (%/s). The parameters in Table 6.2 are set to $r_1 = 0.0003$, $r_2 = 0.0004$, $r_3 = 0.0005$ to classify the stack SoH, and the upper bound of the control input $\bar{u}_0$ are

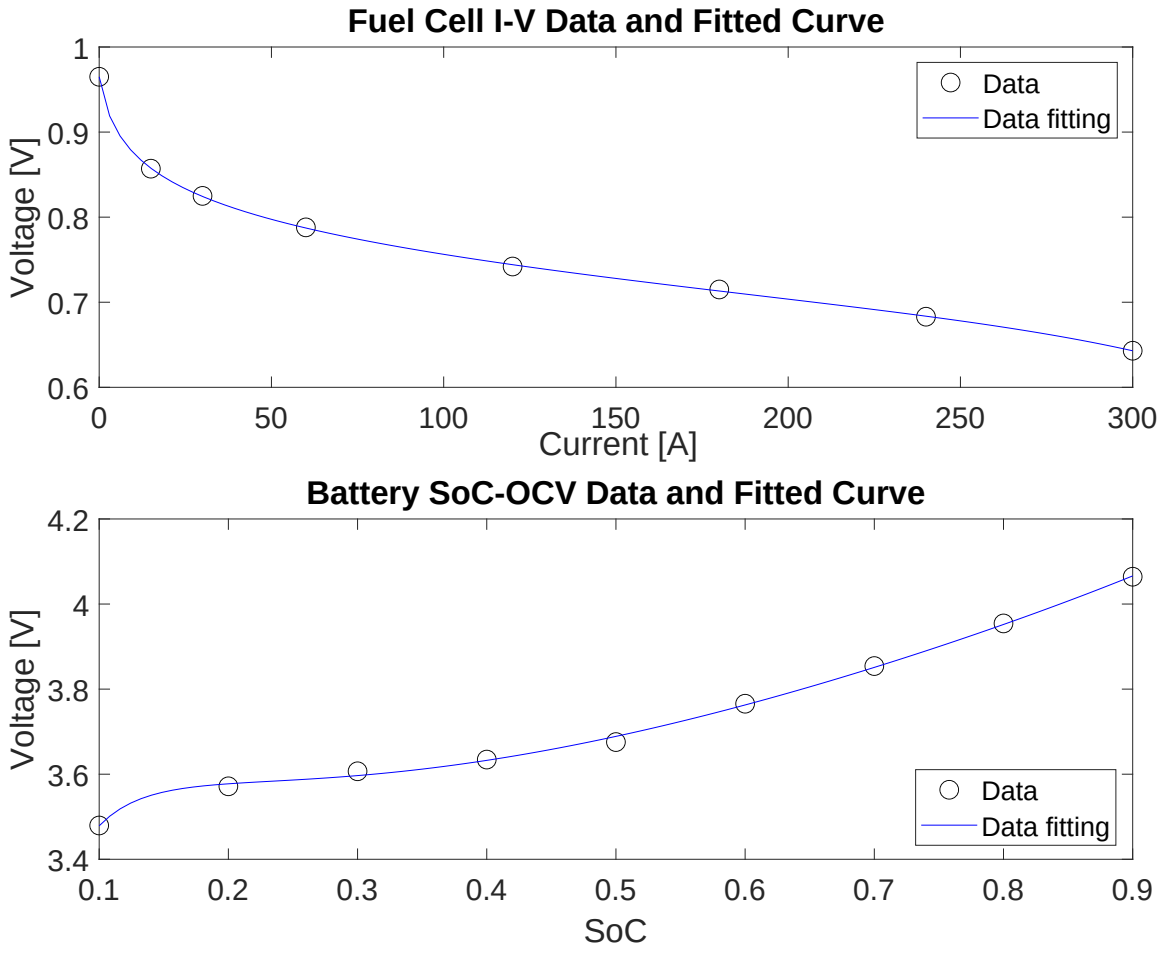

Figure 6.7. Parameters estimation in the battery and fuel cell models

set to 2kW, 3kW, 4kW, 5kW and 6kW in 'Poor', 'Average', 'Good', 'Excellent' status, respectively.

6.4.1 Fuzzy model performance

The control law for the FCV system is obtained under the T-S fuzzy model framework given in Section 6.3.3. It is necessary to validate the effectiveness of the fuzzy model that approximates the FCV nonlinear system and we conduct the following comparison experiment

- Input the dynamic current profiles from the battery experimental data in (CALCE 2020) into the fuzzy model specified in (6.19).

- Compare the voltage response (x_2) and SoC (x_1) between the battery experimental data and fuzzy model output.

Furthermore, two fuzzy models are used in the approximation comparison.

- Off-line fuzzy model. The model approximates the nonlinear system via build-in model (6.19) only.
- MPC fuzzy model. The fuzzy model given in (6.19) incorporates with receding horizon principle to approximate the nonlinear system.

Fig. 6.8 shows the comparison result. It shows that the fuzzy model approximates the battery dynamic response effectively. Moreover, compared with off-line fuzzy model, MPC fuzzy model offers better performance to approximate the FCV nonlinear system. The reason being that new measurements taken at each step with receding horizon principle compensates for the model inaccuracy and disturbance interference due to the uncertain power demand from the driver, whereas there is no corresponding disturbance-compensation functionality in the off-line mode.

6.4.2 Fuel cell stack state of health estimator performance

We assess the estimation accuracy of the proposed fuel cell stack SoH estimator by the following experiments

- Given a dynamic overall internal resistance, we compare the estimated resistance from the estimator with the hypothetical true value based on the stack dynamic V-I response in the simulation.
- We observe the stack SoH estimator performance based on a set of real-world fuel cell experimental data.

Shown in Fig. 6.9 is the simulation result. We observe that the proposed fuel cell stack SoH estimator works effectively in terms of the precision to estimate the stack internal resistance based on the fuel cell empirical model. The results of the estimator performance based on the experimental data are shown in Fig. 6.10. Compared with the V-I

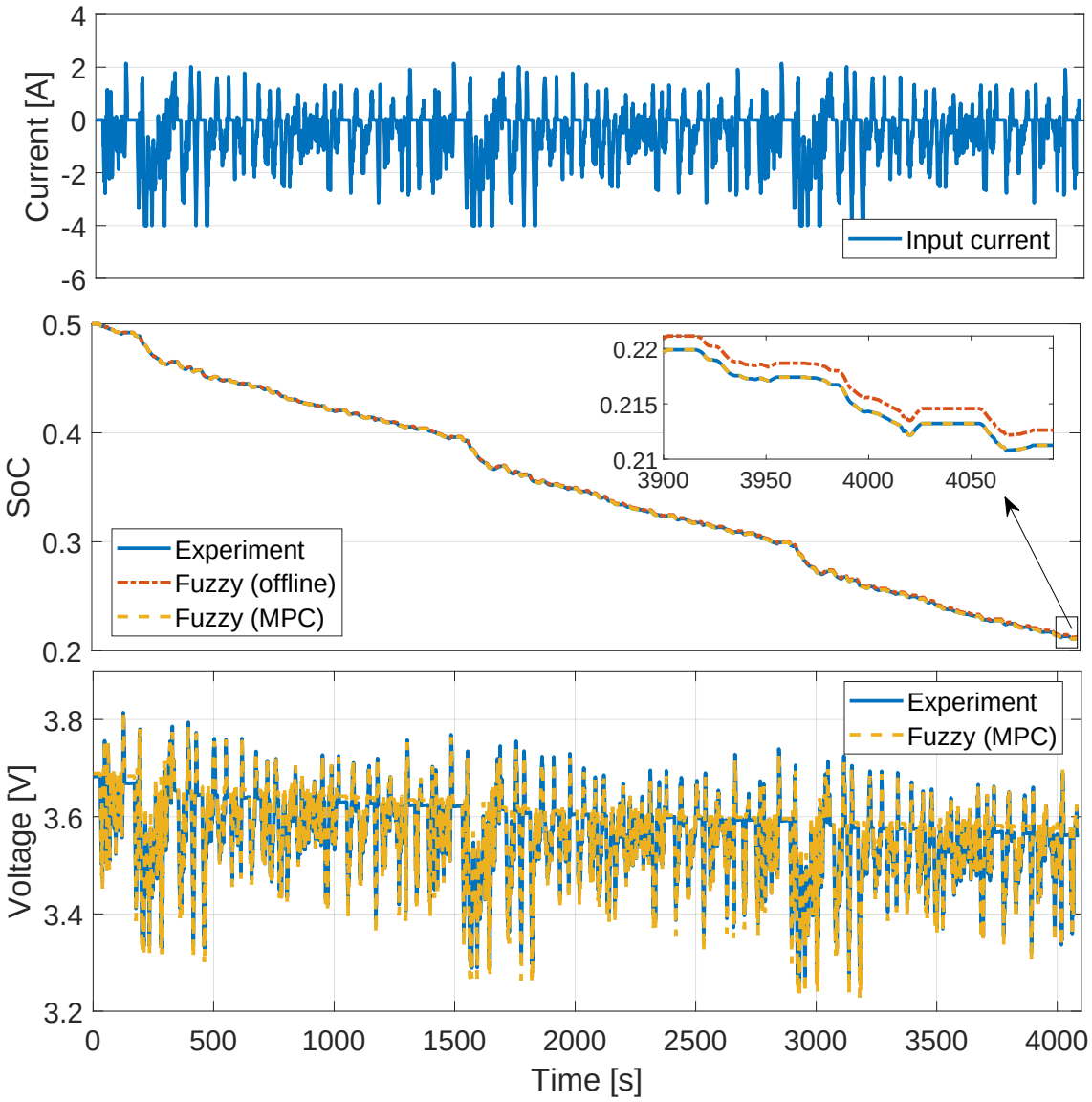

Figure 6.8. Battery dynamic current profiles in the experiment (top), battery SoC (x_1) comparison between the experiment data and fuzzy model output (middle), and battery voltage (x_2) response between the experiment data and fuzzy model output (bottom)

response in the simulation, we observe that there are some atypical measurements in the experimental data caused by sensor measurement error and stack slow dynamic response. From the results, the SoH estimator shows the ability to estimate internal resistance in the presence of senor measurement error and uncertainty and indicates the unusual situations by its 3-sigma error bounds of the estimates.

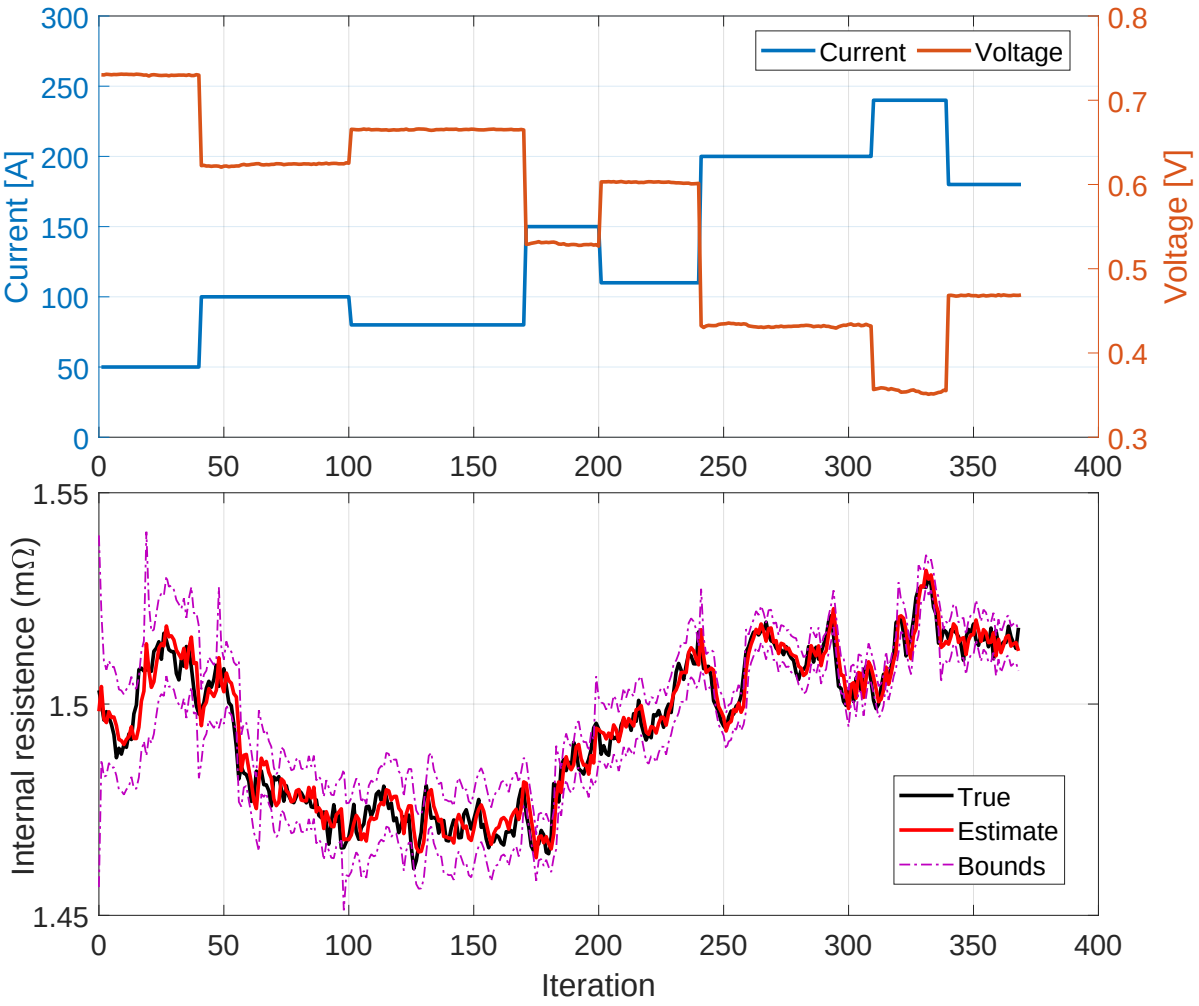

Figure 6.9. Simulated fuel cell stack dynamic response (top); Estimated overall internal resistance with confidence bounds compared with true value (bottom)

6.4.3 Energy management controller performance

We assess the performance of the energy management controller in the developed vehicle simulator under three driving scenarios. They are the Highway Fuel Economy Test (HWFET) to simulate highway driving condition, the Urban Dynamometer Driving Schedule (UDDS) to simulate urban driving condition, and the New York City Cycle (NYCC) to simulate low-speed city driving condition. Fig. 6.11 shows the velocity and power demand profiles of the driving cycles.

The battery reference SoC tracking illustrates the $\mathcal{H}_\infty$ control performance in (6.21) that we adopted in our controller design. The battery SoC responses in Fig. 6.12 show that

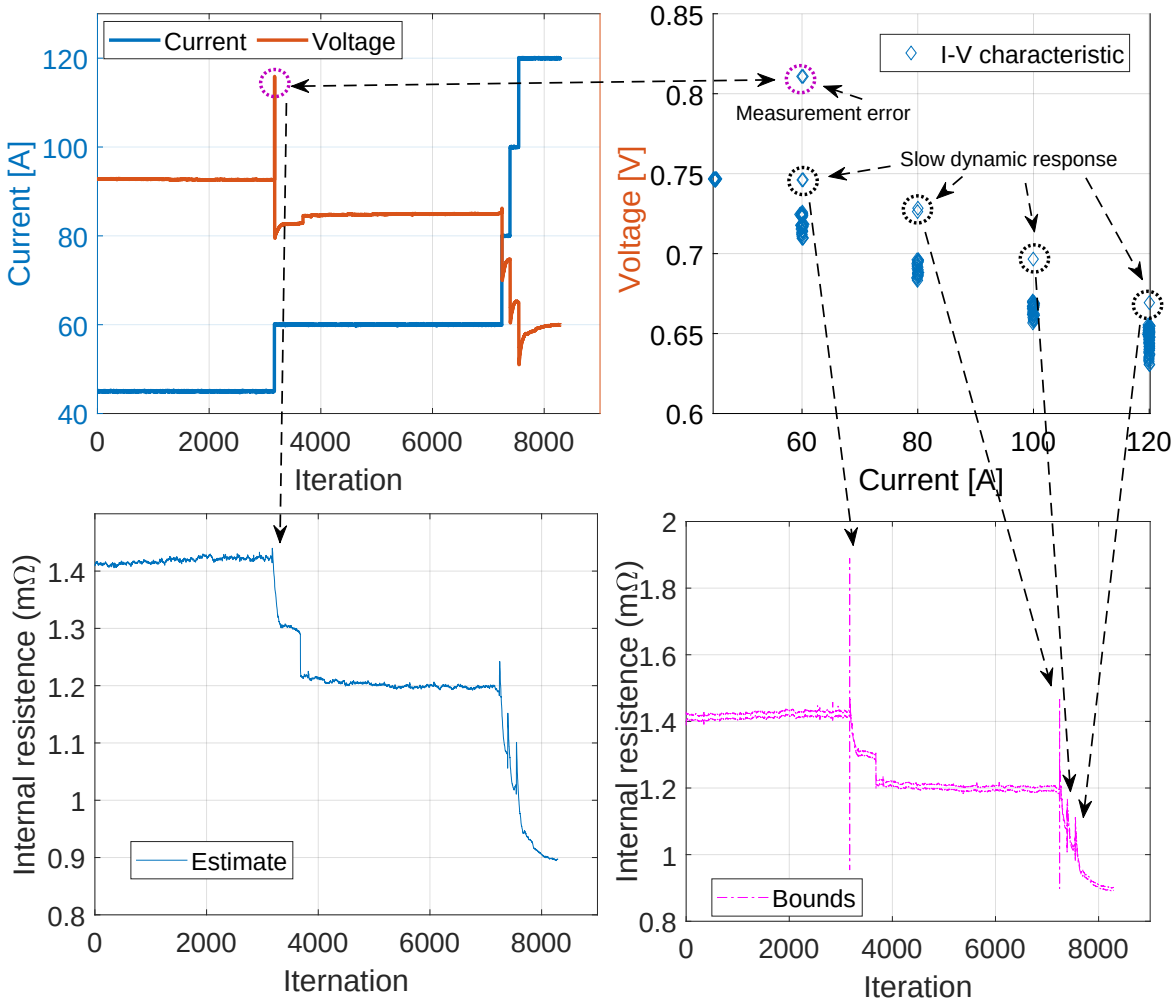

Figure 6.10. Estimated overall internal resistance with the error bounds based on the experimental data

the energy management controller shows the capability to maintain the battery's SoC in an admissible range to track the constant reference under four estimated stack SoH status in all driving scenarios. Consequently, we conclude that even if the estimation performance of the fuel cell stack SoH estimator is poor, the energy management controller shows the ability to maintain the battery SoC in the constant reference tracking case.

Next, we assess the control performance in terms of control input limitation measures to show the fuel cell stack power increment response under the four stack health status. As shown in Fig. 6.13, the load fuel cell stack output power increment is limited

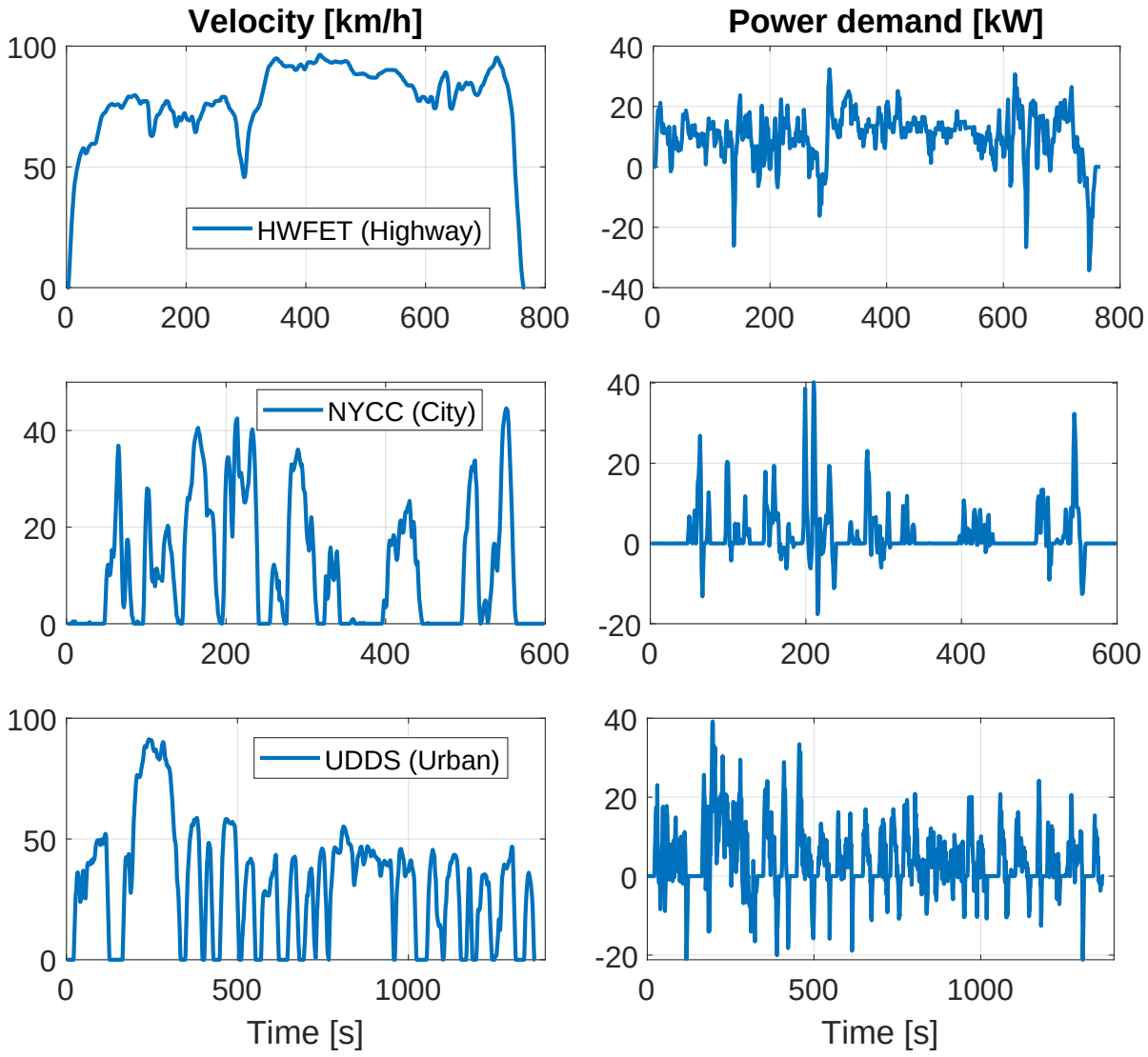

Figure 6.11. Velocity and power demand of the driving cycles used in the simulation

as expected when the fuel cell stack health deteriorating is observed. The observation shows that the energy management controller is capable of effectively reducing sudden load change of the fuel cell stack, which is the primary factor that results in the performance degradation of the fuel cell shown in Table 6.1.

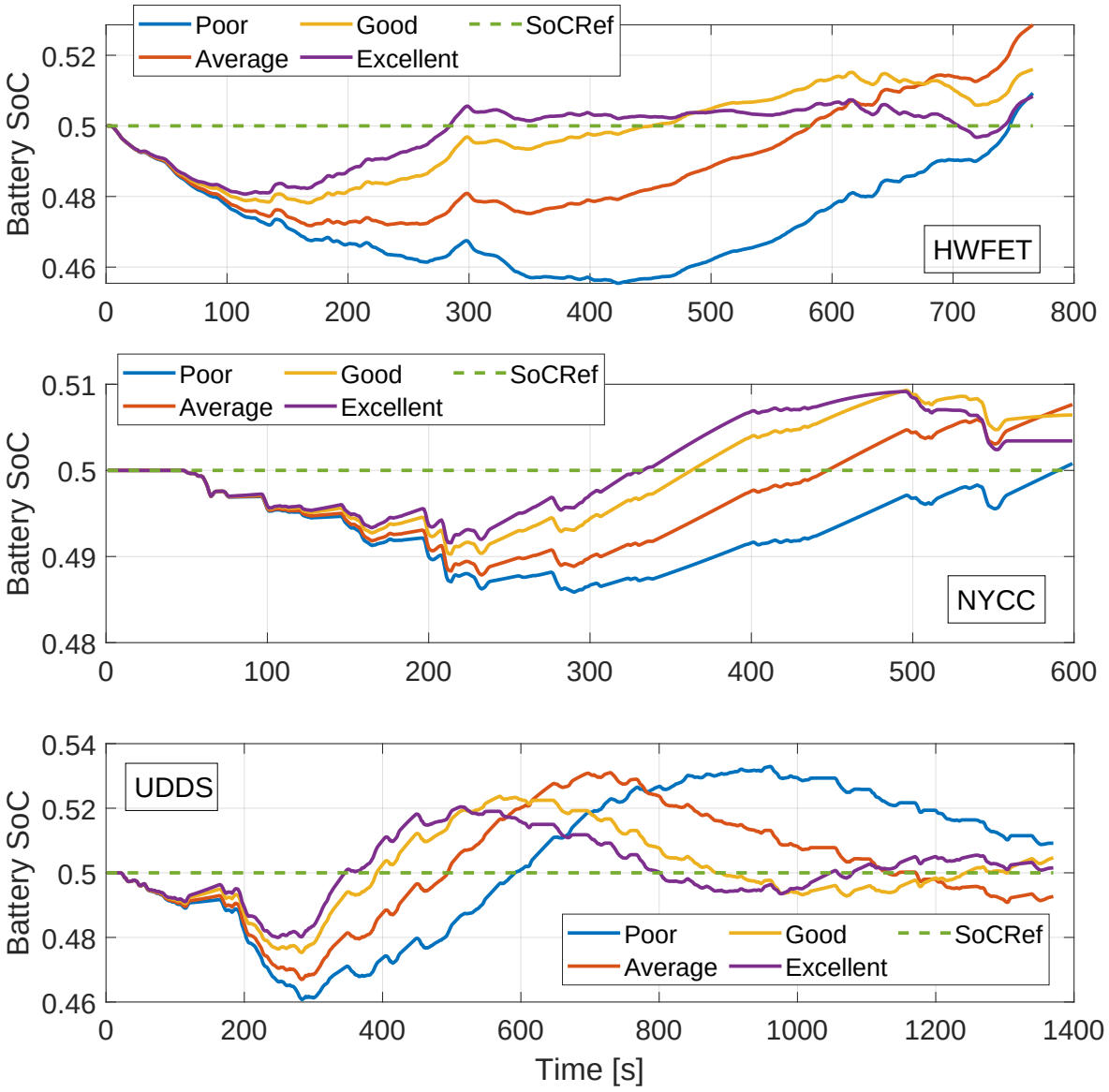

Figure 6.12. Battery SoC response among four stack health status under three driving conditions

6.4.4 Energy management system performance

We assess the overall EMS control scheme (as shown in Fig. 6.3) performance in complex driving scenarios. The following driving route is given in the case study: NYCC - UDDS - HWFET - UDDS - NYCC.

Shown in Fig. 6.14 illustrates the EMS control performance under the two energy storage system schedulers introduced in Section 6.3.2 concerning fuel cell system operational range. Compared with the constant scheduler, the EMS effective to move the

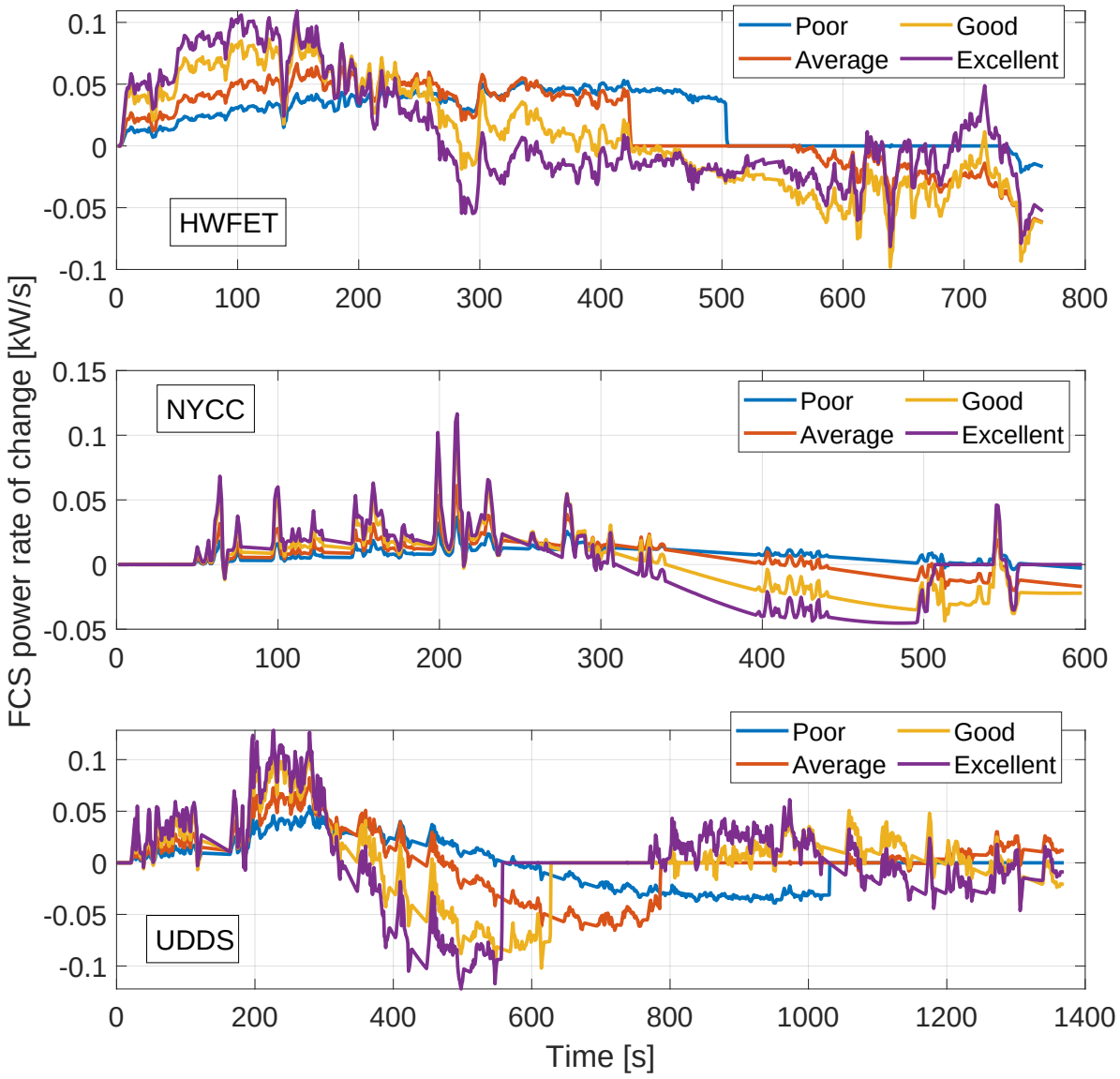

Figure 6.13. Fuel cell system output power change rate among four stack health status

fuel cell system output to the described high-efficient operating range by incorporating the proposed energy storage system schedulers to optimise battery SoC reference set-point. Moreover, Table 6.4 shows the numerical result of the fuel cell stack operational condition under the three energy storage system schedulers. We observe that the negative factors affecting the fuel cell stack performance degradation (according to Table 6.1) is significantly reduced with the frozen-time scheduler.

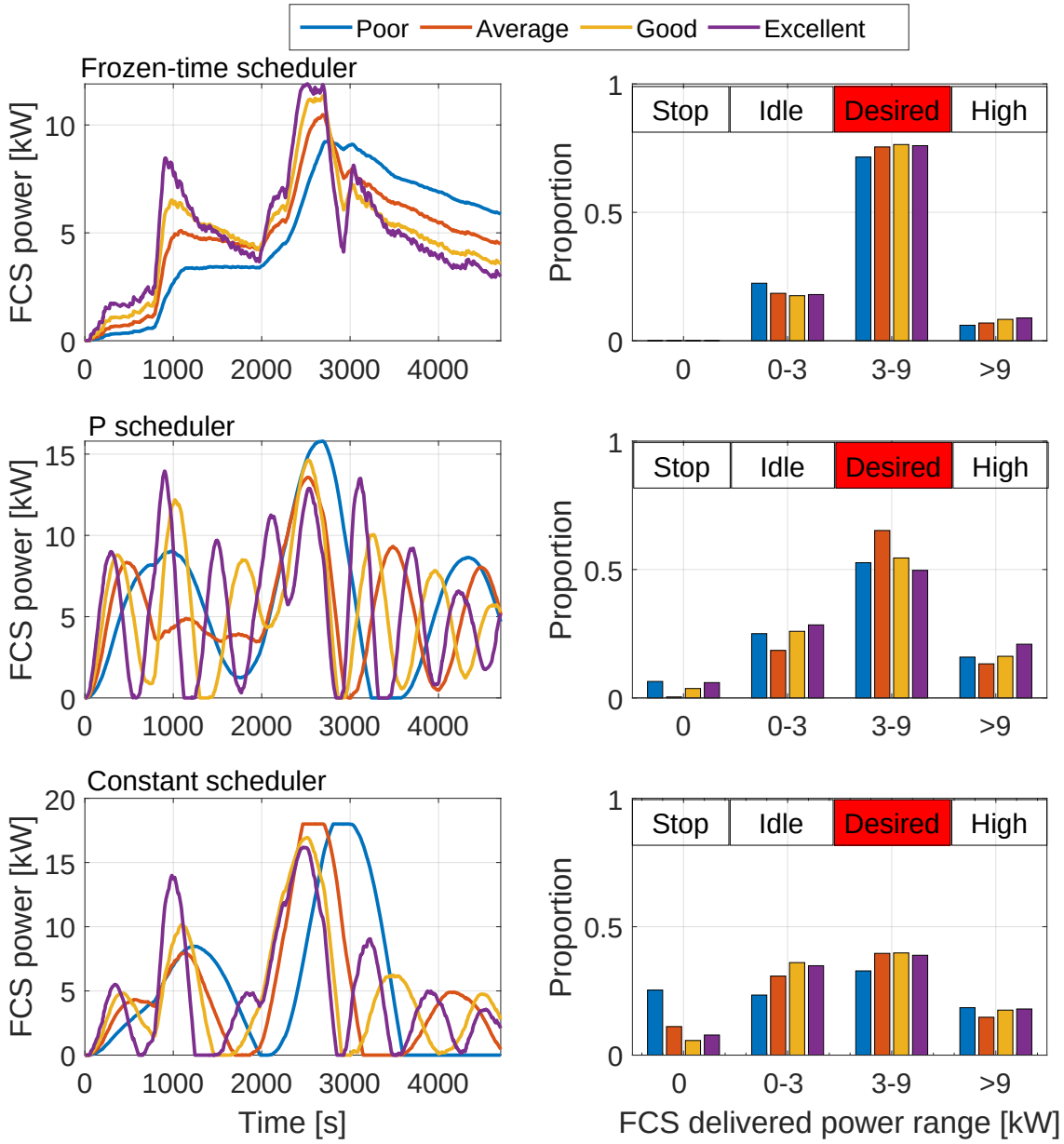

Figure 6.14. Fuel cell system output power during the trip under the three energy storage system schedulers (left) and the proportion of the fuel cell system operating range (right)

The EMS control performance in terms of battery SoC reference tracking is shown in Fig. 6.15. The result shows that both constant and varied battery SoC references are well tracked during operation. Since the EMS enables the fuel cell stack with a faster dynamic response in the 'Excellent' status, we observe that the 'Excellent' condition outperforms other three conditions.

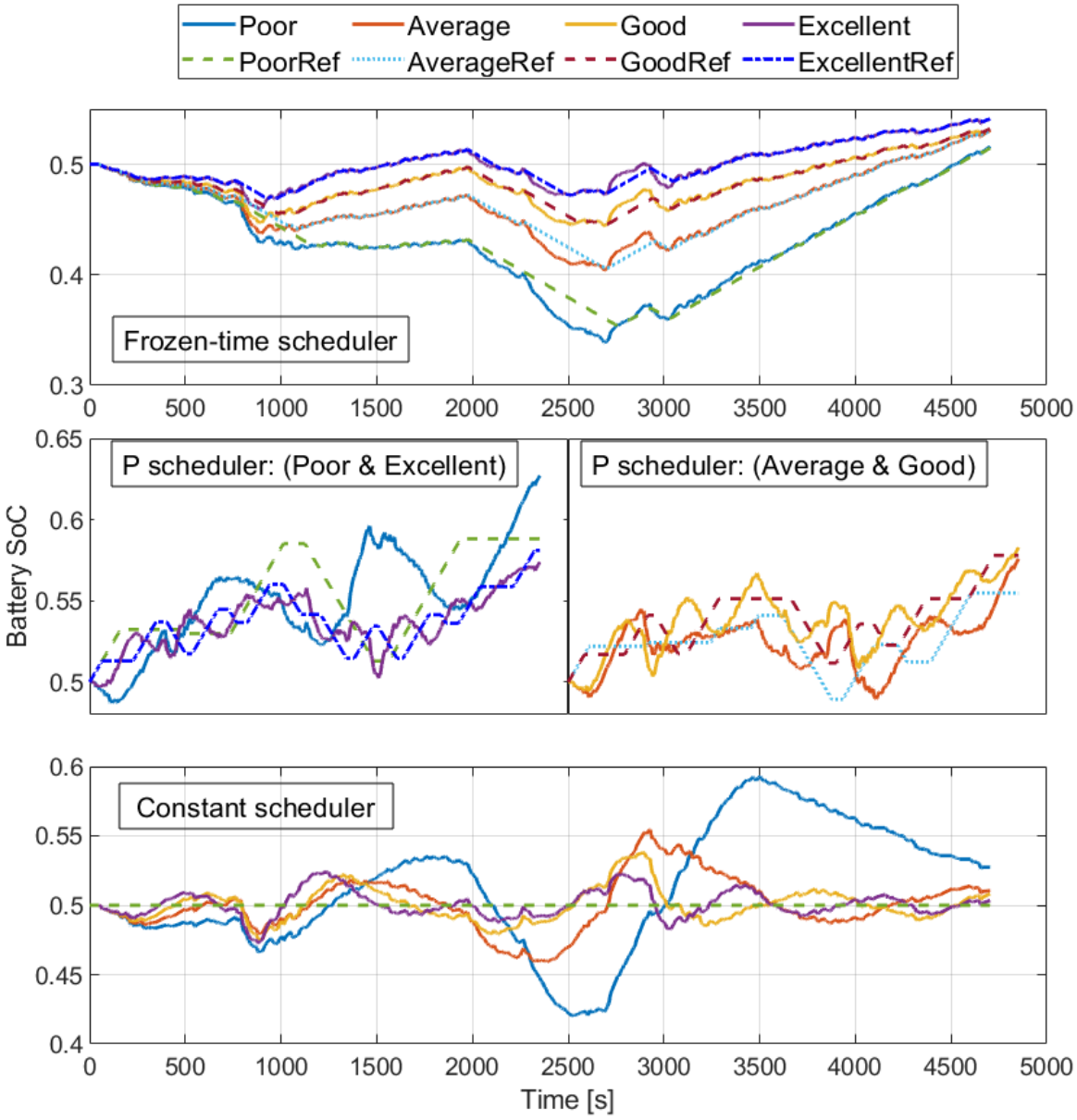

Figure 6.15. Battery SoC reference tracking performance under three energy storage system schedulers in four fuel cell stack state of health status

6.4.5 Computational time

We assess the fourth objective of the EMS design in Section 6.2.2, that is, the computational cost of the EMS. A real-time system is one that must process information and produce a response within a specified time. For a typical sampled data system, the information process should be completed within one sampling interval. In our case, the

Table 6.4. Fuel cell stack operational condition under the three energy storage system schedulers

	Frozen-time	P	Constant
Load change [kW/s]	0.0073	0.0218	0.0164
Start-stop proportion [%]	0.02	4.11	12.49
Idling-time proportion [%]	19.1	24.48	31.26
High-power proportion [%]	7.54	16.58	17.18

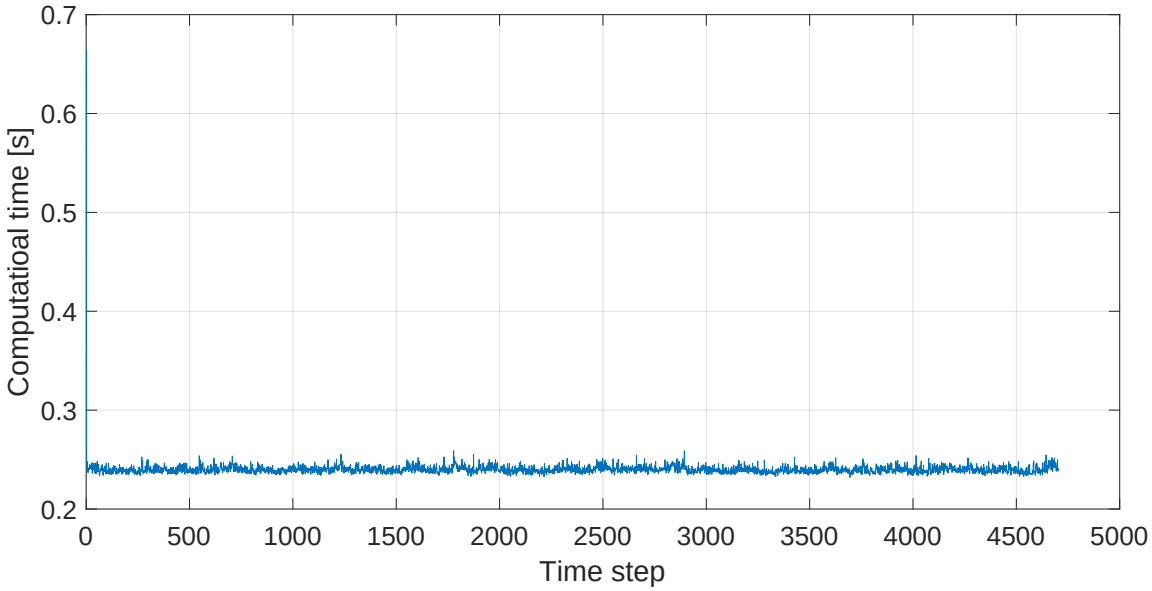

Figure 6.16. Average computational time of the EMS during 20 times driving simulation

sampling interval is one second. Consequently, we set one second as the benchmark to verify the EMS computational performance.

Fig. 6.16 shows the average EMS time consumed during 20 times simulation on a windows PC with Intel® i7-6700 CPU and 16GB Memory. Apart from high time consumed at the initial point due to optimization toolbox initialization, the average computational time to obtain the control gain is 0.2399s during the 20 times driving simulation and maximum computational elapsed time is 0.4388s. The good computational efficiency presents its applicability in real vehicle implementation.

6.5 Chapter summary

This chapter presents a novel control scheme for energy management design in fuel cell vehicles. The energy management system consists of a fuel cell stack state of health estimator, an energy management system scheduler, and an energy management controller in order to achieve optimal control in terms of optimising system efficiency, extending the durability of the fuel cell stack and maintaining battery charge level. The energy management problem is cast as a trajectory tracking problem under online adjustable control input constraints and addressed by the robust fuzzy model predictive control technique. The effectiveness of the energy management system has been demonstrated over typical urban/highway driving scenarios

Chapter 7

Thesis Conclusion

THE research presented in this thesis focuses on addressing the energy management problem in fuel cell vehicles. Four novel energy management systems for fuel cell vehicles have been developed and validated to achieve optimal control in terms of improving fuel economy, optimising fuel cell systems and maintaining battery pack charge level. This chapter concludes this thesis and indicates possible future work.

7.1 Summary

In Chapter 3, we propose a novel energy management system design for fuel cell hybrid vehicles. The predictive model of the future power demand is not required in our new energy management strategy. Instead, a novel framework is designed that uses an average-reward approximator under a partially observable Markov decision process to minimise the long-term cost.

Since the proposed energy management system is based on an average-reward model, the main disadvantage of the method is that it is not applicable to the situation with highly varied driving conditions. However, when the driving path is fixed, such as the bus driving route or in the situation that at the beginning of a trip, the origin, destination and itinerary can be obtained from the navigation unit, the proposed energy management system can achieve high performance.

To increase the applicability of the energy management system for fuel cell vehicle over various driving scenarios, we blend the theoretical analysis and practical issue to develop a new approach for energy management in fuel cell vehicles in Chapter 4. The energy management problem is cast in a mixed H_2/H_∞ framework in which H_2 control regulates the fuel economy and H_∞ control maintains battery charge sustainability in the presence of system uncertainty and disturbance. The proposed optimal control law is implemented in a vehicle simulator, and the performance of the energy management system is shown in simulation against the dynamic programming based benchmark solution.

To further improve the energy management system optimality, we propose an online optimisation-based energy management system in Chapter 5 in order to leverage available driving information. The approach is formulated by the T-S fuzzy modelling framework and robust model predictive control technique. The optimisation problem is cast in the form linear matrix inequalities and solved online. At each sampling step, the state-feedback control law is obtained by minimising the upper bound of the cost function, subject to system constraints. Furthermore, we incorporate traffic condition into the controller design to further improve optimisation performance. A MATLAB/Simulink based simulation serves to illustrate the effectiveness of the control scheme. Although the energy management design is based on fuel cell vehicles in this study, the approach is extensible to traditional hybrid vehicle applications.

In Chapter 6, we incorporate the fuel cell optimisation into the energy management system design for achieving optimal control in terms of battery state of charge maintenance, fuel cell durability protection and fuel economy in real time. The energy management problem is cast as an on-line optimal control problem that incorporates an online fuel cell stack state of health estimator based on the sigma-point Kalman filtering technique for stack health estimation, an energy storage system scheduler for vehicle fuel economy improvement, and a fuzzy robust-model-predictive based energy management controller to ensure system Lyapunov stability. A comprehensive MATLAB based simulation with experimental data serves to validate the effectiveness of the energy management system.

7.2 Future work

Future research includes the following three aspects.

Fuel cell lifetime improvement

The dynamic behaviour of the fuel cell is affected by operating conditions of the stack, such as inlet pressure, humidity, temperature, fuel stoichiometry and load variation (Mueller *et al.* 2007). An effective fuel cell system controller that comprises of fuel, thermal and water management reduces fuel cell performance degradation and improve system durability (Daud *et al.* 2017), which further increases the fuel cell vehicle driving performance and decreases system maintenance costs. Taking energy management system and fuel cell system controller under a unified control scheme could be explored further.

Energy system degradation modelling

High-fidelity models to describe the performance degradation of the energy storage system and fuel cell system have been developed in the literature (Chen *et al.* 2019, Wang *et al.* 2020, Zaccaria *et al.* 2016, Yang *et al.* 2017, Li *et al.* 2020). However, in the existing energy management system design for fuel cell vehicles, the energy system optimisation is limit to the restriction on battery's state of charge, battery charge/discharge

current or the output power increment of the fuel cell system, which hardly quantifies the performance degradation of the energy systems. Incorporating a high-fidelity performance degradation model of the energy system into the energy management system design has a tremendous research potential.

Driving behaviour prediction

In the energy management system design in Chapter 6, the energy storage system scheduler optimises the energy stored in the battery pack for assisting the fuel cell stack to optimally track the high-efficient area of the fuel cell system. Exploring a high-fidelity driving behaviour prediction model is a suitable forward step. This model can be incorporated into the energy storage system scheduler for predicting future power demand of the driver and then indicating the desired SoC set-point of the battery pack to the energy management controller.

Appendix A

Proof of Theorem 4.1 in Chapter 4

THIS appendix chapter provides the proof the Theorem 4.1 in Chapter 4. Section A.1 gives the proof of LMIs (4.32) in terms of H_∞ control performance. Then, Section A.2 provides the proof of the LMIs (4.33) regarding to H_2 performance. We complete this section by giving the proof of LMIs (4.34) concerning system input constraints.

A.1 Proof of H_∞ control performance

Suppose there exists a quadratic function $V(x(k))$ such that

$$V(x(k)) = x^T(k)Px(k), \qquad P > 0. \tag{A.1}$$

For (4.27), H_∞ attenuation level α^2 such that, for all k,

$$\begin{aligned} V(x(k+1)) - V(x(k)) + z^T(k)z(k) \\ - \alpha^2(w^T(k)w(k) + v^T(k)v(k)) \leq 0 \end{aligned} \tag{A.2}$$

Assuming that $x(0) = 0$, from summation in (A.2) in k from 0 until T_n, we have

$$\sum_{k=0}^{T_n}(z^T(k)z(k) - \alpha^2(w^T(k)w(k) + v^T(k)v(k))) \leq 0 \tag{A.3}$$

Therefore, the H_∞ performance index of (4.24) is less than zero if (A.2) holds. We now derive a sufficient linear matrix inequality (LMI) condition from (A.2). The condition (A.2) is equivalent to

$$\begin{aligned} & x^T(k)(P - C_z^T C_z)x(k) + \alpha^2(w^T(k)w(k) + v^T(k)v(k)) \\ & - (A_c X(k) + B_h e(k) + B_i v(k) + C_i w(k))^T \\ & \times P(A_c X(k) + B_h e(k) + B_i v(k) + C_i w(k)) \geq 0 \end{aligned} \tag{A.4}$$

for all $x(k)$ and $e(k)$ satisfying

$$e^T(k)e(k) \leq x^T(k)C_g^T C_g x(k) \tag{A.5}$$

Applying the S-procedure technique (Iwasaki *et al.* 2000), (A.4) and (A.5) hold if there exists $\lambda \in (0, 1]$ such that

$$\begin{aligned} & x^T(k)(P - C_z^T C_z)x(k) + \alpha^2(w^T(k)w(k) + v^T(k)v(k)) \\ & - (A_c X(k) + B_h e(k) + B_i v(k) + C_i w(k))^T \\ & \times P(A_c X(k) + B_h e(k) + B_i v(k) + C_i w(k)) \\ & + \lambda(e^T(k)e(k) - x^T(k)C_g^T C_g x(k)) \geq 0 \end{aligned} \tag{A.6}$$

We obtain the following LMI condition by dropping $[x^T(k), e^T(k), v^T(k), w^T(k)]^T$ and using the Schur complement on (A.6):

$$\begin{bmatrix} P - C_z^T C_z - \lambda C_g^T C_g & \star & \star & \star & \star \\ 0 & \lambda I & \star & \star & \star \\ 0 & 0 & \alpha^2 I & \star & \star \\ 0 & 0 & 0 & \alpha^2 I & \star \\ A_c & B_h & B_v & C_w & P^{-1} \end{bmatrix} \tag{A.7}$$

which is equivalent to

$$\begin{bmatrix} P & \star & \star & \star & \star & \star & \star \\ 0 & \lambda I & \star & \star & \star & \star & \star \\ 0 & 0 & \alpha^2 I & \star & \star & \star & \star \\ 0 & 0 & 0 & \alpha^2 I & \star & \star & \star \\ A_c & B_h & B_v & C_w & P^{-1} & \star & \star \\ C_z & 0 & 0 & 0 & 0 & I & \star \\ C_g & 0 & 0 & 0 & 0 & 0 & 1/\lambda \end{bmatrix} \geq 0 \tag{A.8}$$

where $\star$ denotes terms readily inferred from symmetry. Multiplying the left hand side and the right hand side of (A.8) by a block-diag $[Q, I, I, I, I, I, I]$ and abstracting membership functions $\sum_{i=1}^{2} h_i(z(k)) \sum_{r=1}^{11} v_r(u(k)) \sum_{j=1}^{2} h_j(z(k)))$ give (4.32), where $Q = P^{-1}$.

From (4.32), we have

$$\begin{aligned} V(x(k+1)) - V(x(k)) \\ - \alpha^2(w^T(k)w(k) + v^T(k)v(k)) \leq 0 \end{aligned}$$

Based on the definition of input-to-state practical stable in (Limón *et al.* 2006), closed-loop system (4.23) is input-to-state practical stable and $V(k)$ in (A.1) is the input-to-state practical stability Lyapunov function for the system.

A.2 Proof of H_2 control performance

Suppose there exist a positive scalar β^2 and $x(0) = 0$. For all k, we have

$$\begin{aligned} V(x(k+1)) - V(x(k)) + u^T(k)W_c u(k) \\ - \beta^2(w^T(k)w(k) + v^T(k)v(k)) \leq 0 \end{aligned} \tag{A.9}$$

Summing (A.9) from $k = 0$ to $k = T_n - 1$, we have

$$J_{H_2} = \sum_{k=0}^{T_n-1} u^T(k)W_c u(k) + V(x(T_n)) \tag{A.10}$$

$$\leq \beta^2 \sum_{k=0}^{T_n-1} (w^T(k)w(k) + v^T(k)v(k)) \tag{A.11}$$

Therefore, the upper bound of the H_2 control performance index J_{H_2} is minimized by solving the following optimization problem

$$\min \beta^2, \text{ subject to } (A.9)$$

We now derive a sufficient linear matrix inequality (LMI) condition from (A.9). The condition (A.9) is equivalent to

$$\begin{aligned} & x^T(k)(P - K_h W_c K_h)x(k) + \beta^2(w^T(k)w(k) + v^T(k)v(k)) \\ & - (A_c X(k) + B_h e(k) + B_i v(k) + C_i w(k))^T \\ & \times P(A_c X(k) + B_h e(k) + B_i v(k) + C_i w(k)) \geq 0 \end{aligned} \tag{A.12}$$

for all $x(k)$ and $e(k)$ satisfying

$$e^T(k)e(k) \leq x^T(k)C_g^T C_g x(k) \tag{A.13}$$

where $K_h = \sum_{i=1}^{2} h_i(z(k))K_i$.
The rest of proof is similar to that of H_∞ control performance above and thus is omitted.

A.3 Proof of Control input constraint

Since we assume that the fuel cell vehicle has capable of driving in the battery-only mode and x_1 is represented rate of change of the battery SoC during driving. Based on the component size, we can set a quantity ϕ that guarantee the states are limited the upper bound ϕ at each step, that is, $x^T(k)x(k) \leq \phi^2$. Therefore, we have

$$x^T(k)Px(k) \leq 1 \tag{A.14}$$

if

$$P^{-1} \geq \phi^2 I \tag{A.15}$$

Substituting (4.22) into (4.26), we have

$$\frac{1}{\mu^2}\sum_{i=1}^{2} h_i(z(k)) \sum_{j=1}^{2} h_j(z(k))x^T(k)K_i^T K_j x(k) \leq 1$$

Therefore, if

$$\frac{1}{\mu^2}\sum_{i=1}^{2} h_i(z(k)) \sum_{j=1}^{2} h_j(z(k))x^T(k)K_i^T K_j x(k) \leq x^T(k)Px(k)$$

then (4.26) holds. Substituting $P = Q^{-1}$ and $Y_i = K_i Q$, we can obtain (4.31) and (4.34) by the Schur complement, and thus the proof is completed.

Appendix B

Proof of Theorems in Chapter 5

THIS appendix chapter provides the proof the Theorem 5.1 and Theorem 5.2 in Chapter 5. The first section gives the proof of LMIs (5.36) to provide sufficient conditions for ensuring the recursive feasibility and the second section provides the proof of LMIs in (5.44)-(5.46) for the control law design.

B.1 Proof of Theorem 5.1

For notational convenience, we denote $h_i^r = \sum_{i=1}^{r} h_i(z(k))$.

From (5.29) - (5.34), if there exists $\lambda \in (0,1]$ such that (5.34) is guaranteed, then Y defined in (5.29) is a robust positively invariant for system (5.26). Substituting (5.26) and (5.28) into (5.34) gives:

$$
\begin{aligned}
&\frac{1}{\xi}[x(k+1)^T P x(k+1) - x(k)^T P x(k)] + \lambda[\frac{1}{\xi}x(k)^T P x(k) - \frac{1}{\gamma^2+\delta^2}w(k)^T w(k) \\
&\quad - \frac{1}{\gamma^2+\delta^2}\Delta u(k)^T \Delta u(k)] \\
&= \frac{1}{\xi}\{h_i^r h_j^r[(A_i + B_i K_j)x(k) + B_i \Delta u(k) + E_i w(k)]\}^T \\
&\quad \times P\{h_i^r h_j^r[(A_i + B_i K_j)x(k) + B_i \Delta u(k) + E_i w(k)]\} - \frac{1}{\xi}x(k)^T P x(k) \\
&\quad + \lambda[\frac{1}{\xi}x(k)^T P x(k) - \frac{1}{\gamma^2+\delta^2}w(k)^T w(k) - \frac{1}{\gamma^2+\delta^2}\Delta u(k)^T \Delta u(k)] \\
&= \frac{1}{\xi}[x^T(k)\ \Delta u^T(k)\ w^T(k)]\{h_i^r h_j^r \begin{bmatrix} A_i + B_i K_j & B_i & E_i \end{bmatrix}^T \\
&\quad \times P\{h_i^r h_j^r \begin{bmatrix} A_i + B_i K_j & B_i & E_i \end{bmatrix}\} \begin{bmatrix} x(k) \\ \Delta u(k) \\ w(k) \end{bmatrix} - [x^T(k)\ \Delta u^T(k)\ w^T(k)] \\
&\quad \times \begin{bmatrix} \frac{1-\lambda}{\xi}P & \star & \star \\ 0 & \frac{\lambda}{\gamma^2+\delta^2} & \star \\ 0 & 0 & \frac{\lambda}{\gamma^2+\delta^2} \end{bmatrix} \begin{bmatrix} x(k) \\ \Delta u(k) \\ w(k) \end{bmatrix} \leq 0
\end{aligned}
$$

Using the Schur complement yields

$$
\begin{aligned}
&\begin{bmatrix} \frac{1-\lambda}{\xi}P & \star & \star & \star \\ 0 & \lambda/(\gamma^2+\delta^2) & \star & \star \\ 0 & 0 & \lambda/(\gamma^2+\delta^2) & \star \\ h_i^r h_j^r(A_i + B_i K_j) & h_i^r B_i & h_i^r E_i & (\frac{1}{\xi}P)^{-1} \end{bmatrix} \\
&= h_i^r h_j^r \begin{bmatrix} \frac{1-\lambda}{\xi}P & \star & \star & \star \\ 0 & \lambda/(\gamma^2+\delta^2) & \star & \star \\ 0 & 0 & \lambda/(\gamma^2+\delta^2) & \star \\ A + \frac{B_i K_j + B_j K_i}{2} & \frac{B_i + B_j}{2} & \frac{E_i + E_j}{2} & (\frac{1}{\xi}P)^{-1} \end{bmatrix} \\
&\geq 0
\end{aligned}
$$

Therefore,

$$\begin{bmatrix} \frac{1-\lambda}{\xi}P & \star & \star & \star \\ 0 & \lambda/(\gamma^2+\delta^2) & \star & \star \\ 0 & 0 & \lambda/(\gamma^2+\delta^2) & \star \\ A+\frac{B_iK_j+B_jK_i}{2} & \frac{B_i+B_j}{2} & \frac{E_i+E_j}{2} & (\frac{1}{\xi}P)^{-1} \end{bmatrix} \geq 0$$

for $i \leq j$ subject to $h_i \cap h_j \neq \emptyset$ (B.1)

Substituting $P = \xi Q^{-1}$, $Q > 0$, $M_i = K_i Q$ into (B.1) and then multiplying block-diag $\begin{bmatrix} Q & I & I & I \end{bmatrix}$ on both sides of (B.1), we have (5.36) and the proof is completed.

B.2 Proof of Theorem 5.2

For convenience, we denote
$x_k(i) = x(k+i|k)$, $\Delta u_k(i) = \Delta u(k+i|k)$, $w_k(i) = w(k+i|k)$.

The terminal cost function v_t on state is required to satisfy (5.37). Substituting (5.26) and (5.28) into inequality (5.37) yields

$$\begin{aligned}
&h_i^r h_j^r[(A+B_iK_j)x_k(i)+B_i\Delta u_k(i)+E_iw_k(i)]^T P \times h_i^r h_j^r[(A+B_iK_j)x_k(i)+B_i\Delta u_k(i)+E_iw_k(i)] \\
&\quad - x_k^T(i)Px_k(i) - h_i^r h_j^r[x_k^T(i)K_i^T L_u K_j x_k(i)] - \alpha^2[w_k(i)^T w_k(i) + \Delta u_k(i)^T \Delta u_k(i)] \\
&\geq h_i^r h_j^r[(A+B_iK_j)x_k(i)+B_i\Delta u_k(i)+E_iw_k(i)]^T P h_i^r h_j^r[(A+B_iK_j)x_k(i)+B_i\Delta u_k(i)+E_iw_k(i)] \\
&\quad - x_k^T(i)Px_k(i) - h_i^r[x_k^T(i)K_i^T L_u K_i x_k(i)] - \alpha^2[w_k(i)^T w_k(i) + \Delta u_k(i)^T \Delta u_k(i)] \\
&= [x^T(k)\ \Delta u^T(k)\ w^T(k)]\{h_i^r h_j^r \begin{bmatrix} A+B_iK_j & B_i & E_i \end{bmatrix}^T \\
&\quad \times P\{h_i^r h_j^r \begin{bmatrix} A+B_iK_j & B_i & E_i \end{bmatrix}\} \begin{bmatrix} x(k) \\ \Delta u(k) \\ w(k) \end{bmatrix} - [x^T(k)\ \Delta u^T(k)\ w^T(k)] \\
&\quad \times \begin{bmatrix} P - h_i^r(K_i^T L_u K_i) & \star & \star \\ 0 & \alpha^2 & \star \\ 0 & 0 & \alpha^2 \end{bmatrix} \begin{bmatrix} x(k) \\ \Delta u(k) \\ w(k) \end{bmatrix} \\
&\geq 0
\end{aligned}$$

From the Schur complement, we have

$$\begin{bmatrix} P - h_i^r(K_i^T L_u K_i) & \star & \star & \star \\ 0 & \alpha^2 & \star & \star \\ 0 & 0 & \alpha^2 & \star \\ h_i^r h_j^r (A + B_i K_j) & h_i^r B_i & h_i^r E_i & P^{-1} \end{bmatrix} = \begin{bmatrix} P & \star & \star & \star & \star \\ 0 & \alpha^2 & \star & \star & \star \\ 0 & 0 & \alpha^2 & \star & \star \\ h_i^r h_j^r (A + B_i K_j) & h_i^r B_i & h_i^r E_i & P^{-1} & \star \\ h_i^r K_i L_u & 0 & 0 & 0 & L_u \end{bmatrix}$$

$$= h_i^r h_j^r \begin{bmatrix} P & \star & \star & \star & \star \\ 0 & \alpha^2 & \star & \star & \star \\ 0 & 0 & \alpha^2 & \star & \star \\ A + \frac{B_i K_j + B_j K_i}{2} & \frac{B_i + B_j}{2} & \frac{E_i + E_j}{2} & P^{-1} & \star \\ \frac{K_i + K_j}{2} L_u & 0 & 0 & 0 & L_u \end{bmatrix}$$

$$\geq 0$$

Therefore,

$$\begin{bmatrix} P & \star & \star & \star & \star \\ 0 & \alpha^2 & \star & \star & \star \\ 0 & 0 & \alpha^2 & \star & \star \\ A + \frac{B_i K_j + B_j K_i}{2} & \frac{B_i + B_j}{2} & \frac{E_i + E_j}{2} & P^{-1} & \star \\ \frac{K_i + K_j}{2} L_u & 0 & 0 & 0 & L_u \end{bmatrix} \geq 0$$

$$\text{for } i \leq j \text{ subject to } h_i \cap h_j \neq \emptyset \tag{B.2}$$

Substituting $P = \xi Q^{-1}$, $Q > 0$, and $M_i = K_i Q$ into (B.2), and then pre- and post-multiplying by block-diag $\begin{bmatrix} Q & I & I & I \end{bmatrix}$ on (B.2), we have (5.44).

From (5.42), we can readily obtain (5.46). Now, It remains to prove (5.45). Substituting (5.28) into (5.43) gives

$$\frac{1}{\mu^2} h_i^r h_j^r x^T(k) K_i^T K_j x(k) \leq 1$$

From (5.41), we have

$$\frac{1}{\xi} x^T(k) P x(k) \leq 1$$

If

$$\frac{1}{\mu^2} h_i^r h_j^r x^T(k) K_i^T K_j x(k) \leq \frac{1}{\xi} x^T(k) P x(k) \leq 1$$

then (5.43) holds. Moreover, since

$$h_i^r h_j^r x^T(k) K_i^T K_j x(k) \leq h_i^r x^T(k) K_i^T K_i x(k)$$

if

$$h_i^r x^T(k) [\frac{1}{\mu^2} K_i^T K_i - \frac{1}{\xi} P] x(k) \leq 0 \tag{B.3}$$

(5.43) holds. Substituting $P = \xi Q^{-1}$, $Q > 0$, and $M_i = K_i Q$ into (B.3) gives (5.45) by the Schur complement, and thus the proof is completed.

Appendix C

Proof of Theorem 6.1 in Chapter 6

THIS appendix chapter provides the proof the Theorem 6.1 in Chapter 6. Section C.1 gives the proof of LMIs (6.31) in terms of RPI set. Then, Section C.2 provides the proof of the LMIs (6.30) regarding to the control performance. We complete this section by giving the proof of LMIs (6.32) and (6.33) concerning system input constraints.

For notational convenience, we denote $\Lambda_i = \sum_{i=1}^{4} m(z_{i,k})$.

C.1 Proof of robust positively invariant set

We first derive a sufficient LMI condition from (6.27):

$$\begin{aligned}
&\lambda(\frac{\kappa_k^T\kappa_k}{\sigma_0^2} - \psi_k^T P\psi_k) - (\psi_{k+1}^T P\psi_{k+1} - \psi_k^T P\psi_k) \\
&= \frac{\lambda}{\sigma_0^2}\kappa_k^T\kappa_k - \{\Lambda_i\Lambda_j(\mathcal{A}_i + \mathcal{B}_i K_j)\psi_k + \Lambda_i\mathcal{C}_i\kappa_k\}^T \\
&\times P\{\Lambda_i\Lambda_j(\mathcal{A}_i + \mathcal{B}_i K_j)\psi_k + \Lambda_i\mathcal{C}_i\kappa_k\} + (1-\lambda)\psi_k^T P\psi_k \\
&= \begin{bmatrix}\psi_k & \kappa_k\end{bmatrix}^T \begin{bmatrix}(1-\lambda)P & 0 \\ 0 & \lambda/\sigma_0^2\end{bmatrix} \begin{bmatrix}\psi_k \\ \kappa_k\end{bmatrix} - \begin{bmatrix}\psi_k & \kappa_k\end{bmatrix}^T \{\Lambda_i\Lambda_j \begin{bmatrix}\mathcal{A}_i + \mathcal{B}_i K_j & \mathcal{C}_i\end{bmatrix}\}^T \\
&\times P\{\Lambda_i\Lambda_j \begin{bmatrix}\mathcal{A}_i + \mathcal{B}_i K_j & \mathcal{C}_i\end{bmatrix}\} \begin{bmatrix}\psi_k \\ \kappa_k\end{bmatrix} \geq 0
\end{aligned}$$

From the Schur complement, we obtain the following LMI condition

$$\begin{bmatrix}(1-\lambda)P & \star & \star \\ 0 & \lambda/\sigma_0^2 & \star \\ \Lambda_i\Lambda_j(\mathcal{A}_i + \mathcal{B}_i K_j) & \Lambda_i\mathcal{C}_i & P^{-1}\end{bmatrix} = \Lambda_i\Lambda_j \begin{bmatrix}(1-\lambda)P & \star & \star \\ 0 & \lambda/\sigma_0^2 & \star \\ \frac{\mathcal{A}_i+\mathcal{B}_i K_j+\mathcal{A}_j+\mathcal{B}_j K_i}{2} & \frac{\mathcal{C}_i+\mathcal{C}_j}{2} & P^{-1}\end{bmatrix}$$

where $\star$ denotes terms readily inferred from symmetry. Therefore,

$$\begin{bmatrix}(1-\lambda)P & \star & \star \\ 0 & \lambda/\sigma_0^2 & \star \\ \frac{\mathcal{A}_i+\mathcal{B}_i K_j+\mathcal{A}_j+\mathcal{B}_j K_i}{2} & \frac{\mathcal{C}_i+\mathcal{C}_j}{2} & P^{-1}\end{bmatrix} \geq 0$$
$$i \geq j \text{ s.t. } m(z_i,k) \cap m(z_j,k) \neq \emptyset \tag{C.1}$$

Multiplying the left hand side and the right hand side of (C.1) by a block-diag $\begin{bmatrix}Q & I & I\end{bmatrix}$, LMI (6.31) is obtained, where $Q = P^{-1}$.

C.2 Proof of control performance

Suppose, for system (6.19), there exists a quadratic function $V_{\psi_k} = \psi_k^T P\psi_k$, $P > 0$ such that for all k,

$$V_{\psi_{k+1}} - V_{\psi_k} + \xi_k^T\xi_k - \delta^2\kappa_k^T\kappa_k \leq 0 \tag{C.2}$$

From summation in (C.2) in k from 0 until $T_n - 1$, we have

$$\sum_{k=0}^{T_n-1} (V_{\psi_{k+1}} - V_{\psi_k} + \xi_k^T \xi_k - \delta^2 \kappa_k^T \kappa_k) \leq 0 \tag{C.3}$$

Assuming that initial condition $\psi_0 = 0$, we have

$$V_{\psi_{T_n}} + \sum_{k=0}^{T_n} (\xi_k^T \xi_k - \delta^2 \kappa_k^T \kappa_k) \leq 0 \tag{C.4}$$

Since $V_{\psi_{T_n}} \geq 0$, this implies

$$\frac{||\xi_k||_{\mathcal{L}_2}}{||\kappa_k||_{\mathcal{L}_2}} \leq \delta^2 \tag{C.5}$$

Therefore, the $\mathcal{H}_\infty$ performance index (6.21) is less than zero if (C.2) holds. We now derive a sufficient LMI condition from (C.2).

$$\begin{aligned}
&\delta^2 \kappa_k^T \kappa_k - \xi_k^T \xi_k - (V_{\psi_{k+1}} - V_{\psi_k}) \\
&= \delta^2 \kappa_k^T \kappa_k - (\mathcal{D}\psi_k + \mathcal{E}\kappa_k)^T (\mathcal{D}\psi_k + \mathcal{E}\kappa_k) + \psi_k^T P \psi_k \\
&\quad - \{\Lambda_i \Lambda_j (\mathcal{A}_i + \mathcal{B}_i K_j)\psi_k + \Lambda_i \mathcal{C}_i \kappa_k\}^T P \{\Lambda_i \Lambda_j (\mathcal{A}_i + \mathcal{B}_i K_j)\psi_k + \Lambda_i \mathcal{C}_i \kappa_k\} \\
&= \begin{bmatrix} \psi_k & \kappa_k \end{bmatrix}^T \begin{bmatrix} P - \mathcal{D}^T \mathcal{D} & \mathcal{D}^T \mathcal{E} \\ \mathcal{E}^T \mathcal{D} & \delta^2 - \mathcal{E}^T \mathcal{E} \end{bmatrix} \begin{bmatrix} \psi_k \\ \kappa_k \end{bmatrix} \\
&\quad - \begin{bmatrix} \psi_k & \kappa_k \end{bmatrix}^T \{\Lambda_i \Lambda_j \begin{bmatrix} \mathcal{A}_i + \mathcal{B}_i K_j & \mathcal{C}_i \end{bmatrix}\}^T \times P \{\Lambda_i \Lambda_j \begin{bmatrix} \mathcal{A}_i + \mathcal{B}_i K_j & \mathcal{C}_i \end{bmatrix}\} \begin{bmatrix} \psi_k \\ \kappa_k \end{bmatrix} \\
&\geq 0
\end{aligned}$$

We obtain the following LMI condition by using the Schur complement

$$\begin{bmatrix} P - \mathcal{D}^T \mathcal{D} & \star & \star \\ \mathcal{E}^T \mathcal{D} & \delta^2 - \mathcal{E}^T \mathcal{E} & \star \\ \Lambda_i \Lambda_j (\mathcal{A}_i + \mathcal{B}_i K_j) & \Lambda_i \mathcal{C}_i & P^{-1} \end{bmatrix} =$$
$$\begin{bmatrix} P & \star & \star \\ 0 & \delta^2 & \star \\ \Lambda_i \Lambda_j (\mathcal{A}_i + \mathcal{B}_i K_j) & \Lambda_i \mathcal{C}_i & P^{-1} \end{bmatrix} - \begin{bmatrix} \mathcal{D}^T \\ \mathcal{E}^T \\ 0 \end{bmatrix} \begin{bmatrix} \mathcal{D} & \mathcal{E} & 0 \end{bmatrix} \geq 0$$

The LMI condition is equivalent to

$$\begin{bmatrix} P & \star & \star & \star \\ 0 & \delta^2 & \star & \star \\ \Lambda_i \Lambda_j (\mathcal{A}_i + \mathcal{B}_i K_j) & \Lambda_i \mathcal{C}_i & P^{-1} & \star \\ \mathcal{D} & \mathcal{E} & 0 & I \end{bmatrix}$$

$$= \Lambda_i \Lambda_j \begin{bmatrix} P & \star & \star & \star \\ 0 & \delta^2 & \star & \star \\ \frac{\mathcal{A}_i+\mathcal{B}_i K_j+\mathcal{A}_j+\mathcal{B}_j K_i}{2} & \frac{\mathcal{C}_i+\mathcal{C}_j}{2} & P^{-1} & \star \\ \mathcal{D} & \mathcal{E} & 0 & I \end{bmatrix} \geq 0$$

Consequently,

$$\begin{bmatrix} P & \star & \star & \star \\ 0 & \delta^2 & \star & \star \\ \frac{\mathcal{A}_i+\mathcal{B}_i K_j+\mathcal{A}_j+\mathcal{B}_j K_i}{2} & \frac{\mathcal{C}_i+\mathcal{C}_j}{2} & P^{-1} & \star \\ \mathcal{D} & \mathcal{E} & 0 & I \end{bmatrix} \geq 0$$

$$i \geq j \text{ s.t. } m(z_i, k) \cap m(z_j, k) \neq \emptyset \tag{C.6}$$

Multiplying the left hand side and the right hand side of (C.6) by a block-diag $\begin{bmatrix} Q & I & I & I \end{bmatrix}$, LMI (6.30) is obtained, where $Q = P^{-1}$.

C.3 Proof of control input constraint

Assume that

$$\psi_k^T P \psi_k \leq 1 \tag{C.7}$$

Then,

$$1 - \psi_k^T P \psi_k \geq 0 \tag{C.8}$$

The inequality (C.8) is transformed into (6.33) by the Schur complement procedure.

From the constraint on the control input in (6.22), we have

$$\tilde{u}_k^T \tilde{u}_k = \Lambda_i \Lambda_j \psi_k^T K_i^T K_j \psi_k \leq \bar{u}_0^2$$

there

$$\frac{1}{\bar{u}_0^2} \Lambda_i \Lambda_j \psi_k^T K_i^T K_j \psi_k \leq 1$$

If

$$\frac{1}{\bar{u}_0^2} \Lambda_i \Lambda_j \psi_k^T K_i^T K_j \psi_k \leq \psi_k^T P \psi_k \leq 1$$

then (6.22) holds. Therefore, we have

$$\Lambda_i \Lambda_j \psi_k^T (\frac{1}{\bar{u}_0^2} K_i^T K_j - P) \psi_k \leq 0 \tag{C.9}$$

From (C.9), we have

$$\Lambda_i \begin{bmatrix} P & K_i^T \\ K_i & \bar{u}_0^2 \end{bmatrix} \geq 0 \tag{C.10}$$

Multiplying the left hand side and the right hand side of (C.10) by a block-diag $\begin{bmatrix} Q & I \end{bmatrix}$ yields

$$\Lambda_i \begin{bmatrix} Q & Y_i^T \\ Y_i & \bar{u}_0^2 \end{bmatrix} \geq 0 \tag{C.11}$$

Thus we arrive at condition (6.32).

References

ALESSANDRI-A., BAGLIETTO-M., AND BATTISTELLI-G. (2004). On estimation error bounds for receding-horizon filters using quadratic boundedness, *IEEE Transactions on Automatic Control*, **49**(8), pp. 1350–1355.

ANDÚJAR-J. M., AND SEGURA-F. (2009). Fuel cells: History and updating. a walk along two centuries, *Renewable and Sustainable Energy Reviews*, **13**(9), pp. 2309–2322.

ANSAREY-M., PANAHI-M. S., ZIARATI-H., AND MAHJOOB-M. (2014). Optimal energy management in a dual-storage fuel-cell hybrid vehicle using multi-dimensional dynamic programming, *Journal of Power Sources*, **250**, pp. 359–371.

ARCE-A., ALEJANDRO-J., AND BORDONS-C. (2009). MPC for battery/fuel cell hybrid vehicles including fuel cell dynamics and battery performance improvement, *Journal of Process Control*, **19**(8), pp. 1289–1304.

AXSEN-J., AND KURANI-K. S. (2013). Hybrid, plug-in hybrid, or electric - what do car buyers want?, *Energy Policy*, **61**, pp. 532–543.

BALLARD. (2020). FCvelocity®-9SSL, `https://www.ballard.com/docs/default-source/motive-modules-documents/material-handling/fcvelocity-9ssl.pdf?sfvrsn=2`. Accessed: 2020-04-01.

BEMPORAD-A., AND MORARI-M. (1999). Robust model predictive control: A survey, *Robustness in Identification and Control*, Springer, pp. 207–226.

BERTSEKAS-D. P., AND CASTANON-D. A. (1998). Rollout algorithms for stochastic scheduling problems, *Proceedings of the 37th IEEE Conference on Decision and Control (Cat. No.98CH36171)*, Vol. 2, pp. 2143–2148 vol.2.

BLANCHINI-F. (1999). Set invariance in control, *Automatica*, **35**(11), pp. 1747–1767.

BORUP-R. L., KUSOGLU-A., NEYERLIN-K. C., MUKUNDAN-R., AHLUWALIA-R. K., CULLEN-D. A., MORE-K. L., WEBER-A. Z., AND MYERS-D. J. (2020). Recent developments in catalyst-related pem fuel cell durability, *Current Opinion in Electrochemistry*, **21**, pp. 192 – 200.

BOYD-S., EL GHAOUI-L., FERON-E., AND BALAKRISHNAN-V. (1994). *Linear matrix inequalities in system and control theory*, Vol. 15, SIAM.

BRESSEL-M., HILAIRET-M., HISSEL-D., AND OULD BOUAMAMA-B. (2016). Remaining useful life prediction and uncertainty quantification of proton exchange membrane fuel cell under variable load, *IEEE Transactions on Industrial Electronics*, **63**(4), pp. 2569–2577.

BURKE-A. F. (2007). Batteries and ultracapacitors for electric, hybrid, and fuel cell vehicles, *Proceedings of the IEEE*, **95**(4), pp. 806–820.

BURKE-K. (2003). Fuel cells for space science applications, *1st International Energy Conversion Engineering Conference (IECEC)*, p. 5938.

CAIRANO-S. D., BERNARDINI-D., BEMPORAD-A., AND KOLMANOVSKY-I. V. (2014). Stochastic MPC with learning for driver-predictive vehicle control and its application to HEV energy management, *IEEE Transactions on Control Systems Technology*, **22**(3), pp. 1018–1031.

CALCE. (2020). INR 18650-20R battery experimental data: CALCE battery research group, `https://web.calce.umd.edu/batteries/data.htm#mission`. Accessed: 2020-10-16.

CHEN-B.-S., TSENG-C.-S., AND UANG-H.-J. (2000). Mixed H_2/H_∞ fuzzy output feedback control design for nonlinear dynamic systems: an LMI approach, *IEEE Transactions on Fuzzy Systems*, **8**(3), pp. 249–265.

CHEN-J., XU-C., WU-C., AND XU-W. (2016). Adaptive fuzzy logic control of fuel-cell-battery hybrid systems for electric vehicles, *IEEE Transactions on Industrial Informatics*, **14**(1), pp. 292–300.

CHEN-K., LAGHROUCHE-S., AND DJERDIR-A. (2019). Degradation model of proton exchange membrane fuel cell based on a novel hybrid method, *Applied Energy*, **252**, p. 113439.

CHEN-Z., MI-C. C., XU-J., GONG-X., AND YOU-C. (2013). Energy management for a power-split plug-in hybrid electric vehicle based on dynamic programming and neural networks, *IEEE Transactions on Vehicular Technology*, **63**(4), pp. 1567–1580.

CHIU-H., AND LIN-L. (2006). A bidirectional DC–DC converter for fuel cell electric vehicle driving system, *IEEE Transactions on Power Electronics*, **21**(4), pp. 950–958.

COOK-B. (2002). Introduction to fuel cells and hydrogen technology, *Engineering Science & Education Journal*, **11**(6), pp. 205–216.

CORRÊA-J. M., FARRET-F. A., CANHA-L. N., AND SIMOES-M. G. (2004). An electrochemical-based fuel-cell model suitable for electrical engineering automation approach, *IEEE Transactions on Industrial Electronics*, **51**(5), pp. 1103–1112.

DAUD-W., ROSLI-R., MAJLAN-E., HAMID-S., MOHAMED-R., AND HUSAINI-T. (2017). PEM fuel cell system control: A review, *Renewable Energy*, **113**, pp. 620–638.

EGARDT-B., MURGOVSKI-N., POURABDOLLAH-M., AND MARDH-L. J. (2014). Electromobility studies based on convex optimization: Design and control issues regarding vehicle electrification, *IEEE Control Systems Magazine*, **34**(2), pp. 32–49.

EHSANI-M., GAO-Y., LONGO-S., AND EBRAHIMI-K. (2018). *Modern electric, hybrid electric, and fuel cell vehicles*, CRC press.

ELBERT-P., NÜESCH-T., RITTER-A., MURGOVSKI-N., AND GUZZELLA-L. (2014). Engine on/off control for the energy management of a serial hybrid electric bus via convex optimization, *IEEE Transactions on Vehicular Technology*, **63**(8), pp. 3549–3559.

EL-SOUSY-F. F., AND ABUHASEL-K. A. (2016). Self-organizing recurrent fuzzy wavelet neural network-based mixed H_2/H_∞ adaptive tracking control for uncertain two-axis motion control system, *IEEE Transactions on Industry Applications*, **52**(6), pp. 5139–5155.

GAHINET-P., NEMIROVSKII-A., LAUB-A., AND CHILALI-M. (1994). The LMI control toolbox, *Decision and Control, 1994., Proceedings of the 33rd IEEE Conference on*, Vol. 3, IEEE, pp. 2038–2041.

GARCÍA-TRIVIÑO-P., FERNÁNDEZ-RAMÍREZ-L. M., GIL-MENA-A. J., LLORENS-IBORRA-F., GARCÍA-VÁZQUEZ-C. A., AND JURADO-F. (2016). Optimized operation combining costs, efficiency and lifetime of a hybrid renewable energy system with energy storage by battery and hydrogen in grid-connected applications, *International Journal of Hydrogen Energy*, **41**(48), pp. 23132–23144.

GEMMEN-R., AND JOHNSON-C. (2006). Evaluation of fuel cell system efficiency and degradation at development and during commercialization, *Journal of Power Sources*, **159**(1), pp. 646–655.

GILKS-W. R. (2005). *Markov chain Monte Carlo*, Wiley Online Library.

GOLCHOUBIAN-P., AND AZAD-N. L. (2017). Real-time nonlinear model predictive control of a battery–supercapacitor hybrid energy storage system in electric vehicles, *IEEE Transactions on Vehicular Technology*, **66**(11), pp. 9678–9688.

GRANT-M., AND BOYD-S. (2020). CVX: Matlab software for disciplined convex programming, `http://cvxr.com/cvx/`.

HADDAD-W., AND CHELLABOINA-V. (2011). *Nonlinear dynamical systems and control: A Lyapunov-based approach*, Princeton University Press.

HANSEN-T. M., CHONG-E. K., SURYANARAYANAN-S., MACIEJEWSKI-A. A., AND SIEGEL-H. J. (2018). A partially observable Markov decision process approach to residential home energy management, *IEEE Transactions on Smart Grid*, **9**(2), pp. 1271–1281.

HEGAZY-O., VAN MIERLO-J., AND LATAIRE-P. (2012). Analysis, modeling, and implementation of a multidevice interleaved DC/DC converter for fuel cell hybrid electric vehicles, *IEEE Transactions on Power Electronics*, **27**(11), pp. 4445–4458.

HÖFLINGER-J., HOFMANN-P., MÜLLER-H., AND LIMBRUNNER-M. (2017). FCREEV a fuel cell range extended electric vehicle, *MTZ Worldwide*, **78**(5), pp. 18–23.

HROVAT-D., DI CAIRANO-S., TSENG-H. E., AND KOLMANOVSKY-I. V. (2012). The development of model predictive control in automotive industry: A survey, *2012 IEEE International Conference on Control Applications*, IEEE, pp. 295–302.

HSU-P.-L., AND ROBBINS-H. (1947). Complete convergence and the law of large numbers, *Proceedings of the National Academy of Sciences*, **33**(2), pp. 25–31.

HUANG-Y., WANG-H., KHAJEPOUR-A., HE-H., AND JI-J. (2017). Model predictive control power management strategies for HEVs: A review, *Journal of Power Sources*, **341**, pp. 91–106.

HU-X., JIANG-J., EGARDT-B., AND CAO-D. (2015). Advanced power-source integration in hybrid electric vehicles: Multicriteria optimization approach, *IEEE Transactions on Industrial Electronics*, **62**(12), pp. 7847–7858.

HU-X., MURGOVSKI-N., JOHANNESSON-L., AND EGARDT-B. (2013). Energy efficiency analysis of a series plug-in hybrid electric bus with different energy management strategies and battery sizes, *Applied Energy*, **111**, pp. 1001–1009.

INC.-B. P. S. (2011). *FCvelocity-9SSL V4 Product Manual and Integration Guide*, Ballard Power Systems Inc.

IWASAKI-T., MEINSMA-G., AND FU-M. (2000). Generalized S-procedure and finite frequency KYP lemma, *Mathematical Problems in Engineering*, **6**.

JIANG-Z.-P., AND WANG-Y. (2001). Input-to-state stability for discrete-time nonlinear systems, *Automatica*, **37**(6), pp. 857–869.

KANDEPU-R., FOSS-B., AND IMSLAND-L. (2008). Applying the unscented Kalman filter for nonlinear state estimation, *Journal of Process Control*, **18**(7-8), pp. 753–768.

KASIMALLA-V. K., AND VELISALA-V. (2018). A review on energy allocation of fuel cell/battery/ultracapacitor for hybrid electric vehicles, *International Journal of Energy Research*, **42**(14), pp. 4263–4283.

KOTHARE-M. V., BALAKRISHNAN-V., AND MORARI-M. (1996). Robust constrained model predictive control using linear matrix inequalities, *Automatica*, **32**(10), pp. 1361–1379.

KRITHIKA-V., AND SUBRAMANI-C. (2018). A comprehensive review on choice of hybrid vehicles and power converters, control strategies for hybrid electric vehicles, *International Journal of Energy Research*, **42**(5), pp. 1789–1812.

KURTZ-J. M., SPRIK-S., SAUR-G., AND ONORATO-S. (2019). Fuel cell electric vehicle driving and fueling behavior, *Technical report*, National Renewable Energy Lab.(NREL), Golden, CO (United States).

KWON-W. H., AND HAN-S. H. (2006). *Receding horizon control: Model predictive control for state models*, Springer Science & Business Media.

LARMINIE-J., DICKS-A., AND MCDONALD-M. S. (2003). *Fuel cell systems explained*, Vol. 2, J. Wiley Chichester, UK.

LEE-T. K., ADORNATO-B., AND FILIPI-Z. S. (2011). Synthesis of real-world driving cycles and their use for estimating PHEV energy consumption and charging opportunities: Case study for midwest/U.S., *IEEE Transactions on Vehicular Technology*, **60**(9), pp. 4153–4163.

LEWIS-F. L., VRABIE-D., AND SYRMOS-V. L. (2012). *Optimal control*, John Wiley & Sons.

LIAN-Z., HE-Y., ZHANG-C., AND WU-M. (2020). Stability and stabilization of T–S fuzzy systems with time-varying delays via delay-product-type functional method, *IEEE Transactions on Cybernetics*, **50**(6), pp. 2580–2589.

LIAN-Z., HE-Y., ZHANG-C.-K., SHI-P., AND WU-M. (2019). Robust H_∞ control for T-S fuzzy systems with state and input time-varying delays via delay-product-type functional method, *IEEE Transactions on Fuzzy Systems*, **27**(10), pp. 1917–1930.

LI-J., LANDERS-R. G., AND PARK-J. (2020). A comprehensive single-particle-degradation model for battery state-of-health prediction, *Journal of Power Sources*, **456**, p. 227950.

LIMÓN-D., ALAMO-T., SALAS-F., AND CAMACHO-E. F. (2006). Input to state stability of min–max MPC controllers for nonlinear systems with bounded uncertainties, *Automatica*, **42**(5), pp. 797–803.

LIU-Y., LI-J., CHEN-Z., QIN-D., AND ZHANG-Y. (2019). Research on a multi-objective hierarchical prediction energy management strategy for range extended fuel cell vehicles, *Journal of Power Sources*, **429**, pp. 55 – 66.

LI-X., WANG-Y., YANG-D., AND CHEN-Z. (2019). Adaptive energy management strategy for fuel cell/battery hybrid vehicles using Pontryagin's minimal principle, *Journal of Power Sources*, **440**, p. 227105.

LOFBERG-J. (2004). YALMIP: A toolbox for modeling and optimization in MATLAB, *2004 IEEE International Conference on Robotics and Automation (IEEE Cat. No. 04CH37508)*, IEEE, pp. 284–289.

LU-Q., SHI-P., LAM-H.-K., AND ZHAO-Y. (2015). Interval type-2 fuzzy model predictive control of nonlinear networked control systems, *IEEE Transactions on Fuzzy Systems*, **23**(6), pp. 2317–2328.

MAGNI-L., RAIMONDO-D. M., AND SCATTOLINI-R. (2006). Regional input-to-state stability for nonlinear model predictive control, *IEEE Transactions on Automatic Control*, **51**(9), pp. 1548–1553.

MARTINEZ-J. S., HISSEL-D., PÉRA-M.-C., AND AMIET-M. (2011). Practical control structure and energy management of a testbed hybrid electric vehicle, *IEEE Transactions on Vehicular Technology*, **60**(9), pp. 4139–4152.

MARX-N., HISSEL-D., GUSTIN-F., BOULON-L., AND AGBOSSOU-K. (2017). On the sizing and energy management of an hybrid multistack fuel cell–battery system for automotive applications, *International Journal of Hydrogen Energy*, **42**(2), pp. 1518–1526.

MATHWORKS. (2020). Powertrain blockset - model and simulate automotive powertrain systems, `https://au.mathworks.com/products/powertrain.html`. Accessed: 2020-09-08.

MAYNE-D. (2016). Robust and stochastic model predictive control: Are we going in the right direction?, *Annual Reviews in Control*, **41**, pp. 184–192.

MAYNE-D. Q. (2014). Model predictive control: Recent developments and future promise, *Automatica*, **50**(12), pp. 2967–2986.

MAYNE-D. Q., RAKOVIĆ-S., FINDEISEN-R., AND ALLGÖWER-F. (2006). Robust output feedback model predictive control of constrained linear systems, *Automatica*, **42**(7), pp. 1217–1222.

MAYNE-D. Q., SERON-M. M., AND RAKOVIĆ-S. (2005). Robust model predictive control of constrained linear systems with bounded disturbances, *Automatica*, **41**(2), pp. 219–224.

MESBAH-A. (2016). Stochastic model predictive control: An overview and perspectives for future research, *IEEE Control Systems Magazine*, **36**(6), pp. 30–44.

MOTAPON-S. N., DESSAINT-L.-A., AND AL-HADDAD-K. (2013). A comparative study of energy management schemes for a fuel-cell hybrid emergency power system of more-electric aircraft, *IEEE Transactions on Industrial Electronics*, **61**(3), pp. 1320–1334.

MUELLER-F., JABBARI-F., GAYNOR-R., AND BROUWER-J. (2007). Novel solid oxide fuel cell system controller for rapid load following, *Journal of Power Sources*, **172**(1), pp. 308–323.

MURA-R., UTKIN-V., AND ONORI-S. (2015). Energy management design in hybrid electric vehicles: A novel optimality and stability framework, *IEEE Transactions on Control Systems Technology*, **23**(4), pp. 1307–1322.

MURGOVSKI-N., JOHANNESSON-L., AND SJOBERG-J. (2012). Convex modeling of energy buffers in power control applications, *IFAC Proceedings Volumes*, **45**(30), pp. 92 – 99.

MUSARDO-C., RIZZONI-G., GUEZENNEC-Y., AND STACCIA-B. (2005). A-ECMS: An adaptive algorithm for hybrid electric vehicle energy management, *European Journal of Control*, **11**(4-5), pp. 509–524.

NASSIF-G. G., AND DE ALMEIDA-S. C. (2020). Impact of powertrain hybridization on the performance and costs of a fuel cell electric vehicle, *International Journal of Hydrogen Energy*, **45**(41), pp. 21722–21737.

NGUANG-S. K., AND SHI-P. (2003). H_2/H_∞ fuzzy output feedback control design for nonlinear systems: an LMI approach, *IEEE Transactions on Fuzzy Systems*, **11**(3), pp. 331–340.

NGUYEN-B.-H., GERMAN-R., TROVÃO-J. P. F., AND BOUSCAYROL-A. (2018). Real-time energy management of battery/supercapacitor electric vehicles based on an adaptation of Pontryagin's minimum principle, *IEEE Transactions on Vehicular Technology*, **68**(1), pp. 203–212.

NONOBE-Y. (2017). Development of the fuel cell vehicle Mirai, *IEEJ Transactions on Electrical and Electronic Engineering*, **12**(1), pp. 5–9.

NÜESCH-T., ELBERT-P., FLANKL-M., ONDER-C., AND GUZZELLA-L. (2014). Convex optimization for the energy management of hybrid electric vehicles considering engine start and gearshift costs, *Energies*, **7**(2), pp. 834–856.

ONORI-S., AND TRIBIOLI-L. (2015). Adaptive Pontryagin's Minimum Principle supervisory controller design for the plug-in hybrid GM Chevrolet Volt, *Applied Energy*, **147**, pp. 224–234.

ONORI-S., SERRAO-L., AND RIZZONI-G. (2016). *Hybrid electric vehicles: Energy management strategies*, Vol. 13, Springer.

ORUKPE-P. E., JAIMOUKHA-I. M., AND EL-ZOBAIDI-H. M. (2007). Model predictive control based on mixed H_2/H_∞ control approach, *American Control Conference, 2007. ACC'07*, IEEE, pp. 6147–6150.

OU-K., YUAN-W.-W., CHOI-M., YANG-S., JUNG-S., AND KIM-Y.-B. (2018). Optimized power management based on adaptive-PMP algorithm for a stationary PEM fuel cell/battery hybrid system, *International Journal of Hydrogen Energy*, **43**(32), pp. 15433–15444.

PAGANELLI-G., DELPRAT-S., GUERRA-T., RIMAUX-J., AND SANTIN-J. (2002). Equivalent consumption minimization strategy for parallel hybrid powertrains, *Vehicular Technology Conference, 2002. VTC Spring 2002. IEEE 55th*, Vol. 4, IEEE, pp. 2076–2081.

PAHLEVANINEZHAD-M., DROBNIK-J., JAIN-P., AND BAKHSHAI-A. (2012). A load adaptive control approach for a zero-voltage-switching DC/DC converter used for electric vehicles, *IEEE Transactions on Industrial Electronics*, **59**(2), p. 920.

PEI-P., AND CHEN-H. (2014). Main factors affecting the lifetime of proton exchange membrane fuel cells in vehicle applications: A review, *Applied Energy*, **125**, pp. 60–75.

PLETT-G. L. (2004). Extended Kalman filtering for battery management systems of LiPB-based HEV battery packs: Part 2. modeling and identification, *Journal of Power Sources*, **134**(2), pp. 262 – 276.

RÜCKER-A. (2020). Hydrogen fuel cell cars: everything you need to know, https://www.bmw.com/en/innovation/how-hydrogen-fuel-cell-cars-work.html. Accessed: 2020-09-01.

RHEE-B.-J., AND WON-S. (2006). A new fuzzy Lyapunov function approach for a Takagi–Sugeno fuzzy control system design, *Fuzzy Sets and Systems*, **157**(9), pp. 1211–1228.

RODRIGUES-A., FRONK-M., AND MCCORMICK-B. (2010). *General motors/OPEL Fuel cell activities — driving towards a successful future*, American Cancer Society.

SAMPATHNARAYANAN-B., ONORI-S., AND YURKOVICH-S. (2014). An optimal regulation strategy with disturbance rejection for energy management of hybrid electric vehicles, *Automatica*, **50**(1), pp. 128–140.

SCHOUTEN-N. J., SALMAN-M. A., AND KHEIR-N. A. (2003). Energy management strategies for parallel hybrid vehicles using fuzzy logic, *Control Engineering Practice*, **11**(2), pp. 171–177.

SETHI-S. P., AND THOMPSON-G. L. (2000). *What is optimal control theory?*, Springer.

SHEN-D., LIM-C.-C., AND SHI-P. (2020a). Robust fuzzy model predictive control for energy management systems in fuel cell vehicles, *Control Engineering Practice*, **98**, p. 104364.

SHEN-D., LIM-C., SHI-P., AND BUJLO-P. (2020b). Energy management of fuel cell hybrid vehicle based on partially observable markov decision process, *IEEE Transactions on Control Systems Technology*, **28**(2), pp. 318–330.

SHI-P., SU-X., AND LI-F. (2016a). Dissipativity-based filtering for fuzzy switched systems with stochastic perturbation, *IEEE Transactions on Automatic Control*, **61**(6), pp. 1694–1699.

SHI-P., ZHANG-Y., CHADLI-M., AND AGARWAL-R. K. (2016b). Mixed H-infinity and passive filtering for discrete fuzzy neural networks with stochastic jumps and time delays, *IEEE Transactions on Neural Networks and Learning Systems*, **27**(4), pp. 903–909.

SILVAS-E., HEREIJGERS-K., PENG-H., HOFMAN-T., AND STEINBUCH-M. (2016). Synthesis of realistic driving cycles with high accuracy and computational speed, including slope information, *IEEE Transactions on Vehicular Technology*, **65**(6), pp. 4118–4128.

SONG-Z., HOU-J., HOFMANN-H., LI-J., AND OUYANG-M. (2017). Sliding-mode and Lyapunov function-based control for battery/supercapacitor hybrid energy storage system used in electric vehicles, *Energy*, **122**, pp. 601–612.

SONTAG-E. D., AND WANG-Y. (1995). On characterizations of the input-to-state stability property, *Systems & Control Letters*, **24**(5), pp. 351–359.

SORRENTINO-M., RIZZO-G., AND ARSIE-I. (2011). Analysis of a rule-based control strategy for on-board energy management of series hybrid vehicles, *Control Engineering Practice*, **19**(12), pp. 1433–1441.

SPRINGER-T. E., ZAWODZINSKI-T., AND GOTTESFELD-S. (1991). Polymer electrolyte fuel cell model, *Journal of the Electrochemical Society*, **138**(8), pp. 2334–2342.

STAUNTON-R. H., AYERS-C. W., MARLINO-L., CHIASSON-J., AND BURRESS-B. (2006). Evaluation of 2004 Toyota Prius hybrid electric drive system, *Technical report*, Oak Ridge National Lab.(ORNL), Oak Ridge, TN (United States).

SULAIMAN-N., HANNAN-M., MOHAMED-A., KER-P. J., MAJLAN-E., AND DAUD-W. W. (2018). Optimization of energy management system for fuel-cell hybrid electric vehicles: Issues and recommendations, *Applied Energy*, **228**, pp. 2061–2079.

SUN-C., SUN-F., AND HE-H. (2017). Investigating adaptive-ECMS with velocity forecast ability for hybrid electric vehicles, *Applied Energy*, **185**, pp. 1644–1653.

SUNDSTROM-O., AND GUZZELLA-L. (2009). A generic dynamic programming matlab function, *Control Applications,(CCA) & Intelligent Control,(ISIC), 2009 IEEE*, IEEE, pp. 1625–1630.

TANAKA-K., AND WANG-H. O. (2004). *Fuzzy control systems design and analysis: a linear matrix inequality approach*, John Wiley & Sons.

TANAKA-S., NAGUMO-K., YAMAMOTO-M., CHIBA-H., YOSHIDA-K., AND OKANO-R. (2020). Fuel cell system for honda clarity fuel cell, *eTransportation*, **3**, p. 100046.

TEKIN-M., HISSEL-D., PERA-M., AND KAUFFMANN-J. (2007). Energy-management strategy for embedded fuel-cell systems using fuzzy logic, *IEEE Transactions on Industrial Electronics*, **54**(1), pp. 595–603.

TENG-T., ZHANG-X., DONG-H., AND XUE-Q. (2020). A comprehensive review of energy management optimization strategies for fuel cell passenger vehicle, *International Journal of Hydrogen Energy*, **45**(39), pp. 20293 – 20303.

THOMPSON-S. T., AND PAPAGEORGOPOULOS-D. (2019). Platinum group metal-free catalysts boost cost competitiveness of fuel cell vehicles, *Nature Catalysis*, **2**(7), pp. 558–561.

TOLJ-I., LOTOTSKYY-M. V., DAVIDS-M. W., PASUPATHI-S., SWART-G., AND POLLET-B. G. (2013). Fuel cell-battery hybrid powered light electric vehicle (golf cart): Influence of fuel cell on the driving performance, *International Journal of Hydrogen Energy*, **38**(25), pp. 10630 – 10639.

TSENG-C.-S., AND CHEN-B.-S. (2003). A mixed H_2/H_∞ adaptive tracking control for constrained nonholonomic systems, *Automatica*, **39**(6), pp. 1011–1018.

TÜTÜNCÜ-R. H., TOH-K.-C., AND TODD-M. J. (2003). Solving semidefinite-quadratic-linear programs using SDPT3, *Mathematical programming*, **95**(2), pp. 189–217.

VALMORBIDA-G., AND ANDERSON-J. (2017). Region of attraction estimation using invariant sets and rational Lyapunov functions, *Automatica*, **75**, pp. 37–45.

WAN-E. A., AND VAN DER MERWE-R. (2000). The unscented Kalman filter for nonlinear estimation, *Proceedings of the IEEE 2000 Adaptive Systems for Signal Processing, Communications, and Control Symposium (Cat. No. 00EX373)*, IEEE, pp. 153–158.

WAN-E. A., VAN DER MERWE-R., AND HAYKIN-S. (2001). The unscented Kalman filter, *Kalman Filtering and Neural Networks*, **5**(2007), pp. 221–280.

WANG-F.-K., CHENG-X.-B., AND HSIAO-K.-C. (2020). Stacked long short-term memory model for proton exchange membrane fuel cell systems degradation, *Journal of Power Sources*, **448**, p. 227591.

WANG-H., HUANG-Y., KHAJEPOUR-A., AND SONG-Q. (2016). Model predictive control-based energy management strategy for a series hybrid electric tracked vehicle, *Applied Energy*, **182**, pp. 105–114.

WANG-S., AND JIANG-S. P. (2017). Prospects of fuel cell technologies, *National Science Review*, **4**(2), pp. 163–166.

WANG-Y., MOURA-S. J., ADVANI-S. G., AND PRASAD-A. K. (2019). Optimization of powerplant component size on board a fuel cell/battery hybrid bus for fuel economy and system durability, *International Journal of Hydrogen Energy*, **44**(33), pp. 18283 – 18292.

WIPKE-K., SPRIK-S., KURTZ-J., RAMSDEN-T., AINSCOUGH-C., AND SAUR-G. (2012). National fuel cell electric vehicle learning demonstration final report, *Technical report*, NREL.

WU-K., KUANG-M., MILACIC-M., ZHANG-X., AND SUN-J. (2017). Analysis of effects of fuel cell system dynamics on optimal energy management, *ASME 2017 Dynamic Systems and Control Conference*, American Society of Mechanical Engineers, pp. V003T43A001–V003T43A001.

XIA-Y., YANG-H., SHI-P., AND FU-M. (2010). Constrained infinite-horizon model predictive control for fuzzy-discrete-time systems, *IEEE Transactions on Fuzzy Systems*, **18**(2), pp. 429–436.

YAKUBOVICH-V. (1992). Nonconvex optimization problem: The infinite-horizon linear-quadratic control problem with quadratic constraints, *Systems & Control Letters*, **19**(1), pp. 13–22.

YANG-F., WANG-D., XING-Y., AND TSUI-K.-L. (2017). Prognostics of li (nimnco) o2-based lithium-ion batteries using a novel battery degradation model, *Microelectronics Reliability*, **70**, pp. 70–78.

YANG-W., FENG-G., AND ZHANG-T. (2014). Robust model predictive control for discrete-time Takagi–Sugeno fuzzy systems with structured uncertainties and persistent disturbances, *IEEE Transactions on Fuzzy Systems*, **22**(5), pp. 1213–1228.

YAN-Q., TOGHIANI-H., AND CAUSEY-H. (2006). Steady state and dynamic performance of proton exchange membrane fuel cells (PEMFCs) under various operating conditions and load changes, *Journal of Power Sources*, **161**(1), pp. 492–502.

YIN-H., ZHOU-W., LI-M., MA-C., AND ZHAO-C. (2016). An adaptive fuzzy logic-based energy management strategy on battery/ultracapacitor hybrid electric vehicles, *IEEE Transactions on Transportation Electrification*, **2**(3), pp. 300–311.

YOSHIDA-T., AND KOJIMA-K. (2015). Toyota mirai fuel cell vehicle and progress toward a future hydrogen society, *Electrochemical Society Interface*, **24**(2), p. 45.

YUE-M., JEMEI-S., GOURIVEAU-R., AND ZERHOUNI-N. (2019). Review on health-conscious energy management strategies for fuel cell hybrid electric vehicles: Degradation models and strategies, *International Journal of Hydrogen Energy*, **44**(13), pp. 6844–6861.

YU-Y., LI-H., WANG-H., YUAN-X.-Z., WANG-G., AND PAN-M. (2012). A review on performance degradation of proton exchange membrane fuel cells during startup and shutdown processes: Causes, consequences, and mitigation strategies, *Journal of Power Sources*, **205**, pp. 10 – 23.

YU-Z., ZINGER-D., AND BOSE-A. (2011). An innovative optimal power allocation strategy for fuel cell, battery and supercapacitor hybrid electric vehicle, *Journal of Power Sources*, **196**(4), pp. 2351–2359.

ZACCARIA-V., TUCKER-D., AND TRAVERSO-A. (2016). A distributed real-time model of degradation in a solid oxide fuel cell, part i: Model characterization, *Journal of Power Sources*, **311**, pp. 175–181.

ZANDI-M., PAYMAN-A., MARTIN-J.-P., PIERFEDERICI-S., DAVAT-B., AND MEIBODY-TABAR-F. (2010). Energy management of a fuel cell/supercapacitor/battery power source for electric vehicular applications, *IEEE Transactions on Vehicular Technology*, **60**(2), pp. 433–443.

ZENG-X., AND WANG-J. (2015). A parallel hybrid electric vehicle energy management strategy using stochastic model predictive control with road grade preview, *IEEE Transactions on Control Systems Technology*, **23**(6), pp. 2416–2423.

ZHANG-S., XIONG-R., AND SUN-F. (2017). Model predictive control for power management in a plug-in hybrid electric vehicle with a hybrid energy storage system, *Applied Energy*, **185**, pp. 1654–1662.

ZHANG-Y., ZHANG-C., HUANG-Z., XU-L., LIU-Z., AND LIU-M. (2019). Real-time energy management strategy for fuel cell range extender vehicles based on nonlinear control, *IEEE Transactions on Transportation Electrification*, **5**(4), pp. 1294–1305.

List of Acronyms

BEV ..... Battery electric vehicle

DC-DC ..... Direct current to direct current

DP ..... Dynamic programming

ECMS ..... Equivalent consumption minimisation strategy

EKF ..... Extended Kalman filter

EMS ..... Energy management system

EPA ..... Environmental Protection Agency

FCV ..... Fuel cell vehicle

FTP-75 ..... Federal Test Procedure 75

HEV ..... Hybrid electric vehicle

HWFET ..... Highway Fuel Economy Driving Schedule

ICEV ..... Internal combustion engines vehicle

LMI ..... Linear matrix inequality

MCMC ..... Markov chain Monte Carlo

MPC ..... Model predictive control

MPGe ..... Miles per gallon gasoline equivalent

NYCC ..... New York City Cycle

PEMFCS ..... Proton-exchange-membrane fuel cell system

PMP ..... Pontryagin's minimum principle

POMDP ..... Partially observable Markov decision process

RMPC ..... Robust model predictive control

RPI . . . . . Robust positively invariant

TPM . . . . . Transition probability matrix

T-S . . . . . Takagi–Sugeno

SoC . . . . . State of charge

SoH . . . . . State of health

UDDS . . . . . Urban Dynamometer Driving Schedule

WHVC . . . . . World Harmonized Vehicle Cycle

WLTP . . . . . Worldwide Harmonised Light Vehicles Test Procedure

List of Symbols

List of Symbols in Chapter 3

ac_{mean} ..... Vehicle average acceleration

ac_{std} ..... Vehicle average standard deviation acceleration

ac_{perc} ..... Vehicle average driving time under acceleration

A ..... Vehicle frontal area

b_0, b_1, b_2 ..... Fitting parameters in the fuel cell model

c_0, c_1 ..... Fitting parameters in the battery model

C_{drag} ..... Air resistance coefficient

C_{rollR} ..... Rolling resistance coefficient

C_n ..... Cell's nominal capacitor

de_{mean} ..... Vehicle average deceleration

de_{perc} ..... Vehicle average driving time under deceleration.

de_{std} ..... Vehicle average standard deviation deceleration

F_a ..... Vehicle acceleration resistance

F_f ..... Vehicle rolling resistance

F_t ..... Vehicle driving force

F_w ..... Vehicle air resistance

g ..... Acceleration of gravity

i_0, i_k ..... Vehicle transmission ratio

$i(t)$ ..... Instantaneous cell current

M ..... Column number of the road information class

m ..... Vehicle total mass

N ..... Length of the generated cycle

P_a ..... Power consumption of the auxiliary systems

P_{bin} ..... Battery internal power

P_{bloss} ..... Battery internal power loss

P_{bo} ..... Output power from the battery pack

P_{dcdc} ..... Output power from the DC-DC converter

P_{eloss} ..... Electric motor internal power loss

P_{fcs} ..... Output power from the fuel cell stack

P_{h_2} ..... Hydrogen input power

$P_{require}$ ..... Power demand by the electric motor

P_v ..... Power demand from the vehicle

R ..... Battery internal resistance

R_{wheel} ..... Vehicle wheel radius

SoC ..... Battery state of charge

u_{soc} ..... Battery open-circuit voltage

u_t ..... Control action which is selected by the energy management system

v_{mean} ..... Vehicle average velocity

v_{std} ..... Vehicle average standard deviation velocity

$v(t)$ ..... Vehicle speed

V_c ..... Current velocity of the vehicle

z ..... Index selected by the Markov chain Monte Carlo sampling

α ..... Road slope angle

α_{mean} ..... Road average slope

α_{std} ..... Road average standard deviation slope

α_{max} ..... Road maximal slope

α_{min} ..... Road minimal slope

β_{h2} ..... Price of hydrogen

β_b ..... Price of electricity

$\boldsymbol{\kappa}_i$ ..... Velocities in previous k time steps.

$\boldsymbol{\Phi}$ ..... Transition probability matrix of the velocity and the road information

ε_{soc} ..... Battery state of energy

$\dot{m}_f$ ..... Instantaneous fuel flow rate

Δt ..... Time step

ϵ ..... Rotating mass conversion factor

η_b ..... Cell's Faraday efficiency

η_r ..... Transmission efficiency

γ ..... Total number of cells in the battery pack

Ω ..... Road information

ρ ..... Air density

ρ_{avg} ..... Driver's driving behaviours

τ ..... Motor output torque

$\triangle P_{fcs}(t)$ ..... Increase rate of the output power of the fuel cell stack

ω ..... Motor rotational speed

List of Symbols in Chapter 4

A_{fc} ..... Tafel slope in the fuel cell model

b_0, b_1 ..... Fitting parameters in the battery model

C_1 ..... Value of the capacitor in the RC-branch

C_n ..... Battery nominal capacitor

E_{batt} ..... Battery open circuit voltage

E_{fc} ..... Fuel cell open-circuit voltage

$H, E_r P$ ..... Known matrices in the fuzzy model

h_i ..... Fuzzy membership function of rule i.

i_0 ..... Exchange current density on a proton exchange membrane

i_b ..... Instantaneous battery current

i_{fc} ..... Fuel cell output current

i_{R_1} ..... Diffusion resistor current

J ..... Objective function

J_{H_2} ..... H_2 performance indexes

J_{H_∞} ..... H_∞ performance indexes

k ..... Discrete time step

K ..... Control gain

L^r ..... Fuzzy term that associates control input in rule r

m_{H_2} ..... Hydrogen consumption

$M(z)$ ..... Fuzzy membership function

n_{fcs} ..... Number of cells in the fuel cell stack

n_p ..... Number of cells in parallel in the battery pack

n_s ..... Number of cells in series in the battery pack

P ..... Terminal cost on states.

P_{bout} ..... power delivered from the battery pack

P_{dc} ..... Output power from the fuel cell boost converter

P_{drive} ..... Power demand from the driver.

P_{fcs} ..... Power delivered from the fuel cell stack

R_0 ..... Battery internal resistance

R_1 ..... Value of the resistor in the RC-branch

R_{fc} ..... Fuel cell internal ohmic

SoC ..... Battery state of charge

SoC_{ref} ..... Reference value of battery's state of charge

T_n ..... Finite driving time

u ..... Control input in the system dynamic model

V_{batt} ..... Battery terminal voltage

V_{fc} ..... Output voltage of a fuel cell

v_r ..... Fuzzy membership function of rule r.

W_c ..... Weighting scalar on control input

w ..... Disturbance acting on the system

x ..... States in the system dynamic model

z ..... Premise variable in the fuzzy system

α ..... H_∞ attenuation level to reject the disturbance

ΔS_r ..... Uncertainty of the operational fuel cell voltage

Δt ..... Sampling period

η_f ..... Battery Faraday efficiency

η_{dc} ..... Fuel cell boost converter efficiency

μ ..... Upper bound of the control input

θ ..... Fitting parameter in the fuel cell model

Ω_b ..... Terminal set of the battery state of charge

List of Symbols in Chapter 5

A_{fc} ..... Tafel slope in the fuel cell model

C_n ..... Cell capacity

co_{fc} ..... Corresponding constant coefficient in fuel cell model

E_{batt} ..... Battery open-circuit voltage

E_{oc} ..... Open-circuit voltage of the fuel cell

h_i ..... Fuzzy membership function of rule i.

i_0 ..... Exchange current density on a proton exchange membrane

i_b ..... Output current of the battery pack

i_{dc} ..... Output current of the boost converter

i_{fc} ..... Output current of the fuel cell

i_{fcs} ..... Output current of the fuel cell stack

$J(k)$ ..... Performance index

K ..... State feedback matrices

L_{h2} ..... Weighting scalar in the performance index

L_u ..... Weighting scalar in the performance index

$M(z)$ ..... Fuzzy membership function

m_{h2} ..... Hydrogen consumption in standard liter per minute

N_{fc} ..... Number of fuel cells

n_{pb} ..... Number of battery in parallel

n_{sb} ..... Number of battery in serial

P ..... Weighting scalar in the performance index

p_a, p_b ..... Fitting parameters in the battery model

P_{batt} ..... Power delivered from the battery pack

P_{boost} ..... Output power from the boost converter

P_{fcs} ..... Power delivered from the fuel cell system

P_{h2} ..... Output power of the hydrogen tank

P_{motor} ..... Power demand from the motor

R_b ..... Battery internal resistance

R_{ohmic} ..... Internal resistance of the fuel cell

S_{batt} ..... Battery state of charge

$S_{batt \cdot ref}$ ..... Reference values of the battery state of charge

T_n ..... Travel time

u ..... Control input in the system dynamic model

V_{bus} ..... Terminal voltage of the battery pack

$V_{bus \cdot ref}$ ..... Reference values of the DC-BUS voltage

V_{fcs} ..... Terminal voltage of the fuel cell stack

w ..... Disturbance acting on the system

x ..... States in the system dynamic model

z ..... Premise variable in the fuzzy system

α ..... Disturbance rejection level

Δt ..... Sampling time period

Δu ..... Uncertainty on the control input

ΔV_{act} ..... Activation overvoltage

δ ..... Upper bound of the control input uncertainty

γ ..... Upper bound of the disturbance

γ^* ..... Upper bound of the power demand based on the traffic condition

η_{boost} ..... Boost converter efficiency

η_{fcs} ..... Fuel cell system efficiency

η_i ..... Faraday efficiency of the battery

ν_t ..... Terminal cost on state

Ω_b ..... Terminal constraints set of the battery state of charge

Y ..... Robust positively invariant candidate

List of Symbols in Chapter 6

a_0, a_1, a_2, a_3, a_4 . Fitting parameters in the battery model

b_0, b_1 ..... Fitting parameters in the fuel cell model

b_f ..... Tafel constant in the fuel cell model

C_n ..... Battery capacity

E_f ..... Open-circuit voltage of the fuel cell stack

I_b ..... Output current of the battery pack

I_f ..... Output current of the fuel cell stack

i_l ..... Exchange current density on a proton exchange membrane

K ..... State feedback matrices

L_k ..... Kalman filter gain

M, N ..... Fuzzy membership function

m_i ..... Fuzzy membership function of rule i.

n_p ..... Number of battery in parallel

n_s ..... Number of battery in serial

P_{aux} ..... Power consumption of the auxiliary systems

P_b ..... Power delivered from the battery pack

P_d ..... Power demand from the motor

P_{dc} ..... Output power from the boost converter

P_{fcs} ..... Power delivered from the fuel cell system

$P_{fcs,max}$ ..... Fuel cell system admissible maximum load

$P_{fcs,r}$ ..... Desired fuel cell system output power

P_v ..... Power demand from the vehicle

R_b ..... Battery internal resistance

r_f ..... Overall resistance of the fuel cell

SoC ..... Battery's state of charge

u ..... Control input in the model

v_b ..... Battery open-circuit voltage

V_{bus} ..... Terminal voltage of the battery pack

V_f ..... Terminal voltage of the fuel cell stack

v_k ..... model process noise

w ..... Disturbance acting on the system

x ..... System states in the model

y ..... System output in the model

z ..... Premise variable in the fuzzy system

α_i ..... Weighting scalar for each sigma point

$\bar{v}$ ..... Mean value of the measurement noise v_k

$\bar{\rho}$ ..... Mean value of the process noise ρ_k

$\bar{u}$ ..... Upper bound on the control input

β_i ..... Weighting scalar for each sigma point

χ_k^{a+} ..... Augmented sigma points set

$\chi_{k,i}^{r+}$ ..... State portion in augmented sigma points set

$\chi_{k,i}^{\rho+}$ ..... Process-noise portion in augmented sigma points set

ΔSoC_r ..... Admissible increment of the battery state of charge

Δt ..... Sampling time period

δ ..... $\mathcal{H}_\infty$ Attenuation level

η_{dc} ..... Efficiency of the fuel cell boost converter

η_f ..... Faraday efficiency of the battery

γ ..... Scaling parameter in the sigma-point Kalman filter

$\hat{r}_k^{a+}$ ..... Augmented a posteriori state estimate vector

$\hat{r}_k^{+}$ ..... Posteriori estimated state

$\hat{V}_{f,k}$ ..... Output estimate in the sigma-point Kalman filter

ρ_k ..... Zero mean white noise perturbation

Ψ ..... Candidate invariant set

σ_0 ..... Upper bound on the disturbance

$\Sigma_{\tilde{v},k}$ ..... Covariance of the output estimate

$\Sigma_{\tilde{r},k}^{a+}$ ..... Augmented a posteriori covariance estimate

$\Sigma_{\tilde{r}}$ ..... Covariance of the measurement noise v_k

$\Sigma_{\tilde{\rho}}$ ..... Covariance of the process noise ρ_k

τ ..... Battery State of charge reference

ξ ..... Error between the output measurement and reference value